AN ABSTRACT OF THE DISSERTATION OF

Benjamin L. Clark for the degree of Doctor of Philosophy in Chemistry presented on May 3, 2001. Title: Electroluminescent and Photoluminescent Phosphor Development and a Facile Approach to Synthesis of Refractory Silicates at Low Temperatures.

Abstract Approved: Redacted for Privacy

Douglas A. Keszler

Several phosphors of importance for alternating-current thin-film electroluminescent (ACTFEL) device applications have been synthesized and studied. Particular attention was paid to synthesis of a bright and efficient green ACTFEL phosphor by using codopants, solid-solution, and ceramic processing techniques.

Emission from SrS:Cu has been studied. The specific emission color depends strongly on the local environment surrounding the Cu^+ ion in the SrS lattice. Both blue and green emissions have been reported previously, and there remains considerable debate as to the origins of these emissions. A new model emphasizing the structural environment of the Cu atom in its ground state is used to account for new and previously reported data on the SrS:Cu system. The model is described, extended to emission colors in other Cu-doped alkaline-earth sulfides, and used to account for the performance characteristics of EL devices.

The differences in ACTFEL performance of ZnS and SrS were studied by comparing the EL emission spectra of each with a series of lanthanide dopants. On the basis of these spectra and the electrical characteristics of the device, it was confirmed that the electron distribution for ZnS is not hot enough at higher energies to efficiently excite luminescent impurities in the blue region of the spectrum and this results in inefficient blue EL emission as compared to SrS.

Hydrothermal dehydration, a simple method for preparing refractory silicates at low temperatures and pressures, is introduced. The method involves precipitation of a hydroxylated silicate, followed by dehydration under equilibrium conditions. Three silicates were synthesized using this method: Zn_2SiO_4, $SnSiO_3$, and Mg_2SiO_4.

Electroluminescent and Photoluminescent Phosphor Development and a Facile Approach to Synthesis of Refractory Silicates at Low Temperatures

by

Benjamin L. Clark

A DISSERTATION

submitted to

Oregon State University

in partial fulfillment of
the requirements for the
degree of

Doctor of Philosophy

Completed May 3, 2001
Commencement June 2001

Doctor of Philosophy dissertation of Benjamin L. Clark presented on May 3, 2001.

APPROVED:

Redacted for Privacy

Major Professor, representing Chemistry

Redacted for Privacy

Head of Department, representing Chemistry

Redacted for Privacy

Dean of the Graduate School

I understand that my dissertation will become part of the permanent collection of Oregon State University libraries. My signature below authorizes release of my dissertation to any reader upon request.

Redacted for Privacy

Benjamin L. Clark, Author

ACKNOWLEDGEMENTS

I would like to first thank my major professor, Doug Keszler. His unwavering support, guidance, encouragement, and seemingly unending stream of ideas have greatly helped me the last several years.

I would next like to extend my gratitude to my committee members, Arthur Sleight, Janet Tate, Milo Koretsky, Richard Peterson, and Richard Tuenge, for their support in both my coursework and in my research.

This work would not have been possible without the help and collaborative research efforts of the department of Electrical and Computer Engineering. I especially have to thank Paul Keir, whom without, this thesis would not be complete. Beau Baukol and John Hitt were very helpful in helping me with the finer points of electrical characterization techniques and in helping me with energy transfer experiments. Jeff Bender was very helpful with many low temperature annealing techniques. I am also grateful to John "The Bossman" Wager for allowing me to work with his research group in ECE.

I need to thank both former and present members the Keszler Power Group for their support, encouragement, and helpful discussions: Ki-Seog Chang, Dong Li, Greg Peterson, Judith Kissick, Sangmoon Park, Jennifer Stone, Jeremy Anderson, T. Cho, Youhyak Kim, and Mike Hruschka. I especially need to thank Dong Li for helping me in the initial stages of this work and for encouraging me to work with Dr. Wager's group in ECE.

The faculty and staff here at OSU were all tremendously helpful, and I need to thank them for their support. I have also made a lot of new friends in this department including Geoffrey Barber, David Blanchard, Kevin Cantrell, Englene Chyrsostom, George Law, and Towy Masiella. My old friends Bill Suckow and Jon Tichenor have always been there for me.

My parents Judy and Kerry Murray, and Larry and Debbie Clark, have been tremendously supportive, even though they have always teased me about being a professional student. I have to also thank my in-laws, George and Mary Copeland, and Donna and Doug Goldsmith, who I'm sure thought twice about me after finding out that I was going to attempt to support their daughter, and myself, on a graduate student's stipend for four years. But they have always been there for us, and I appreciate them for that.

By far most importantly, I need to thank my wife, Sara. Her undying love and support of me the last few years have been remarkable. Without her, I wouldn't be where I am today.

CONTRIBUTION OF AUTHORS

This work would not have been possible without the help of several collaborators. These collaborators and their respective contributions are given here. Dong Li was essential in the introductory phases of examining the photoluminescence of SrS and ZnS for chapters 2 and 3. Paul Keir contributed in chapters 2-4 by helping manufacture the ACTFEL devices used for testing. He is also responsible for most of the electrical characterization of the ACTFEL devices. Beau Baukol and Crystal Maddix contributed in chapter 4 by developing and testing the ACTFEL devices. He is also responsible for part of the electrical and optical characterizations conducted. Jeremy Anderson helped synthesize and test SrS powders used in chapter 5. Tom Reynolds is responsible for providing the single crystal of $LaSc_3(BO_3)_4$ used in Appendix A.

TABLE OF CONTENTS

TABLE OF CONTENTS (continued)

TABLE OF CONTENTS (continued)

TABLE OF CONTENTS (continued)

TABLE OF CONTENTS (continued)

LIST OF FIGURES

LIST OF FIGURES (continued)

LIST OF FIGURES (continued)

LIST OF TABLES

ELECTROLUMINESCENT AND PHOTOLUMINESCENT PHOSPHOR DEVELOPMENT AND A FACILE APPROACH TO SYNTHESIS OF REFRACTORY SILICATES AT LOW TEMPERATURES

CHAPTER 1

INTRODUCTION

For years, the information-display market has been dominated by the cathode-ray tube (CRT). CRT displays offer the consumer excellent color, high contrast, and high resolution. Being a mature technology, CRTs are also relatively inexpensive. Their bulky size, however, prohibits incorporation into smaller, portable systems such as notebook computers.

Within the past decade, an increasing number of portable devices have evolved to make our everyday lives easier and more enjoyable. Many of these devices, including cellular phones, pagers, personal electronic planners, and portable gaming systems, rely on some type of display technology to interface with the user. Users demand high resolution, wide viewing angles, low operating costs, and high durability in these displays. Because of these needs, chemists, materials scientists, and engineers work closely to improve display performance through phosphor and process development as well as device-structure evolution.

The Flat Panel Display (FPD) industry has filled the niche for portable display applications. Presently, the largest FPD technology encompasses the liquid crystal display (LCD). LCDs are found on virtually every notebook computer,

making it difficult for other technologies to enter this market. There are, however, drawbacks to LCD technology such as low viewing angles, limited operational temperatures, and relatively high power consumption. For these reasons, many other forms of FPDs have been developed, including field emission displays (FEDs,) organic light-emitting diodes (OLEDs,) electroluminescent displays (ELDs,) and plasma display panels (PDP.) The development of phosphors for these types of displays has not been studied as extensively as those for CRT, thus the focus of this study is on the development of phosphors for ELD and PDP displays. The purpose of this chapter is to give some preliminary concepts before presenting results on the phosphor development.

Luminescence Process

Luminescence can best be described by using the configurational coordinate diagram as shown in Figure 1.1. In this diagram, two potential wells are plotted with energy (E) on the ordinate and interatomic distance (R) on the abscissa. The lower and upper parabolas represent the ground and excited states, respectively, of the luminescent center. A photon is absorbed by the luminescent center, giving rise to an electronic transition from the lowest vibrational level in the ground state to an upper vibrational level in the excited state (EX). At this point, nonradiative decay or relaxation occurs, and the electron relaxes to the lowest vibrational level in the excited state. Decay to the ground state results in the release of a photon of lower energy than that of the exciting photon (EM). This process is called emission.

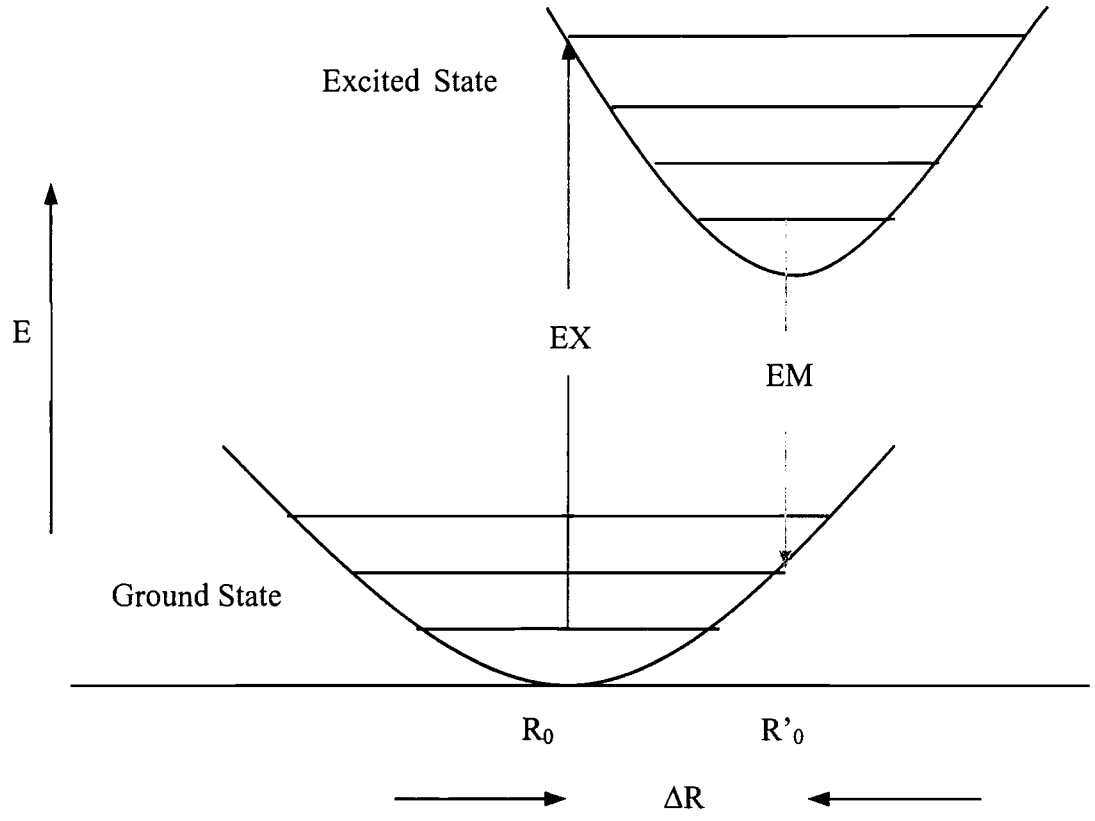

Figure 1.1. Configurational coordinate diagram.

The horizontal difference in position of the parabolas is equal to ΔR and represents atomic displacement. Additional details can be found in the literature.[1-3]

Color and Light [4,5]

Visible light constitutes only a small part of the electromagnetic spectrum. The portion perceived by the human eye covers a fairly narrow band of the total spectrum with the sensitivity ranging from approximately 380 to 780 nm. Obviously not all human eyes react the same, so a quantitative method for

describing color is necessary. One way to quantify color is by testing color perception on a large number of individuals and averaging the results. This average is termed the standard observer.

Luminosity (or sensitivity) curves are obtained by testing hundreds of individual's response to color. A luminosity curve is a plot of spectral sensitivity of the human eye. Obviously, it is important for the spectral output of a phosphor to match with the eye's response. The luminosity curve for a standard observer is given in Figure 1.2.

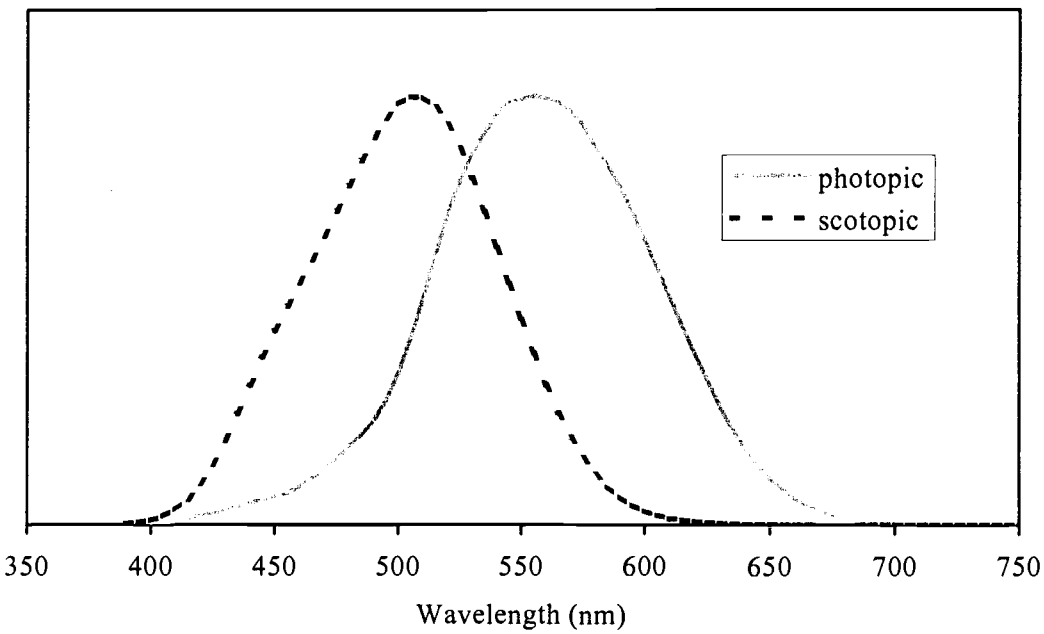

Figure 1.2. Luminosity curves for CIE standard observer.

The brightest part of the spectrum in the photopic range (vision under high levels of illumination) occurs near 555 nm, in the green-yellow region. Under low levels of illumination, or the scotopic range, the region of highest response is near 510 nm, or in the blue-green region of the spectrum. This difference in spectral response under different illumination levels arises from the distinct receptors in the human eye; rods are responsible for scotopic vision, while cones are responsible for photopic.

Color perceived from a self-emitting object is typically described by its hue, brightness, and saturation. Hue is the attribute that we denote by red, yellow, and green, therefore hue is determined by the dominant wavelength. The degree to which a color differs from white describes a color's saturation. Saturation provides a description of the purity of the chromatic color. Finally, the brightness or luminance is the attribute we use to describe the perceived intensity of light.

These attributes describe color in a qualitative manner. For scientific purposes, a quantitative method of describing color is necessary. To do this, we employ the CIE system developed by the Commission Internationale de I'Eclairage (International Commission on Illumination.) It is based on trichromatic theory and deals with three fundamental aspects of color – the object, the light source, and the observer. A set of tristimulus values (X, Y, Z) are used to denote quantities of primary colors in any arbitrary sample color. One can think of these values as the amount of blue, green, and red in a sample, although this is a simplified way of thinking of the tristimulus values.

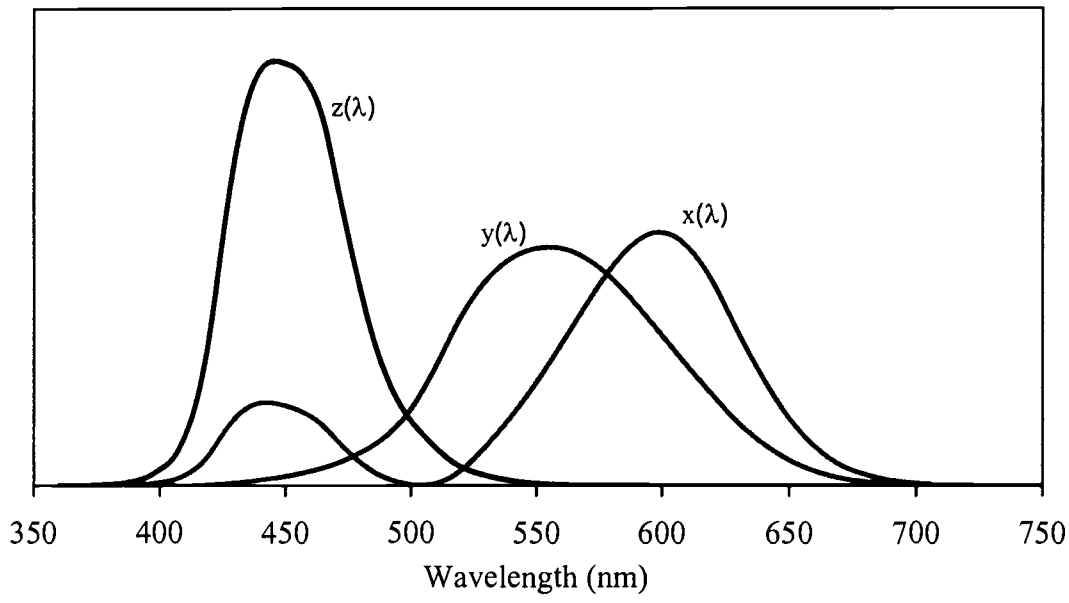

Figure 1.3. Color matching functions for CIE 1931 standard observer.

The tristimulus values X, Y, Z can be calculated by using the color matching functions given in Figure 1.3. As noted previously, these functions have been derived by determining the average response to the human eye. Each tristimulus value for a sample of interest is calculated by integrating the product of the power output of the sample and the color matching function:

$$X = \int S(\lambda) \cdot x(\lambda) \cdot d\lambda$$

$$Y = \int S(\lambda) \cdot y(\lambda) \cdot d\lambda$$

$$Z = \int S(\lambda) \cdot z(\lambda) \cdot d\lambda$$

Chromaticity coordinates x, y, and z are then derived by normalizing each of the tristimulus values:

$$x = \frac{X}{X+Y+Z}$$

$$y = \frac{Y}{X+Y+Z}$$

$$z = \frac{Z}{X+Y+Z}$$

Since the sum of x, y, and z must equal 1, we need only consider the pair x, y, which is commonly plotted on a CIE chromaticity diagram (Figure 1.4.) This gives a quantitative value of color. Colors with chromaticity coordinates near the perimeter of the diagram are regarded as being saturated. True white light has equivalent chromaticity coordinates, i.e., x = y = 0.33.

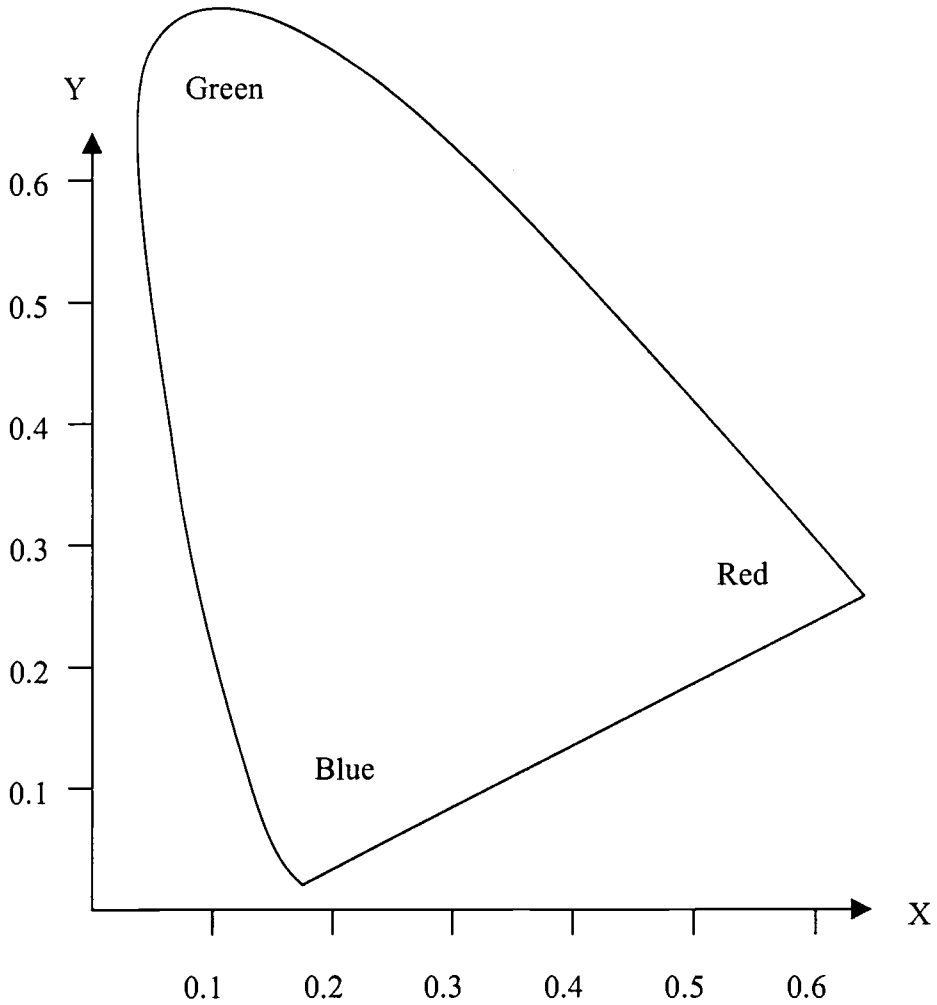

Figure 1.4. CIE chromaticity diagram.

In the display industry, the production of saturated white light is required. On the basis of the triphosphor system, the chromaticity requirements for each phosphor have been determined,[6] and they are summarized in Table 1.1. In addition to the required CIE coordinates, the intensities of blue, green, and red must be in the ratio of 1:6:3 in order to achieve a balanced white.

Table 1.1. CIE coordinates for phosphors in the trichromatic system.

Coordinate	Blue	Green	Red	White
X	<0.15	<0.3	>0.55	0.33
Y	<0.15	>0.5	<0.3	0.33

ACTFEL Devices[7-9]

Since the flat-panel display market is dominated by the LCD, alternative flat-panel display technologies must be gauged in terms of LCD performance and characteristics. Several advantages of an alternating-current thin-film electroluminescent (ACTFEL) display over a conventional LCD include the ability to pattern much smaller pixels, better performance over a wider range of temperatures, greater ruggedness, and a wider viewing angle. Disadvantages include larger power consumptions, lack of adequate trichromatic phosphors, and larger driving voltages. Of these three, the most serious disadvantage is the lack of adequate chromaticity. The main hindrance to production of full-color ACTFEL displays has historically been the lack of a bright and efficient blue phosphor. Recent developments, however, on a bright and efficient blue phosphor may lead to improved full-color ACTFEL displays in the near future.[10]

Device Structure

ACTFEL devices consist of a phosphor layer, at least one insulator, an opaque conductor, and a transparent conductor, all deposited on a substrate made of glass or ceramic. Three general types of structures are commonly employed.[8] The two more common types of ACTFEL structures are depicted in Figure 1.5. The "standard" structure is given in 1.5(a). In this structure, a transparent substrate is coated with a transparent electrode, such as tin-doped indium oxide (ITO.) The first of two insulators is deposited on the ITO, followed by a thin film of phosphor. A second insulator is added on top of the phosphor, and finally, an opaque conductor completes the device. Light reaches the viewer through the transparent conductor, as indicated in the figure.

The second structure is known as the "inverted" structure, and it also consists of a phosphor layer encased by two insulating layers. The main difference, however, between this and the first structure is the transparent electrode is deposited last. Because of this, the substrate can be opaque or transparent, since the light reaches the viewer through the top, transparent conductor, as depicted in Fig. 1.5(b).

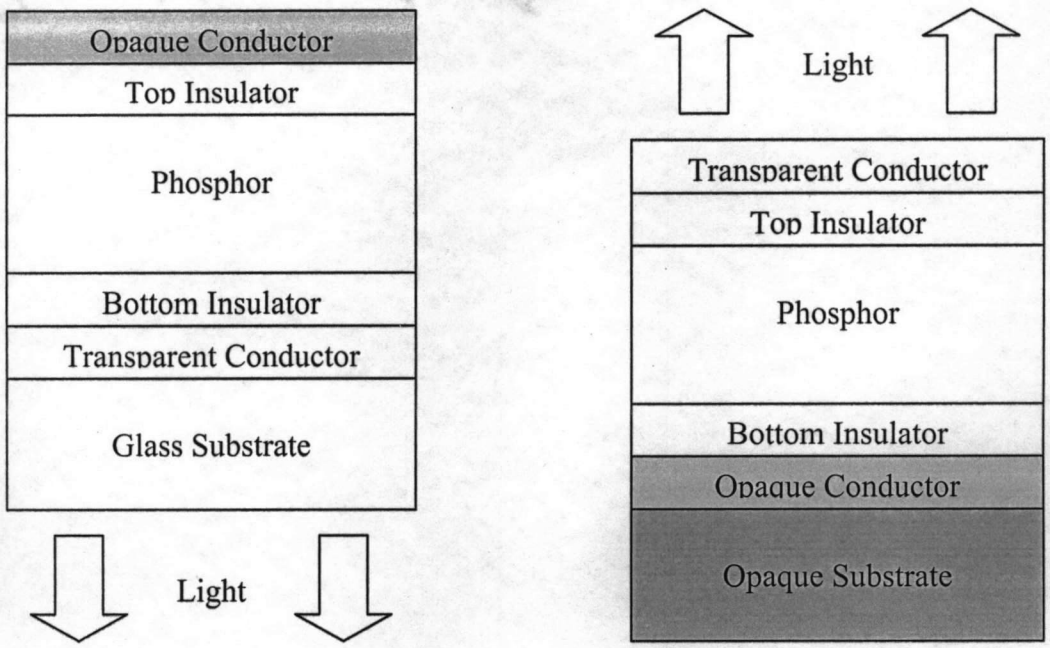

Figure 1.5 The standard ACTFEL device structure (left) and the inverted device structure (right).

The choice of structure is dictated by the process requirements, limitations, and intended applications for the ACTFEL device. The standard structure is the most common, and it is the one used throughout this work, unless otherwise noted. It is the preferred structure for testing purposes, because its fabrication is simpler than that of the inverted structure. Also, the active device layers are shielded from the viewer by the glass substrate. The inverted structure has several distinct advantages, however, for certain applications. For instance, the use of color filtering is easier in the inverted structure. Color filters are typically organic polymers that are sensitive to high processing temperatures, thus incorporation of a color filter should be the final process in manufacturing a device. By using the standard structure, this filter would have to be placed on the glass substrate first,

before any other layers are deposited, and thus would be subject to all subsequent processes. Because of the way light is directed out of the inverted device structure, glass substrates are not necessary and higher processing temperatures can be achieved by using the inverted structure. Glass substrates begin to soften near 873 K, so if higher temperatures are needed for extended periods of time, a ceramic or silicon substrate is used.

A third, less common ACTFEL device structure sometimes used for testing purposes is the "one-insulator" structure. It is essentially the same as the inverted structure, minus either of the insulators. Details of this structure and its applications can be found elsewhere.[11]

ACTFEL Operation[8,9]

Since the advent of the ACTFEL device[12] in the mid-1970s, researchers have studied their operation and it is believed that the basic operation of an ACTFEL device is well understood. In this section basic operation of an ACTFEL device will be summarized.

Before threshold voltage in an ACTFEL device is achieved, the electrical characteristics of the device are equivalent to a simple capacitor. The phosphor layer and insulating layers all have equivalent capacitances, following the formula given for the capacitance of parallel plates:

$$C = \frac{\varepsilon A}{t}$$

where ε is the permittivity, A is the area, and t is the thickness of the layers. Since the ACTFEL device consists of successive layers, the total capacitance is equal to the capacitances of the individual layers in series:

$$C_{total} = \frac{C_p C_{i,t} C_{i,b}}{C_p C_{i,t} + C_p C_{i,b} + C_{i,t} C_{i,b}}$$

where C_p is the capacitance of the phosphor layer and $C_{i,t}$ and $C_{i,b}$ are the capacitances of the top and bottom insulator, respectively. The insulators can be modeled as a single contribution:

$$C_{total} = \frac{C_i C_p}{C_i + C_p}$$

At voltages below threshold, the ACTFEL device acts as a capacitor. Above threshold, electrons are tunnel emitted from the insulator-phosphor interface (essentially, the phosphor layer "shorts out") where they feel the strong electric field generated by the electric potential. This is shown schematically as process 1 in Figure 1.6. Once in the phosphor, the electron rapidly accelerates toward the anodic interface because of the high electric field in the phosphor layer (process 2.) The electron may eventually collide with a luminescent impurity, such as a Mn^{2+} ion, causing the ion to become excited (process 3.) Relaxation of the ion is accompanied by either the release of a photon, or by a nonradiative phonon. Obviously, the latter of the two processes is unwanted and should be minimized. After impact excitation, the electron continues to accelerate toward the anode, where along the way, it can excite other impurities. Finally (process 4,) the electron is trapped at the phosphor-insulator interface. Since these are AC driven

devices, the process is repeated in the opposite direction when the AC waveform changes signs. This time, however, there are some remnants of charge left in the phosphor that lowers the turn-on voltage for the opposite pulse. For this reason, the turn-on voltage is always lower than the threshold voltage.

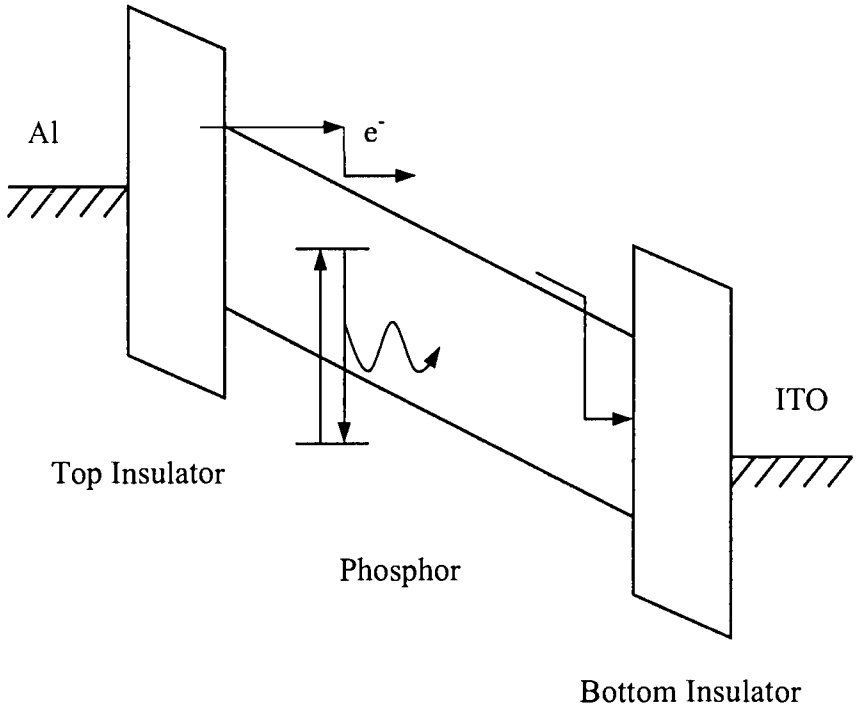

Figure 1.6. Band structure model of an ACTFEL device.

This simple picture works well in describing the basics of ACTFEL devices. One complication of this basic model is space charge. Space charge is basically a polarization of the charge in the phosphor layer that arises from electron ionization of an atom in the phosphor. This is sometimes called carrier multiplication; two electrons are now present leaving a positive hole behind. The

internal electric field of the phosphor will no longer be uniform and band bending will occur (Figure 1.7), resulting in the formation of positive space charge.

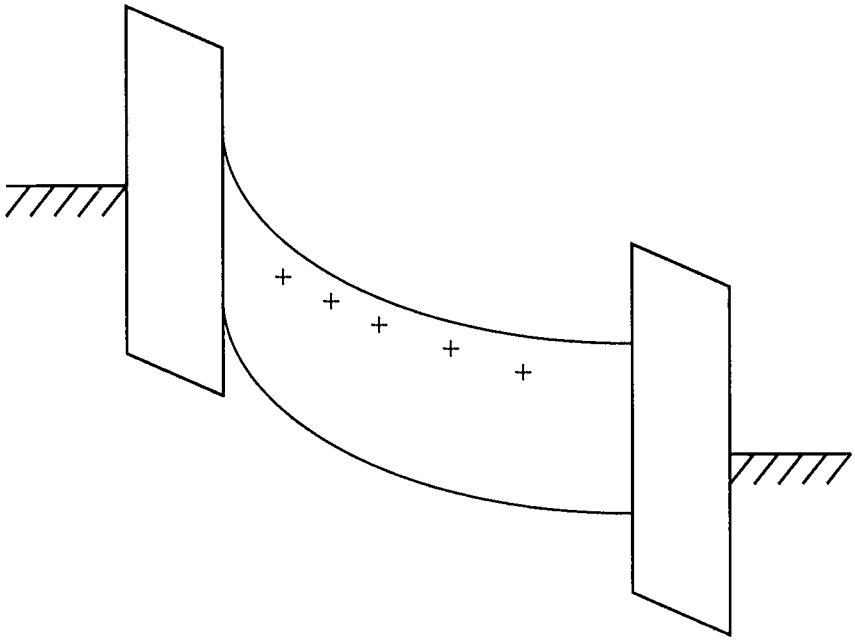

Figure 1.7. Energy band diagram of an ACTFEL device with positive space charge.

ACTFEL Optical Characterization

There are three important optical characteristics of ACTFEL devices: the color or chromaticity of the emitted light, the amount of light emitted and the amount of power required to generate the light. Color and chromaticity have been discussed above. The other two characteristics are discussed below.

Luminance (or brightness) is defined as the luminous flux spreading outward per steradian in a given direction per square meter of perceived surface area. Its units are usually denoted as candela per meter squared (cd/m^2.) The

luminance of an ACTFEL device is generally measured versus the applied voltage. A typical luminance-voltage (L-V) curve is depicted in Figure 1.8. The voltage in increased and the luminance is measured with a photometer or photomultiplier tube until a predetermined maximum voltage has been reached. For most measurements, the luminance at 40 volts over threshold, L_{40}, is reported.

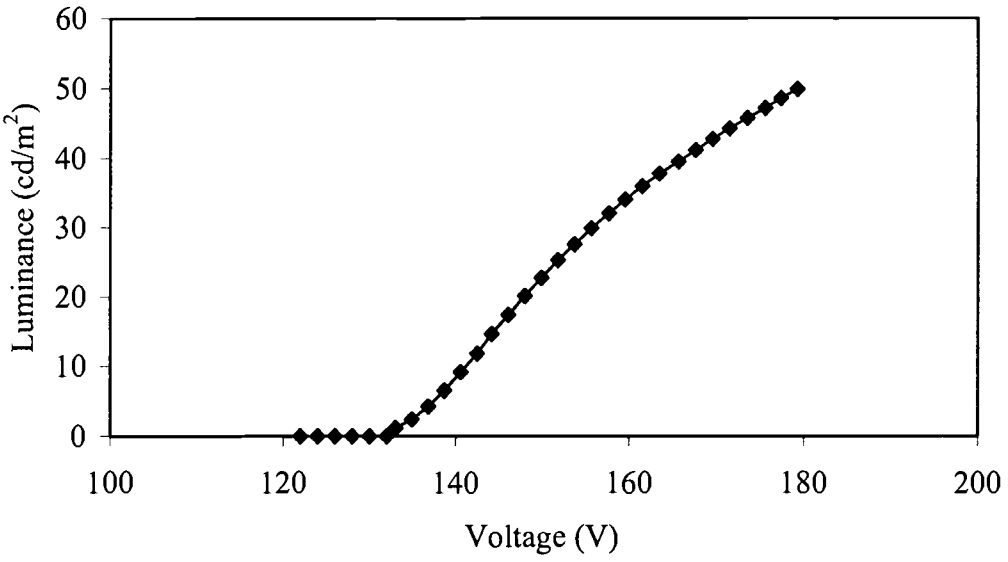

Figure 1.8. A typical L-V curve for an ACTFEL device.

Since most ACTFEL devices are intended to run in portable devices, the power consumption of the device needs to be as small as possible. For this reason, the efficiency is measured. Efficiency (η) is essentially the amount of light emitted per unit power and has units of lm/W. It is calculated from the following:

$$\eta = \pi \frac{L}{P}$$

where L is the luminance, P is the power density, and π accounts for the assumption of a perfectly diffuse surface. This last factor is included because the desired measurement is the emitted light from all directions, and one usually only obtains the quantity normal to the surface. Just like the L-V curve, the efficiency is measured versus the applied voltage. A typical η-V (or E-V) curve is given in Figure 1.9. For consistency, the efficiency is generally reported at 40 volts over threshold.

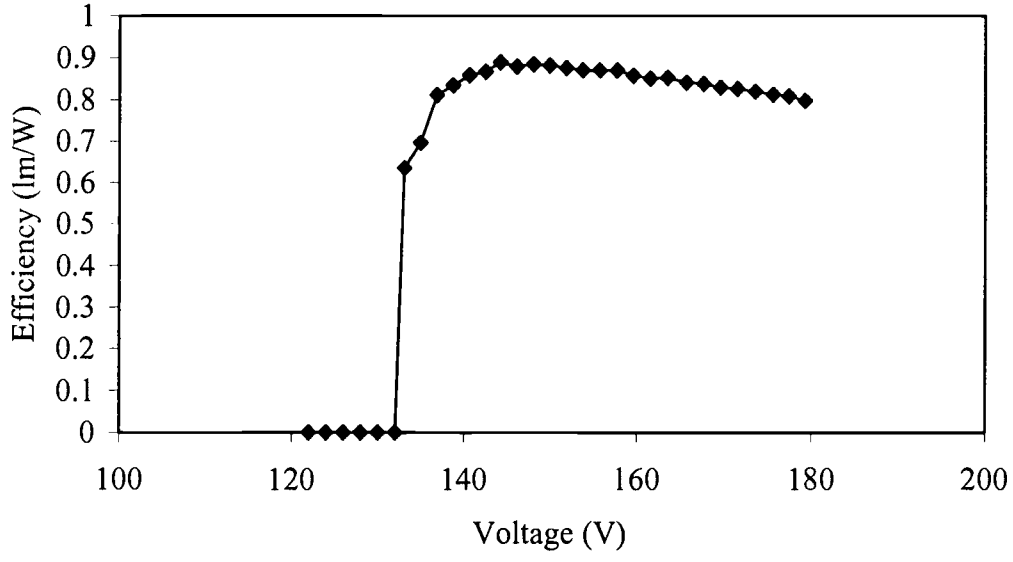

Figure 1.9. Typical η-V curve for a generic ACTFEL device.

Processing of ACTFEL Devices

A thin-film can be deposited by many different methods. Thin-film deposition can be broken down into two main categories: physical processes and chemical processes. Some methods, such as reactive sputtering, could be

considered as a combination of physical and chemical processes. The most common methods employed in research labs are evaporation, sputtering, and chemical vapor deposition. These and other methods will be discussed below along with advantages and disadvantages of each.

Evaporation[13]

Evaporation is perhaps one of the simpler deposition methods. It offers the researcher a quick, low-cost technique to deposit films of various metals. A film is created by applying heat to the source material under vacuum. As long as a sufficient vacuum exists, the vaporized materials will likely deposit on the substrate. An insufficient vacuum will result in a small mean free path, whereby the vaporized atoms will collide into gas molecules before ever reaching the substrate. This slows down the deposition rate, and it can also lead to nonuniform films with pinholes or other unwanted defects such as incorporation of residual gases.

Some advantages of evaporation include high deposition rates, low energy of impinging atoms, and the ability to produce high purity films. The deposition rate can be estimated from the following relationship:

$$R \approx \frac{P_{vap}}{\sqrt{TM}}$$

where R is the rate, P_{vap} is the vapor pressure, T is the temperature, and M is the molecular weight of the material. For reasonable deposition rates, P_{vap} must be greater than 1-10 mtorr.

The purity of the film depends on the pressure, therefore a low ultimate pressure is required. This represents a disadvantage since a large amount of time must be committed to pump down the chamber. Poor step coverage is also a problem in evaporation. This refers to how well a film maintains uniformity as it encounters a step, or channel, in a device. For these reasons, evaporation is generally not used in industry, but due to its simplicity and low-cost, it is used widely in academic research.

Resistive heating and electron-beam evaporation are the most common techniques in evaporation. In the former, a voltage is applied to a resistive material, such as tungsten, which then heats the source material sufficiently to cause vaporization and produce the thin-film. For more refractory materials, it may become necessary to use electron-beam evaporation. In this technique, a flow of electrons is directed to the source material by using magnetic field lines. The basic schematic the electron-beam evaporation method is given in Figure 1.10. This is the preferred method for depositing binary sulfide materials, as will be discussed in subsequent chapters.

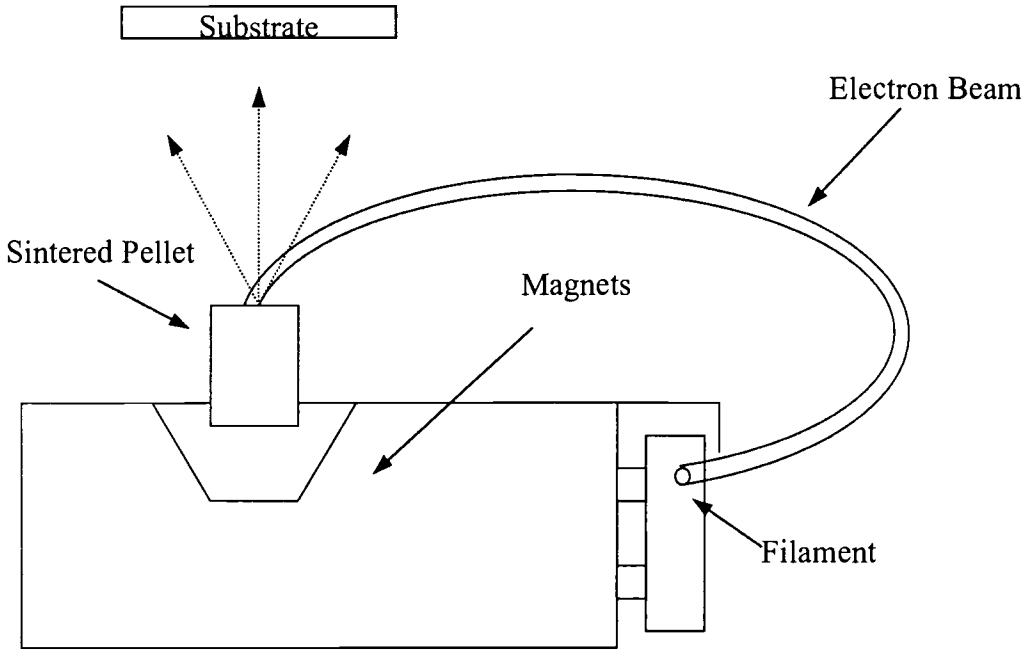

Figure 1.10. Schematic diagram of electron beam evaporation.

Sputtering[14,15]

Another common deposition method is sputtering. Sputtering is perhaps the most common thin-film deposition technique used in industry today.[16] It is usually a physical deposition method in which atoms are removed from the surface of the source material, or target, after bombardment of particles from a glow discharge. Advantages of sputtering over evaporation include better film uniformity, more control of thickness and composition, and better step coverage. Disadvantages include higher setup and maintenance costs, slower deposition rates, and a greater chance for incorporation of impurities because of the nature of the higher operating pressures used.

The sputtering process is shown schematically in Figure 1.11. A bombarding ion collides with the surface atoms of the target, and if the ion has sufficient kinetic energy, an atom from the surface will be dislodged. The dislodged, or sputtered atom then traverses the chamber and deposits on the substrate surface.

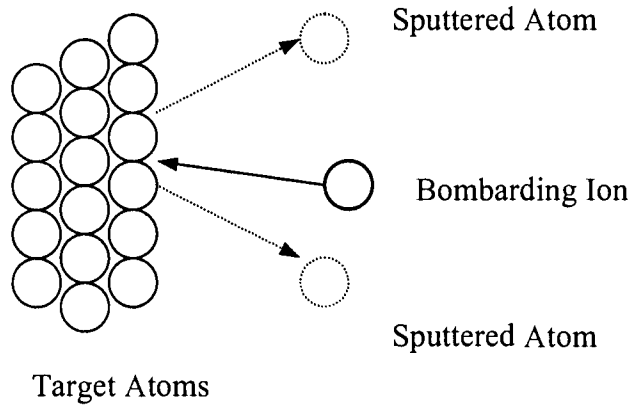

Figure 1.11. Schematic of the sputtering process.

Sputtering can actually occur at both electrodes (the target and the substrate.) To prevent this from happening, the relative areas of the electrodes must be controlled. More details can be found in the literature,[15,17] but briefly, the ions in the glow discharge will gain all of their kinetic energy near the electrodes in the sheath voltage. To control the sheath voltage, one simply needs to alter the areas of each electrode. The sheath voltage therefore depends on the following relationship:

$$\frac{V_a}{V_b} = \left(\frac{A_b}{A_a}\right)^4 .$$

where V_a and V_b represent the sheath voltages for each electrode, and A_a and A_b represent the areas of each electrode. Theoretical calculations result in an exponent equal to 4, but it has been experimentally determined to be less than 2. The smaller the area of the electrode a, the larger will be the sheath voltage, V_a. Thus, to prevent sputtering of the substrate instead of the target, the area of the substrate electrode must be as large as possible. This is usually accomplished by grounding the substrate electrode to the entire chamber.

Plasma Enhanced Chemical Vapor Deposition[14]

Plasma enhanced chemical vapor deposition (PECVD) is another common deposition technique. In this chemical deposition process, a thin film is formed by reacting gas phase chemicals in the presence of a glow discharge, or plasma. The chemicals react in the plasma, are deposited on the substrate and the excess material is transported out of the chamber. This is the technique used to create the top insulator in the ACTFEL devices to be discussed in subsequent chapters.

Advantages include low processing temperatures, fast deposition rate, and good step coverage. Since this process is mainly used to create silicon containing compounds, e.g., silicon oxide nitrides, toxic gases such as silane and silicon tetrachloride are generally used. Another disadvantage is contamination; the

pressures used for PECVD are generally slightly higher than those used in evaporation, therefore residual gases can be incorporated.

Atomic Layer Epitaxy[18]

Atomic layer epitaxy (ALE) is a technique used commonly employed in industry to deposit high-quality films of ZnS for ACTFEL devices. Excellent step coverage, high crystallinity, and low concentration of defects are a few advantages. A couple disadvantages of ALE are the high startup costs slow deposition rates.

In the ALE method, the film is grown one monolayer at a time, commonly employing the reaction below. The deposition of ZnS is depicted in Figure 1.12. First, a gaseous precursor ($ZnCl_2$) flows into the chamber, where it adsorbs onto the substrate surface in several layers, followed by a short burst of inert gas to expel all but a single monolayer of material. Next the second gaseous species (H_2S) is introduced, where it reacts with the adsorbed monolayer. The reaction products include crystalline ZnS and gaseous HCl. A second blast of inert gas is introduced, carrying away the HCl; the process is continuously repeated until the desired film thickness is achieved.

$$ZnCl_2\,(g) + H_2S\,(g) \rightarrow ZnS\,(s) + 2HCl\,(g)$$

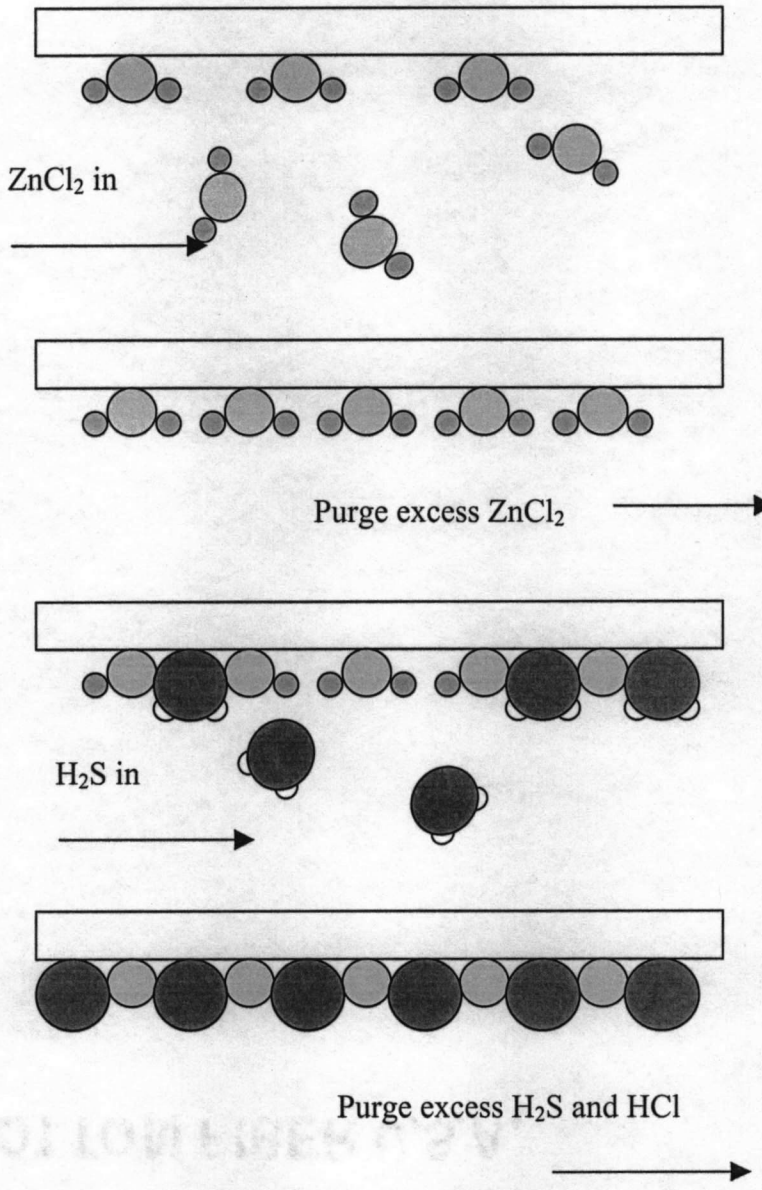

Figure 1.12. Deposition of one monolayer of ZnS by ALE.

Phosphor Development

Since the main focus of this work will be on the development of the phosphor layer in ACTFEL devices, a brief history of inorganic luminescent materials and their development should be reviewed. First, a general history of

phosphors will be discussed, followed by the development of lamp phosphors, concluding with phosphor development for ACTFEL devices. Although not closely related to most of this thesis, the section on lamp phosphors is included since it is the most established area of inorganic luminescent materials, its history is well known, and some similarities between it and ACTFEL phosphors development should become clear.

General History of Phosphors

Phosphor development is generally considered to have begun toward the end of the 19th century following the introduction of equipment for the production of electron beams, X-rays, and UV rays. General literature, however, indicates that luminescent materials have been known for centuries. In 1948, Jorrissen suggested that Romans might have prepared calcium sulfide phosphors as early as 186 B.C. by heating sulfur with chalk, lime, or oyster shells. He based these findings on the writings of the Euripides tragedy *Bacchae*, which describes a festival where Romans, carrying blazing torches, plunged them into the Tiber River, causing the torches to glow without being lit on fire.[19]

In 1603, Vincenzo Cascariolo, an Italian shoemaker, first prepared what is known as the Bolognian, or Bononian phosphor. He had discovered that the material, now known to be barium sulfate, glowed in the dark after being exposed to daylight.[19] To some, this discovery is considered the origin of inorganic phosphors.

Lamp Phosphor Development

Although the discovery of the Bolognian phosphor seemed to arouse great interest at the time, the equipment, methods, and materials of that time were insufficient to fully characterize the observations. In wasn't until the late 1800s and beyond that phosphor development really started. Becquerel, in 1867, described how he caused a phosphor to fluoresce in an electric-discharge tube pressured at 1-2 mmHg.[20] Almost three decades later, Edison filed a patent in which he described introducing $CaWO_4$ into a glass tube as it was being blown, thereby coating the inside with a thin layer of phosphor. Then, using two electrodes (no filament) to produce a discharge of residual gas, he excited the phosphor.[21] He called this a fluorescent electric lamp.

No real new developments occurred until forty years later, when in 1938, General Electric Company in Britain announced that they had produced a set of phosphors that coated lamps 8 feet, 6 inches in length. The phosphors Zn_2SiO_4 (green), $CaWO_4$ (blue), and $CaWO_4$ (pink) were used in three separate lamps and combined to create white light.[22] These lamps, however, required a high-voltage transformer to turn on, as well as the long lengths to obtain high efficiencies. Thus, they were mainly used for advertising displays rather than for illumination. That same year, General Electric (GE) of the United States announced that they had developed a fluorescent lamp that could be used at low household voltages.[23-24] The lamps were also shorter in length, making it more convenient to use; this also led to the production of the phosphor $Cd_2B_2O_5$:Mn.

The Japanese, intrigued, astounded, and quite behind in their own phosphor research, sent researchers from Toshiba to GE to learn the technology of lamps and phosphors. A little over a year later, Toshiba developed a white light lamp, which used the phosphors $MgWO_4$, $(Zn,Be)_2SiO_4$:Mn and $Cd_2B_2O_5$:Mn.[25] The outbreak of World War II, however, temporarily put a halt to all Japanese research.

In 1946, the Japanese resumed phosphor research, mainly out of the need to produce efficient lamps for attracting moths and insects as the desperate need for providing food increased. Lamp production increased from 2400 pieces in 1947 to 140,000 pieces in 1949.[25] Because of the toxicity of BeO, however, a suitable replacement for $(Zn,Be)_2SiO_4$:Mn was needed. $CaSiO_3$:Pb,Mn eventually replaced $(Zn,Be)_2SiO_4$:Mn as the red (pink) lamp phosphor.[26]

Research in the U.S. was ongoing throughout the war. In 1942, Jenkins and co-workers[27] discovered that replacement of Cd in $Cd_5(PO_4)_3Cl$:Mn with Ca and doping with Sb^{3+} resulted in efficient UV absorption and white-light production by combining the blue emission of Sb^{3+} and the orange emission of Mn^{2+}. They later learned how to control the ratio of blue to orange emission, increasing the efficiency. [28] Large-scale production of calcium halophosphate phosphor began in 1951, even though it presented some unique manufacturing challenges. To obtain consistent emission from the phosphor, strict heating regimes were required, and controls had to be established to limit the volatility of the starting materials.

To increase the efficiency of the calcium halophosphate phosphors, several processing improvements were made during the 1960s, including strict control of

particle size,[29] the use of $CaHPO_4$ as a starting material,[30] and modifications in compound stoichiometry.[31] From these improvements and others, efficiencies of the calcium halophosphate phosphors rose from ~20 lm/W in the 1940s to over 75 lm/W in the 1960s.[25]

Other improvements to the efficiency and luminous output came by adding deeper red emitting phosphors, such as $CaSiO_3$:Pb,Mn or $(Ca,Sr)_3(PO_4)_2$:Sn.[32] A broader luminescence spectrum, providing improved color rendition, was obtained by adding deep-blue emitting $CaWO_4$ and deep-red emitting $6MgO \cdot As_2O_5$:Mn.[33]

Research continued into the 1970s with separate groups at Philips and Westinghouse suggesting that white emitting lamps could be obtained by using the line emission from lanthanide ions.[34-35] One lamp phosphor introduced by the latter of these groups was $Y_2O_3:Eu^{3+}$, which had been developed in the late 1960s for the red component in color television tubes. Philips developed[36] two new phosphors in 1974: $MgAl_{11}O_{19}$:Ce,Tb and $BaMg_2Al_{16}O_{27}:Eu^{2+}$.

During the 1980s, a large increase in the number of new phosphors were produced, including a several aluminate phosphors developed by Smets and co-workers at Philips.[37-39] They obtained detailed crystallographic results on many of these aluminates, including $BaMgA_{11}O_{17}$ (BAM,) which was originally thought to have composition $BaMg_2Al_{16}O_{27}$. The real composition of BAM was found to have better mechanical properties than those of the composition $BaMg_2Al_{16}O_{27}$.

Today, much of the focus on lamp development is on miniaturization.[40] Fluorescent lamps with narrow diameters are necessary for backlighting in liquid

crystal displays and other handheld devices. Efforts are also being directed to the development of phosphors exhibiting quantum efficiencies above unity,[71] which could lead to the doubling of the performance of fluorescent lamps.

ACTFEL Phosphor Development

High-field electroluminescence was first discovered by Destriau[41] in 1936. He observed light emission after applying a high ac voltage to a ZnS phosphor dispersed in oil and sandwiched between two electrodes. No effort was made to develop a practical device until 1950 when the transparent conductor ITO (indium tin oxide) was developed. During the 1950s basic research and development focused on developing powder EL devices for lighting applications. With the use of ITO, Sylvania produced the first ac powder EL device called Palelite.

Display applications, however, were limited by poor multiplexing ability, low luminance, poor contrast, and significant degradation over a short period of time.[42] Research in powder EL devices for display applications all but halted with the emergence of thin-film technology. In 1960, Vlasenko and Popkov developed the first thin-film EL device.[43] They observed a much greater luminance in the yellow-emitting ZnS:Mn thin-film device with respect to the powder EL devices. The reliability of the thin-film devices, however, was insufficient for display applications.

Almost a decade later, Kahng reported[44] a new thin-film EL device using ZnS as the host and TbF_3 as the luminescent center. This was the first reported

green EL device, whereas all other thin-film EL devices up to this point had been obtained with the yellow-amber ZnS:Mn. This development was made possible by the advances in electronics and material science, especially with respect to new processing techniques and new phosphors. Reliability, however, was still a major problem, and again, research in the field stalled.

In 1974, Inoguchi and coworkers reported that luminances of over 3400 cd/m^2 at 5 kHz driving voltages could be maintained for more than 10,000 hours by using a double insulating layer device structure. This discovery triggered renewed interest in thin-film electroluminescent device applications, especially with respect to finding new phosphors for developing full color EL devices.

With one exception,[44] research for full color EL device applications did not take place until the 1980s. Most researchers continued to focus on ZnS, doping the system with various alkaline earth ions such as Tm, Tb, and Sm for blue, green, and red EL emission, respectively.[45-47] Luminance for these devices was still low, even after improvements to the phosphors were made, such as using $LnCl_3$, instead of LnF_3 (where Ln is a lanthanide) for the dopants.[48] Red emission was also obtained by using a thin-film filter of CdSSe over ZnS:Mn.[49]

The approach to using color filters in order to obtain red, green, and blue EL emission, however, is not desirable because of the decrease in luminance of the emitted light. To obtain efficient color EL phosphors, many researchers abandoned the ZnS system, turning their attention to finding new hosts and new luminescent impurities. The first alkaline earth sulfide to be used in EL device applications was

SrS doped with Ce,[50] which was reported to be 100 times brighter than ZnS:Tm. Soon after, many researchers were using SrS and CaS as EL phosphor hosts.[51-53] CaS doped with Eu was reported to be a deep red emitting phosphor with high luminance.[51] In 1997, a new blue EL phosphor was introduced based on Cu doped SrS.[54] Two years later, green EL emission was reported[55] in this same system by adding alkali-metal coactivators.

The use of thiogallate phosphors for EL applications has also been reported.[56] In particular, $CaGa_2S_4$:Ce emits in the deep blue region of the spectrum with high luminance. Improved luminance was obtained by substituting Sr for Ca.[57] Also, in this same study, Eu^{2+} was used as the activator, giving saturated green emission.

White-emitting phosphors have been investigated for EL device applications. By obtaining a white-emitting phosphor, full color emission can be obtained by using appropriate color filters. To obtain a white-emitting phosphor, Ono and coworkers used the blue-green emitting SrS:Ce and the red emitting SrS:Eu to give white light.[58] Tanaka and coworkers used a combination SrS:Ce/CaS:Eu to obtain white light.[59-60] A layered device based on ZnS:Mn has also been demonstrated.[61] While the luminance is better than those mentioned above, the color is not a true white because of the strength of the yellow-amber component from the ZnS:Mn emission.

Because of the relative instability of sulfide phosphors, many oxide materials have also been examined for EL display applications. Oxide phosphors

have potential advantages over sulfide phosphors such as greater hydrolytic stability, ease of manufacture, and greater development.

Ga_2O_3 has been used as an ACTFEL phosphor, and it has been activated with manganese,[62] chromium,[63] and europium.[64] Minami and coworkers have recently demonstrated a method for depositing Ga_2O_3 by using a dip-coating technique.[65] This eliminated the need for a vacuum chamber and other expensive deposition equipment. Miyata and coworkers have recently demonstrated a new EL emission from Ga_2O_3 by doping the host with tin, resulting in blue emission.[66] The reported luminance, however, was rather low even at 1 kHz driving frequencies.

Zinc silicate and zinc germanate have received much attention as ACTFEL phosphor materials.[62,67-69] Zinc germanate ACTFEL devices emit saturated green light when activated with manganese, and they have good luminance and efficiency.[70]

This Work

The topics in this thesis concern the investigation of sulfide phosphors for ACTFEL device applications and a novel method for creating refractory materials at low temperatures.

In chapters 2-5, the phosphors SrS and ZnS for both electro- and photoluminescence are described. In chapter 2, the photoluminescence results from varying defect concentrations in SrS:Cu and ZnS:Mn are examined. In chapter 3,

the characteristics of electroluminescent SrS:Cu devices prepared by using electron-beam evaporation techniques are considered. In chapter 4, the hot electron distributions are compared for SrS and ZnS by doping each with the same lanthanide ions and examining the resulting ACTFEL emission spectra. In chapter 5, further insight into the emission of SrS:Cu is given, proposing a shallow potential-well model to explain the differences in emission colors for different dopants and temperatures.

In chapters 6 and 8, details are given on a new, low-cost, low-temperature technique for producing Sn^{2+}-containing compounds and forsterite, Mg_2SiO_4. This method may lead to low-temperature annealing techniques for producing crystalline oxide ACTFEL devices, details of which are given in chapter 7.

References

1. Blasse, G.; Grabmaier, B.C. Luminescent Materials. Springer-Verlag, 1994.

2. Kitai, A.H. Solid State Luminescence: Theory, Materials, and Devices. Chapman and Hall, 1993.

3. Vij, D.R. Luminescence in Solids. Plenum, 1998.

4. Williamson, S.J.; Cummins, H.Z. Light and Color in Nature and Art. John Wiley and Sons, 1983.

5. Berger-Schunn, A. Practical Color Measurement. John Wiley and Sons, 1994.

6. Sun, S-S. Private communication, May 20, 1998.

7. Vecht, A.; Gibbons, C; Davies, D.; Jing, X.; Marsh, P.; Ireland, T.; Silver, J.; Newport, A.; Barber, D. *J Vac Sci Tech.* **17**, 750 (1999).

8. Kitai, A.H. Solid-State Luminescence. Chapman and Hall, 1993.

9. Ono, Y.A. Electroluminescent Displays. World Scientific, 1995.

10. Sun, S-S.; Dickey, E.; Kane, J.; Yocom, P.N. *Proc. 17th Int. Display Research Conf.;* Morreale, J., Ed.; Society for Information Display: Santa Ana, CA, 1997. p 301.

11. Minami, T.; Miyata, T.; Takata, S.; Fukuda, I. *Jpn. J. Appl. Phys.* **33**, L117 (1991).

12. Inguchi, T.; Takeda, M.; Kakihora, Y.; Yoshida, M. SID Digest. **5**, 84 (1974).

13. Ohring, M. The Materials Science of Thin Films. Academic Press, 1992.

14. Schuegraf, K.K. Handbook of Thin-Film Deposition Processes and Techniques. Noyes Publications, 1988.

15. Wolf, S.; Tauber, R.N. Silicon Processing for the VLSI Era, vol. 1. Lattice Press, 1986.

16. Koretsky, M. Electronic Materials Processing, Class Notes, Fall, 1997.

17. Keir, P.D. Fabrication and Characterization of ACTFEL Devices. PhD Thesis, Oregon State University, 2000.

18. Suntola, T.; Hyvarinen, J. *Ann. Rev. Mat. Sci.* 15, 177 (1985).

19. Harvey, E.N. A History of Luminescence. The American Philosophical Society, 1957.

20. Becquerel, E. La Lumiere. F. Didot Freres, Paris, 1867.

21. Edison, T.A. U.S. Patent #865367, 1896.

22. Jenkins, H.G.; Bowtell, J.N. *Trans. Illum. Eng. Soc.* **13**, 61 (1938).

23. Inman, G.E. *Trans. Illum. Eng. Soc.* **34**, 65 (1939).

24. Tayer, R.N.; Barnes, B.T. *J. Opt. Soc. Am.* **29**, 131 (1939).

25. Shionoya, S.; Yen, W.H. Phosphor Handbook. CRC Press, 1999.

26. Merril, J.B.; Schulman, J.H. J. Opt. Soc. Am. 38, 471 (1948).

27. Jenkins, H.G.; McKeag, A.H..; Ranby, P.W. *J. Electrochem. Soc.* **96**, 1 (1949).

28. McKeag, A.H.; Ranby, P.W. U.S. Patent #2488733, 1952.

29. Butler, K.H.; Homer, H.H. *Illum. Eng.* 55, 396 (1960).

30. Aia, M.A. Kokoku (Japanese patent) 39-1121, 1964.

31. Gillooly, G.R.; Rabatin, J.G. Kokoku 40-6843, 1965.

32. Butler, K.H. *J. Electrochem. Soc.* **100**, 250 (1953).

33. Nakajima, S.; Honda, Y.L. *J. Illum. Eng. Japan.* **40**, 305 (1956).

34. Koedamn, M.; Opstelten, J.J. *Lighting Res. Technol.* **3**, 205 (1971).

35. Thornton, W.A. *J. Opt. Soc. Am.* **61**, 1155 (1971).

36. Verstegen, J.M.P.J. *J. Electrochem. Soc.* **121**, 1623 (1974).

37. Ronda, C.R.; Smets, B.M.J. *J. Electrochem. Soc.* **136**, 570 (1989).

38. Smets, B.; Rutten, J.; Hoeks, G.; Verlijsdonk, J. *J. Electrochem. Soc.* **136**, 2119 (1989).

39. Stevels, A.L.N. *J. Lumin.* **17**, 121 (1978).

40. Kamiya, S. *Proc. 6th Int. Symp. Sci. Tech. Light Sources*, Budapest, 37, 1995.

41. Destriau, G. *J. Chim. Physique.* **33**, 587 (1936).

42. Lehmann, W. *J. Electrochem. Soc.* **113**, 40 (1966).

43. Vlasenko, N.A.; Poplov, I.A. *Optics & Spectroscopy.* **8**, 39 (1960).

44. Kahng, D. *Appl. Phys. Lett.* **13**, 210 (1968).

45. Ohnishi, H.; Yamamoto, K.; Katayama, Y. *Conference Record of the 1985 International Display Research Conference.* 159, 1985.

46. Ohnishi, H.; Yamasaki, Y.; Iwase, R. *Digest of 1987 SID International Symposium.* 238, 1987.

47. Ogura, T.; Mikami, A.; Tanaka, K.; Taniguchi, K.; Yoshida, M. Nakajima, S. *Appl. Phys. Lett.* **48**, 1570 (1986).

48. Hirabayashi, K.; Kozawaguchi, H.; Tsujiyama, B. *Jpn. J. Appl. Phys.* **26**, 1472 (1987).

49. Tuenge, R.T.; Kane, J. *Digest of 1991 SID International Symposium*, 279, 1991.

50. Barrow, W.A.; Coovert, R.E.; King, C.N. *Digest of 1984 SID International Symposium*, 249, 1984.

51. Tanaka, S.; Deguchi, H.; Mikami, Y.; Shiiki, M.; Kobayashi, H. *Proc. SID.* **26**, 255 (1985).

52. Tanaka, K.; Mikami, A.; Ogura, T.; Taniguchi, M.; Yoshida, M.; Nakajima, S. *Appl. Phys. Lett.* **48**, 1730 (1986).

53. Tanaka, S. *J. Crystal Growth.* **101**, 958 (1990).

54. Sun, S-S.; Dickey, E.; Kane, J.; Yocum, P.N. *Proceedings of the 17th International Display Research Conference*, p. 301, 1997.

55. Keir, P.D.; Wager, J.F.; Clark, B.L.; Li, D.; Keszler, D.A. *Appl. Phys. Lett.* **75**, 1398 (1999).

56. Barrow, W.A.; Coovert, R.E.; Dickey, E.; King, C.N.; Laakso, C.; Sun, S.S.; Tuenge, R.T.; Wentross, R.C.; Kane, J. *Digest of 1993 SID International Symposium*, 761, 1993.

57. Benalloul, P.; Barthou, C.; Benoit, J. *J. Alloys Compnd.* 275 (1998).

58. Ono, Y.A.; Fuyama, M.; Onisawa, K.; Tamura, K.; Ando, M. *J. Appl. Phys.* **66**, 5564 (1989).

59. Tanaka, S.; Yoshiyama, H.; Nishiura, J.; Ohshio, S.; Kawakami, H.; Kobayashi, H. *Appl. Phys. Lett.* **51**, 1661 (1987).

60. Tanaka, S.; Mikami, Y.; Deguchi, H.; Kobayashi, H. *Jpn. J. Appl Phys.* **25**, L225 (1986).

61. Tanaka, S.; Ohmi, K. Fujimoto, K.; Kobayashi, H.; Nire, T.; Matsuno, A.; Miyakoshi, A. *Eurodisplay '93*, 237, 1993.

62. Minami, T.; Yamada, H.; Yoshihiro, K. Toshihiro, Miyata. *Proc. SPIE Int. Soc. Opt. Eng.* 3242, 1997.

63. Minami, T.; Kubota, Y.; Yamada, H.; Miyata, T. *Ext. Abstr., Internat. Conf. Sci. Technol. Display Phosphors.* 207, 1997.

64. Minami, T.; Sakagami, Y.; Miyata, T. *Ext. Abstr., Internat. Conf. Sci. Technol. Display Phosphors.* 37, 1997.

65. Minami, T.; Miyata, T.; Nakatani, T. *Proc. Electrochem. Soc.* 99, 2000.

66. Miyata, T.; Nakatani, T.; Minami, T. *J. Lumin.* **89**, 1183 (2000).

67. Minami, T. *Mater. Res. Soc. Symp. Proc.* 558, 2000.

68. Miyata, T.; Minami, T.; Ito, J.; Takata, S. *Proc. 6th Int. Workshop Electroluminescence.* 228, 1992.

69. Bondar, V. *Mater. Sci. Eng. B.* **69**, 510.

70. Clark, B.; Keszler, D.; Bender, J.; Wager, J. *Ext. Abstr., Internat. Conf. Sci. Technol. Display Phosphors.* 145 (2000).

71. Feldmann, C.; Justel, T.; Ronda, C.R.; Wiechert, D.U. *J. Lumin.* **92**, 245 (2001).

CHAPTER 2

COLOR CONTROL IN SULFIDE PHOSPHORS: TURNING UP THE LIGHT FOR ELECTROLUMINESCENT DISPLAYS

For publication in Chemistry of Materials

Abstract

Control of defect concentration and type in the phosphors SrS and ZnS results in a broad range of colors in the visible part of the spectrum. Photoluminescent (PL) data on the blue to green emitting system SrS:Cu is presented and explained on the basis of coordination about the Cu ion. Saturated red PL is obtained by introducing Zn vacancies into ZnS:Mn. Some preliminary results of electroluminescent (EL) data on both systems are also presented. An efficiency of about 1 lm/W is achieved for the green-emitting SrS:Cu, K EL device.

Introduction

Commercial flat-panel electroluminescent devices operate on the basis of the phosphor ZnS:Mn, which gives yellow-amber emission. Despite the absence of full-color output, the high-performance characteristics of these monochrome displays have led to their use in a variety of niche-market applications. Of course, a full-color device could find use in various hand held devices such as personal organizers and notebook computers.

Two methods are currently being examined to realize full color output. In the color-by-white method, suitable phosphors broadly emitting in the blue and yellow portions of the spectrum are combined to produce a solid-state EL source of white light; this light is then passed through a set of color filters. The phosphor ZnS:Mn is under investigation for this application, but much improved performance could be realized by inducing the material to luminesce at a slightly

longer wavelength. To replicate the full red, green, blue (RBG) performance of a cathode-ray tube, efficient EL-active red, green, and blue phosphors having specific emission colors (chromaticity) must be available. To date, such a color set has not been demonstrated, but recently the prospects for production of a full-color EL display have brightened considerably, following the discovery and efficient operation of the blue-emitting phosphor SrS:Cu[1] and its modifications.[2]

In this contribution, we describe results on controlling the emission colors of the phosphors ZnS:Mn and SrS:Cu and on the performance characteristics of new red- and green-emitting EL devices. By manipulating the defect chemistry and crystal properties in the stated materials, virtually any color can be specified across the entire portion of the visible spectrum important for display applications. For the first time, true, chromatically red emission is observed from ZnS:Mn with Ga_2S_3 doping, and chromatically green emission is observed in SrS:Cu, M (M=alkali metal) systems.

Color tuning of emission wavelengths for ZnS phosphors has previously been accomplished by altering energy gaps of materials. For example, a progressive increase in the concentration of Cd in the series $Zn_{1-x}Cd_xS$:Ag ($0<x<1$) leads to longer wavelength emission: ZnS:Ag, blue; $Zn_{0.68}Cd_{0.32}S$:Ag, green; and $Zn_{0.13}Cd_{0.87}S$:Ag, red. The emission color is primarily determined by the magnitude of the band gap rather than the intrinsic nature of the dopant atom (Ag,) and the resulting donor-acceptor emission is not EL active. In much the same way,

quantum-size effects have been used in nanocrystalline II-VI materials to adjust energy gaps and affect emission colors.[3-7]

Various electronic and structural features can be considered for inducing a red shift to the luminescence of Mn in crystalline ZnS while retaining potential EL activity. From consideration of the Tanabe-Sugano diagram for the d^5 cation Mn^{2+}, such a shift will be produced on increasing the crystal-field strength. Shrinkage of the lattice and associated interatomic distances should increase the crystal field. Such shrinkage is expected to occur by substitution of smaller or more highly charged cations for Zn^{2+}. The only suitable isovalent cation available for this substitution is Be^{2+}. Because of the hazards in working with Be, we elected to examine substitutions with more highly charged ions. Al^{3+} and Ga^{3+} are suitable for this purpose, and they provide some potential, additional advantages. Substitution of Al^{3+} or Ga^{3+} for Zn^{2+} in ZnS produces cation vacancies. To maintain charge compensation on substitution, Zn defects will be formed according to the representative formula $Zn_{1-3/2x}\square_{x/2}Ga_xS{:}Mn$, thereby lowering the coordination number of some S atoms. Such S atoms will bond more strongly to Mn in comparison to those not associated with a Zn vacancy, producing a stronger crystal field and a red shift in the emission. In addition, greater relaxation is expected for the Mn-Zn vacancy-complex excited state, also leading to a red shift in the emission.

Experimental

For the preparation of $Zn_{1-3/2x}Ga_xS$:Mn, stoichiometric amounts of ZnS (Aldrich, 99.99%), Ga_2S_3, MnS (Cerac, 99.9%), and 5 wt% Li_2CO_3 (Cerac, 99.9%) were mixed and charged in a graphite crucible and heated under Ar/CS_2 at 1123 K for 6 h. Ga_2S_3 was made in-house by dissolving Ga metal (Cerac, 99.999%) in nitric acid, followed by precipitation of $Ga(OH)_3$ by addition of ammonium hydroxide. The hydrated precipitate was heated under Ar bubbled through CS_2 to 973 K for 10 h. Powder X-ray diffraction (XRD) patterns were obtained on a Siemens D-5000 diffractometer equipped with Cu Kα radiation.

SrS:Cu was prepared by grinding stoichiometric amounts of $SrCO_3$, $CuSO_4 \cdot 5H_2O$ and MNO_3 (where M = Na, K), and passing H_2S over the sample at 1323 K for 1 h. Powder XRD patterns were obtained to verify preparation of single-phase material.

Luminescence spectra were recorded with a right-angle spectrometer. The excitation wavelength was selected with a Cary model 15 prism monochromator, and the sample emission was passed through an Oriel 22500 1/8 m monochromator prior to detection with a Hamamatsu R636 photomultiplier tube (PMT.) Current from the PMT was measured with a Keithley 486 picoammeter that was interfaced to a computer.

Luminescence decay curves were measured by using a Nd:YAG laser (pulse width = 10 ns) equipped with a frequency mixing crystal to provide excitation at 355 nm. The emission was passed through a filter to remove the excitation light

and detected with a PMT connected to a Tektronix digital oscilloscope (model TDS 350). Fifty waveforms were averaged for each sample.

Results and Discussion

As shown in Figure 2.1, the emission color of the ZnS:Mn phosphor can be specifically controlled in the system $Zn_{1-3/2x}Ga_xS$:Mn, i.e., a systematic wavelength shift occurs with increasing Ga concentration. For samples prepared at 1123 K, increasing Ga concentrations lead to a decrease in volume of the hexagonal cell of ZnS from 79.5 $Å^3$ at x = 0 to 77.0 $Å^3$ at x = 0.35, the approximate solubility limit. Luminescent decay times and chromaticity values are summarized in Table 1. The decay curves are readily fit by single-exponential functions, and the resulting lifetimes are consistent with direct emission from the Mn center, rather than a donor-acceptor recombination. As seen from the chromaticity values x = 0.64 and y = 0.36 for composition $Zn_{0.55}Ga_{0.3}S$:Mn, a true red phosphor can be produced in this series. A red shift in the luminescence of ZnS:Mn has also been observed by substitution of Zn with Al.

Table 2.1. Luminescent lifetimes and chromaticity values for $Zn_{1-3/2x}Ga_xS$:Mn.

	x	Lifetime (ms)	Chromaticty (x,y)
ZnS	0	0.85	0.54, 0.46
$Zn_{0.85}Ga_{0.2}S$	0.1	0.75	0.58, 0.43
$Zn_{0.7}Ga_{0.2}S$	0.2	0.83	0.62, 0.38
$Zn_{0.56}Ga_{0.3}S$	0.3	0.75	0.64, 0.36

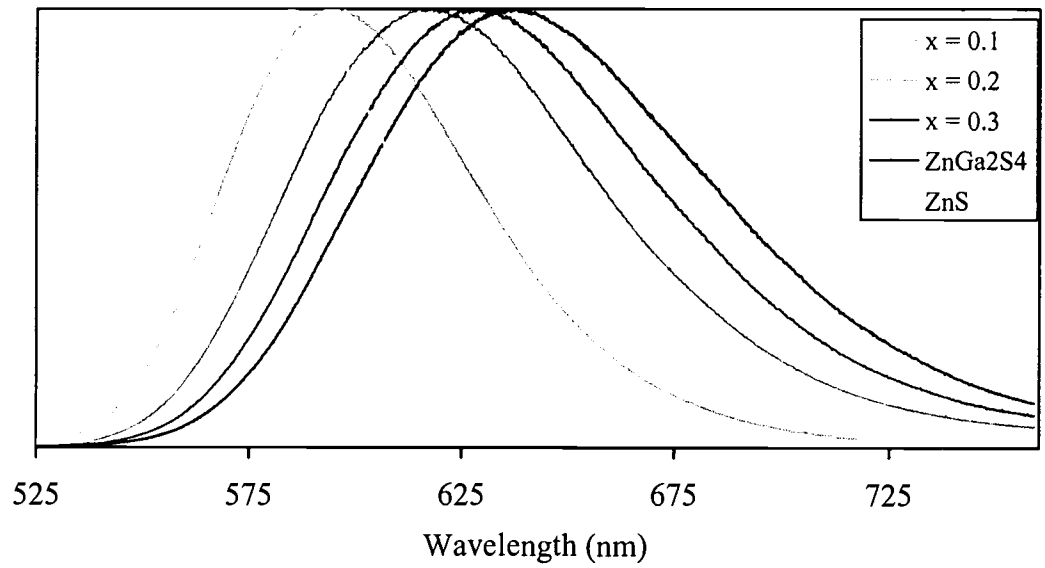

Figure 2.1. Photoemission spectra for the series Zn1-3/2xGaxS:Mn (1 atom %)

Cathodoluminescence in the system SrS:Cu has been described by Lehmann[8] and results of photoluminescence measurements have been detailed by Yamashita and co-workers.[9] In general, either blue or green luminescence has been observed – blue in lightly doped samples and green in heavily doped samples. On the basis of lifetime data, short-wavelength green emission has been associated

with isolated Cu centers, and longer-wavelength green emission with aggregates of Cu centers.[10] The blue emission has been associated with an equilibrium occupation between excited-state levels.[11]

Our conclusions from interpretation of the available SrS:Cu spectra data are different. Because the Cu atoms enter the matrix in the +1 oxidation state, Cu doping results in the formation of S vacancies. Two types of Cu sites can exist, one without an adjacent S vacancy (six-coordinate Cu) and one with an adjacent S vacancy (likely a five-coordinate Cu). If this is the case, we should be able to control their relative concentration, hence, the emission color of the phosphor. This result should be achieved by substitution of the trivalent cation in conjunction with Cu to decrease the concentration of S vacancies, and substitution of a monovalent cation in conjunction with Cu to increase S vacancies.

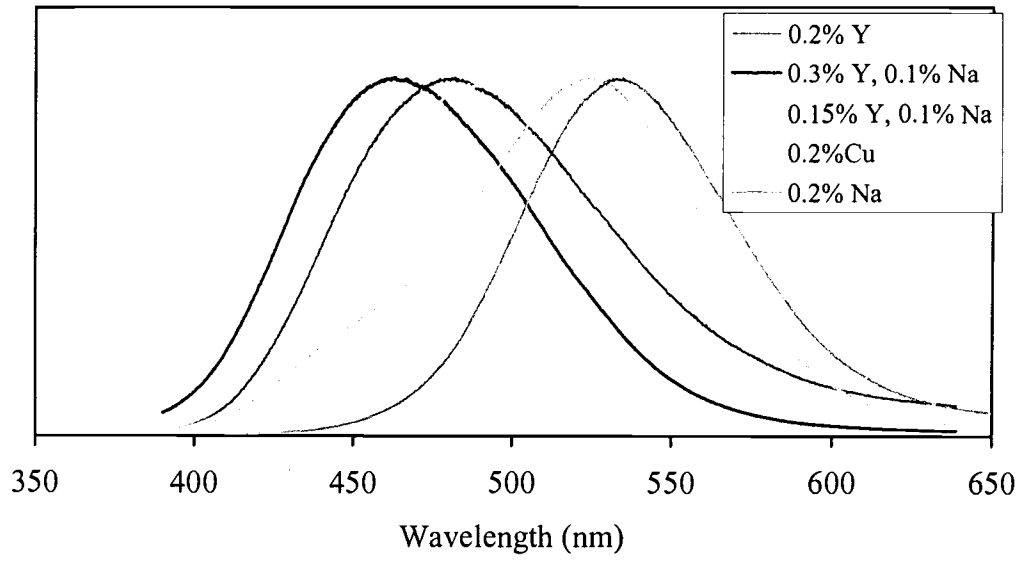

Figure 2.2. Photoemission spectra for SrS codoped with Na, Y, and 0.2 atom % Cu.

In accordance with these ideas, we have prepared SrS:Cu powder phosphors exhibiting controlled emission wavelengths spanning the blue and green regions of the spectrum (Figure 2.2). Importantly, these colors are achieved by fixing the Cu concentration at 0.2 atom % and carefully adjusting the concentrations of the codopants Y^{3+} and Na^{+}; a number of other M^{3+} and M^{+} cations can be used to produce the same results. On the basis of optical studies and solid-state NMR data,[12] we believe the emission color arises from distinct surroundings of the Cu centers, i.e., likely a six-coordinate site for the blue-emitting Cu atoms and a five-coordinate site for the green-emitting Cu atoms. Charge compensation of Cu^{+} with an M^{3+} cation in the NaCl-type host of $Sr^{2+}S^{2-}$ preserves a six-coordinate environment for the Cu^{+} ion, leading to a predominant blue emission. Incorporation of a sufficient quantity of M^{+} cations, i.e., Na^{+} or other alkali-metal

cation, leads to an increased formation of S vacancies. Cu^+ ions distributed through such a matrix occupy sites associated with these vacancies.[13] A reduced coordination number results for the Cu^+ ions, and a green emission can be observed. By varying the relative concentration of the M^{3+} and M^+ codopants, the concentration of the two types of emission centers and the resulting emission color can be controlled. The larger breadth of the emission band peaking near 505 nm (cf., Figure 2) relative to those at shorter and longer wavelengths is likely a reflection of the bimodal distribution of the Cu atoms between the two different types of coordination environments.

The overall effects of manipulating codopant concentrations in the systems (Zn,Ga)S:Mn and (Sr,Y,Na)S:Cu are illustrated by the photoluminescence of samples shown in Figure 3. Yellow to red emission is observed in the ZnS system and blue to green in the SrS system.

A series of luminescent materials has been developed on the basis of the two important EL hosts ZnS and SrS. For the first time, full range emission color control has been achieved in phosphor hosts having demonstrated utility in EL displays. While the optical results presented above were obtained by photoexcitation of powders, we have observed the same emission characteristics in thin-film EL devices that have been fabricated by evaporation, electron-beam, and sputtering methods of deposition. Very thin (~500 nm thick,) deep-red emitting films of (Zn,Ga)S:Mn exhibit thresholds near 47 V with levels of luminance near 1 cd/m^2.[14] For devices containing thin-film SrS codoped with Cu and K, performance

is characterized by a luminance of 53 cd/m^2 and a luminous efficiency of 0.97 lm/W (40 V above threshold and a frequency of 60 Hz.).[15] Color coordinates are x = 0.29 and y = 0.60, indicating the attainment of a saturated green color. Insofar as we know, the efficiency is unsurpassed by any other EL device operating in a saturated green mode under commercially realistic conditions.

Conclusions

By controlling the vacancy concentration in SrS and ZnS, full color PL was achieved. Saturated red emission from ZnS:Mn was achieved by substituting Ga in the matrix. The red shift was observed by changing the crystal field around the Mn ion. Saturated green emission from SrS:Cu, M was explained on the basis of different Cu centers – blue emission arises from fully coordinated Cu while green emission arises from Cu ions associated with a S vacancy. EL devices for both systems have been manufactured, resulting in emission that correlates well with the PL reported.

Acknowledgments

This work was supported by the National Science Foundation under grants DMR-9617031 and DMR-9710207 and by the Defense Advanced Research Projects Agency through the Phosphor Technology Center of Excellence, Grant MDA-972-92-1-0030.

References

1. Sun, S-S.; Dickey, E.; Kane, J.; Yocom, P.N. *Proc. 17th Int. Display Research Conf.;* Morreale, J., Ed.; Society for Information Display: Santa Ana, CA, 1997. p 301.

2. Sun, S.-S. *Extended Abstracts, 4th Int. Conference on Science and Technology of Display Phosphors.* Bend, OR. Society for Information Display: Santa Ana, CA, 1998.

3. Colvin, V.L.; Schlamp, M.C.; Alvisatos, A.P. *Nature.* **370**, 354 (1994).

4. Bhargava, B.N.; Gallagher, D.; Hong, X.; Nurmikko, A. *Phys Rev. Lett.* **72**, 416 (1994).

5. Gan, L.M.; Liu, B.; Chew, C.H.; Xu, S.J.; Chua, S.J.; Loy, G.L. *Langmuir.* **13**, 6427 (1997).

6. Xu, S.J.; Chua, S.J.; Liu, B.; Gan, L.M.; Chew, C.H.; Xu, G.Q. *Appl. Phys. Lett.* **4**, 478 (1998).

7. Yu, J.; Liu, H.; Wang, Y.; Jia, W. *J. Lumin.* **79**, 191 (1998).

8. Lehmann, W. *J. Electrochem. Soc.* **117**, 1389 (1970).

9. Yamashita, N. *Jpn. J. Appl. Phys.* **30**, 3355 (1991).

10. Yamashita, N.; Ebisumori, K.; Nakamura, K. *Jpn. J. Appl. Phys.* **32**, 3840 (1993).

11. Li, W.M.; Ritala, M.; Leskela, M.; Niinisto, L.; Soininen, E. Sun, S.S.; Tong, W. Summers, C.J. *J. Appl. Phys.* **86**, 5017 (1999).

12. Janesky, J.; Warren, W.; Li, D.; Keszler, D.A. Unpublished results.

13. Wager, J.F.; Hitt, J.C.; Baukol, B.A.; Bender, J.P.; Keszler, D.A. *Unpublished results.*

14. Dimitrova, V.; Draeseke, A.; Tate, J.; Yokoyama, T.; Clark, B.L.; Li, D.; Keszler, D.A. *Appl. Phys. Lett.* **75**, 2353 (1999).

15. Keir, P.D.; Wager, J.F.; Clark, B.L.; Li, D.; Keszler, D.A. *Appl. Phys. Lett.* **75**, 1398 (1999).

CHAPTER 3

ALKALI METAL COACTIVATORS IN SrS:Cu THIN-FILM ELELCTROLUMINESCENT DEVICES

For publication in Applied Physics Letters

Abstract

A unique approach for obtaining bright and efficient saturated green phosphors for alternating-current thin-film electroluminescent (ACTFEL) device applications is presented. The approach involves color-shifting blue SrS:Cu ACTFEL phosphors into the green region of the spectrum via the incorporation of alkali metal ions into the SrS lattice. Alkali metals are incorporated into the SrS:Cu phosphors by using LiF, NaF, KF, RbF, or CsF coactivators. The best result to date is obtained by using a KF coactivator and results in a saturated green brightness and efficiency of 52.7 cd/m^2 and 0.97 lm/W (at a frequency of 60 Hz and an overvoltage of 40 V.) In addition to providing a color shift, the alkali-metal fluorides improve the overall performance of the ACTFEL device by increasing the magnitude of the electric field and its uniformity across the phosphor through suppression of positive space charge.

Introduction

For several decades, the development of alternating-current thin-film electroluminescent (ACTFEL) devices for full-color flat-panel displays has been hampered by the lack of an efficient blue phosphor.[1] With the recent development and improvement of SrS:Cu as a blue ACTFEL phosphor,[2-5] this situation appears to be changing so that the ultimate performance of first-generation full-color commercial ACTFEL displays may actually be determined by the performance of the green phosphor, not the blue. The purpose of the work described herein is to

report a novel approach for obtaining a bright and efficient green ACTFEL phosphor.

The basic idea is to begin with the efficient blue SrS:Cu phosphor system and to add appropriate coactivators, i.e., alkali metal ions, to color shift from blue to green. The model underlying this color shift and the procedure for selecting appropriate coactivators via monitoring the photoluminescence (PL) of coactivated phosphor powders is described elsewhere.[6,7] Briefly, the green-color shift is ascribed to a self-compensation driven process in which S vacancies are formed when Cu and alkali metal ions are intentionally incorporated into the SrS host. These S vacancies associate with Cu luminescent impurities to form Cu-S vacancy complexes such that the Cu coordination number is reduced. This reduced coordination leads to green emission, whereas normal six-fold coordinated Cu gives blue emission. The primary focus of this letter is to demonstrate that this color-shift approach, which was first applied to shift the PL spectrum of powder phosphors, is equally viable for shifting the electroluminescence (EL) spectrum of thin-film phosphors.

Experimental

The ACTFEL devices employed in this study are fabricated as follows. First, a SrS:Cu thin-film phosphor layer with a typical thickness of 800-1000 nm is deposited onto a glass substrate previously coated with layers of indium tin oxide and aluminum-titanium oxide, which serve as the bottom transparent contact and

the bottom insulator, respectively, of the ACTFEL device. The SrS:Cu deposition is accomplished by electron-beam evaporation of SrS and simultaneous thermal co-evaporation of CuF_2. Next, a thin layer of the appropriate alkali metal fluoride coactivator (i.e., MF, where M = Li, Na, K, Rb, Cs) is deposited by thermal evaporation over one half the sample area. Subsequently, rapid thermal annealing of the sample is performed, typically at 1083 K for 2 min. Finally, a top insulator of silicon oxynitride is deposited by plasma-enhanced chemical vapor deposition, and aluminum dots are thermally evaporated as the top contact.

Since the ACTFEL fabrication sequence involves the deposition of the coactivator over only half of the sample area, a direct comparison of the PL and EL performance of the coactivated and non-coactivated portions of the sample is possible.

Results and Discussion

A comparison of the EL spectra of a coactivated SrS:Cu, Na (subsequently denoted the "green device") and a non-coactivated SrS:Cu ACTFEL device (subsequently denoted the "blue device") which were prepared on the same sample substrate, is given in Figure 3.1. Note the dramatic green shift in the spectrum for the coactivated sample. The CIE color coordinates for the coactivated sample are CIEx = 0.32 and CIEy = 0.59, which are consistent for an ideal green phosphor.[1] In contrast, the non-coactivated EL CIE color coordinates of the SrS:Cu phosphor are CIEx = 0.16 and CIEy = 0.27, which is in the blue region of the spectrum. These

values, however, are not quite those desired for an ideal, fully saturated blue phosphor (CIEx = 0.15 and CIEy = 0.10.)

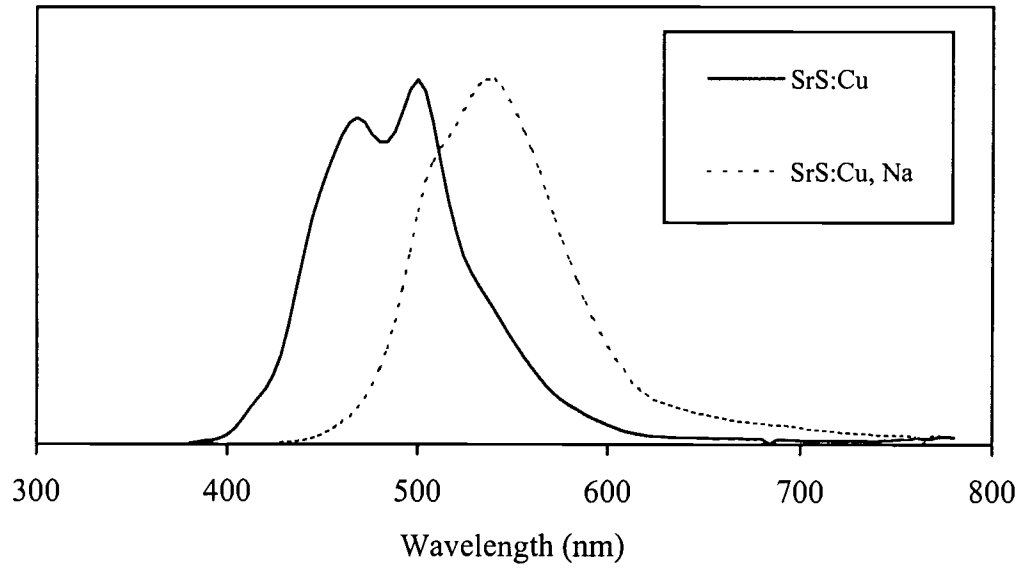

Figure 3.1. Normalized electroluminescent spectra for a coactivated SrS:Cu, Na (green) and a non-coactivated SrS:Cu (blue) ACTFEL device.

Comparisons of the EL luminance-voltage (L-V) and efficiency-voltage (E-V) characteristics for green and blue ACTFEL devices, each prepared on the same sample substrate, are depicted in Figures 3.2 and 3.3. The dramatic increase in brightness and improvement in efficiency from captivation is clearly evident from these figures. All of the L-V and the E-V results reported herein are obtained at 60 Hz by using bipolar trapezoidal voltage pulses with 5 μs rise and fall times and a pulse width of 30 μs.

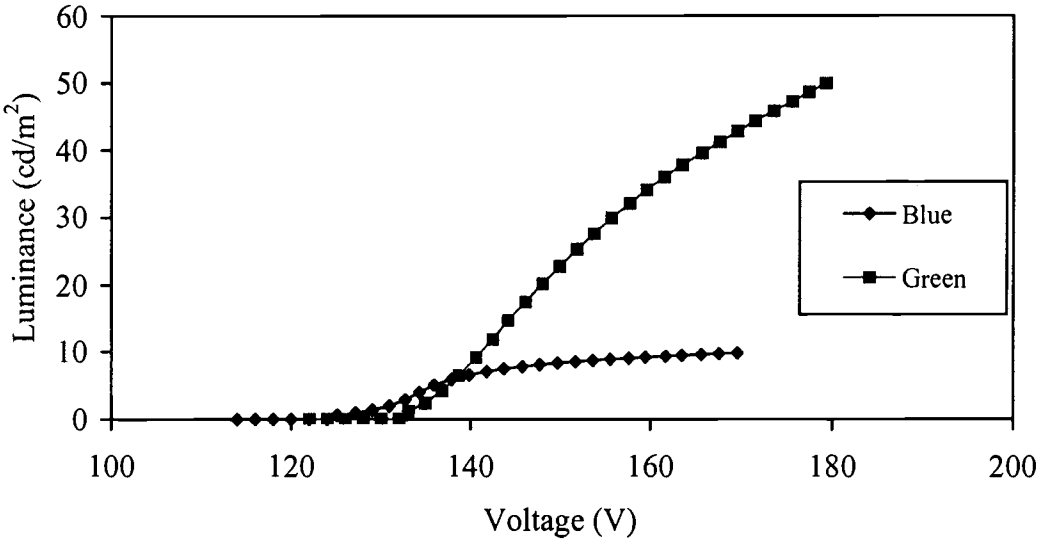

Figure 3.2. Luminance-Voltage (L-V) curves (60 Hz) for a coactivated green and non-coactivated blue ACTFEL device.

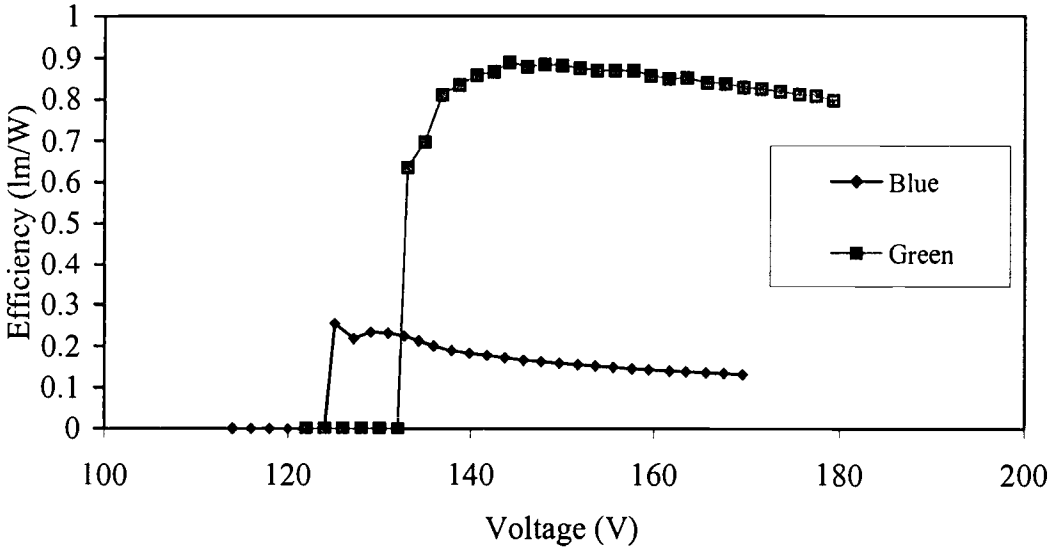

Figure 3.3. Efficiency-Voltage (E-V) curves (60 Hz) for a coactivated green and non-coactivated blue ACTFEL device.

A summary of the improved luminance and efficiency results obtained to date, with corresponding CIE color coordinates, is presented in Table 1 for each of the five green samples codoped with alkali metal coactivator and for the blue SrS:Cu reference. Note that all of the alkali metal atoms employed in this study, except for Li, provided excellent color shifting so that the CIE color coordinates correspond well with those desired for saturated green emission. We believe that the efficiency reported for SrS:Cu,K in Table 1 is equal to the highest ever reported[1] for a saturated green ACTFEL phosphor operating under realistic waveform driving conditions (40 V above threshold at 60 Hz.)

Table 3.1. Performance comparison of blue and green SrS ACTFEL devices.

Phosphor	L40 (cd/m2)	E40 (lm/W)	CIEx, CIEy
SrS:Cu	9.57	0.14	0.16, 0.27
SrS:Cu, Li	4.53	0.05	0.29, 0.56
SrS:Cu, Na	45.8	0.82	0.32, 0.59
SrS:Cu, K	52.7	0.97	0.29, 0.60
SrS:Cu, Rb	30.6	0.19	0.28, 0.58
SrS:Cu, Cs	21.6	0.14	0.29, 0.58

Some of the coactivator-induced L-V and the E-V improvement depicted in Figures 3.2 and 3.3 and in Table 3.1 is a simple consequence of the color shift and of the human eye's greater sensitivity to the green portion of the visible spectrum. There appear to be other factors inherent in the coactivator processing procedure, which also contribute to the improvement in the phosphor performance. There are

two primary observations that point to the coactivator improvement of the phosphor performance.

First, the coactivator treatment leads to an improvement in the phosphor crystallinity and the diffuse reflectance. This may be deduced visually by the rather milky appearance of the coactivated portion of the phosphor. Additionally, the improvement in crystallinity is confirmed by x-ray diffraction. Improved crystallinity leads to more efficient electron transport and radiative recombination in the phosphor. The increase in diffuse reflectance improves the optical outcoupling.

The second beneficial aspect of the coactivator treatment is that there is a noticeable improvement in the electrical characteristics of the coactivated, green ACTFEL device. For example, the internal charge-phosphor field (Q-F_p) characteristics[8] of a blue and a green ACTFEL device prepared on the same substrate are compared in Figure.3.4. There are three important trends that should be noted from Figure 3.4. (i) In comparison to the blue device, less charge is transported across the phosphor of the green device (even though the luminance of this device is greater.) (ii) Less power is dissipated in the green ACTFEL device, as established by the fact that this Q-F_p curve encloses less area.[8] (iii) The steady-state phosphor field of the green device is greater than that of the blue device (~1.7 MV/cm versus ~1.5 MV/cm.) This larger phosphor field leads to a more energetic hot electron distribution, more efficient impact excitation of the Cu luminescent impurities and hence, greater luminance. (iv) More overshoot is present in the Q-F_p

characteristics of the blue device; overshoot is more clearly evident in corresponding capacitance-voltage (C-V) or in the transferred charge capacitance curves (not given.) The presence of overshoot implies the existence of positive space charge within the phosphor layer and a corresponding non-uniform electric field across the phosphor layer. Observations (iii) and (iv) taken together imply that the electric field is larger and more uniform across the phosphor for the green device, which leads to greater luminance. Further details of the electrical characterizations can be found elsewhere.[10]

Conclusions

Note that our original purpose for adding alkali metal ions to the SrS:Cu phosphor was to shift the emission color from blue to green. The fact that the alkali metal fluorides employed lead to additional improvements in the phosphor performance implies that these coactivators behave as "flux" agents. Other researchers have recently used chloride flux agents to improve the performance of ZnS:Mn ACTFEL devices.[9] These flux agents are incorporated into the phosphor layer after deposition of the phosphor in a manner similar to that employed here. Additionally, a reduction of the positive space charge and a concomitant increase in the phosphor field has been proposed to explain the observed flux agent induced performance improvement.

In summary, the incorporation of alkali metal ions into SrS:Cu phosphors is demonstrated as a new methodology for obtaining bright and efficient green

ACTFEL phosphors. In addition to providing a color shift from blue to green, the alkali metal fluorides are found to act as flux agents that improve the ACTFEL device performance by increasing the magnitude and uniformity of the electric filed across the phosphor through suppression of positive space charge in the phosphor.

References

1. Ono, Y.A. Electroluminescent Displays. World Scientific, 1995.
2. Sun, S-S.; Dickey, E.; Kane, J.; Yocum, P.N. *Proceedings of the 17th International Display Research Conference*, p. 301, 1997.
3. Sun, S-S. presented at the *Fourth International Conference on the Science and Technology of Display Phosphors*, Bend, Oregon, September 14-17, 1998.
4. Troppenz, U.; Huttl, B.; Storz, U.; Kratzert, P.; Velthaus, K.O. presented at the *Fourth International Conference on the Science and Technology of Display Phosphors*, Bend, Oregon, September 14-17, 1998.
5. Menkara, H.M.; Park, W.; Chaichimansour, M.; Jones, T.C.; Wagner, B.K.; Summers, C.J.; Sun, S-S. presented at the *Fourth International Conference on the Science and Technology of Display Phosphors*, Bend, Oregon, September 14-17, 1998.
6. Li, D. Ph.D. Thesis, Oregon State University, 1999.
7. Li, D.; Clark, B.L.; Keszler, D.A.; Keir, P.D.; Wager, J.F. *Chem. Mater.* **12**, 268 (2000).
8. Wager, J.F. and Keir, P.D. *Annu. Rev. Mater. Sci.* **27**, 223 (1997).
9. Lewis, J.; Waldrip, K.E.; Davidson, M.R.; Morehead, D.; Holloway, P.H.; Sun, S-S. presented at the *Fourth International Conference on the Science and Technology of Display Phosphors*, Bend, Oregon, September 14-17, 1998.
10. Keir, P.D. *Ph.D. Thesis*, Oregon State University, 2000.

CHAPTER 4

LANTHANIDE DOPING IN ZnS AND SrS THIN-FILM ELECTROLUMINESCENT DEVICES

For publication in *Journal of Applied Physics*

Abstract

The relative high field transport efficiency and short wavelength electroluminescence (EL) potential of the phosphors ZnS and SrS for alternating-current thin-film electroluminescent (ACTFEL) device flat-panel display applications are assessed via a comparison of the EL spectra of ZnS and SrS ACTFEL devices prepared in a very similar manner and doped with the same lanthanide luminescent impurities: Dy, Er, Ho, Tb, and Tm. For all of the lanthanide luminescent impurities studied, it is found that the higher energy EL peaks are much more intense for SrS than for ZnS, even thought the average phosphor field in SrS is smaller than in ZnS. These observations show SrS to be a superior high-field electron transport material compared to ZnS. All of the ZnS EL spectra have a dramatic cut off in their EL intensities at about 440-460nm; this suggests that ZnS is not an appropriate phosphor for blue light emission since its electron distribution does not appear to be adequately heated to efficiently excite blue luminescent impurities.

Introduction

ZnS and SrS are the two most common phosphors employed in alternating-current thin-film electroluminescent (ACTFEL) flat-panel displays.[1] To obtain electroluminescence (EL) from these materials, the phosphor is intentionally doped with transition metal or lanthanide luminescent impurities.

Several studies have reported the EL spectra of lanthanide ZnS[2-4] or SrS[5-7] phosphors for a variety of lanthanide luminescent impurities. These studies reveal that there are often differences in the relative peak intensities in the EL spectra of the same lanthanide luminescent impurity, depending on whether it is present in ZnS or in SrS. This result is somewhat surprising, especially for lanthanides whose spectra arises from 4f-4f transitions which are well shielded from the surrounding lattice so that crystal field effects are not expected to play a major role in determining the luminescent spectra. Okamoto et al. point out that although some of these differences in the EL spectra arise from differences in the branching ratios of the emitting level, which may be attributed to the crystal field effects, there is a distinct tendency for the higher energy lanthanide transitions to be more intense when doped in SrS; they assert that it is unlikely that this trend is due to crystal field effects.[5-7] Rather, Okamoto et al. believe that these high energy trends are more likely due to either the nature of the luminescent impurity excitation mechanism (i.e., impact excitation of impact ionization[8]) or due to more of an energetic hot electron distribution in SrS compared to ZnS.

The present work is a comparative study of the EL spectra of ZnS and SrS ACTFEL devices prepared in a very similar manner and doped with the same lanthanide luminescent impurities, namely Dy, Er, Ho, Tb, and Tm. This direct comparison provides evidence that the electron distribution is significantly hotter is SrS than in ZnS, even though the average phosphor field is smaller in SrS. Moreover, the ZnS ACTFEL devices fabricated for this study exhibit very little, if

any, positive space charge in the phosphor whereas all of the SrS ACTFEL devices possess some space charge. Therefore, it is likely that at least part of the reason that SrS ACTFEL devices exhibit superior high field transport properties is related to the tendency of SrS phosphors to possess more space charge than ZnS phosphors. Finally, the hot electron distribution in ZnS does not appear to be sufficiently energetic to efficiently excite the luminescent impurities appropriate for short wavelength portion of the visible spectrum, as witnessed by the fact that the ZnS EL spectra invariably cuts off at about 480 nm, independent of the luminescent impurity employed.

Experimental

The ACTFEL devices employed in this study are fabricated as follows. First, a SrS:LnF_3 (where LnF_3 = DyF_3, ErF_3, HoF_3, TbF_3, or TmF_3) thin-film phosphor layer, with a typical thickness of 800-1000 nm, is deposited onto a glass substrate coated with layers of indium tin oxide and aluminum-titanium oxide which serve as the bottom transparent contact and the bottom insulator, respectively, of the ACTFEL device. The SrS:LnF_3 deposition is accomplished by electron beam evaporation of SrS and simultaneous thermal coevaporation of the lanthanide fluoride. Next, rapid thermal annealing of the sample is performed, typically at 1083 K for two minutes. Finally, a top insulating layer of silicon oxynitride is deposited by plasma-enhanced chemical vapor deposition and thermally evaporated aluminum dots are used as the top contact.

Electro-optic assessment of ACTFEL devices is accomplished via luminance-voltage (L-V) analysis and by determination of the Commission Internationale de l'Eclairage (CIE) color coordinates with a Photo-Research PR-650 Spectra Calorimeter. Additional electro-optic characterization involves assessment of trailing edge (TE) luminescence which is accomplished via measurement of the transient luminance [L(t)] by using a Hamamatsu Photosensor Module H5783 photomultiplier. Electrical evaluation of ACTFEL devices is accomplished via charge-voltage (Q-V), capacitance-voltage (C-V), internal charge-phosphor field ($Q\text{-}F_p$), maximum transferred charge-maximum applied voltage ($Q_{max}\text{-}V_{max}$), and transferred charge capacitance ($dQ_{max}/dV_{max}\text{-}V_{max}$) analysis.[9]

Results and Discussion

The EL spectra of the ZnS and SrS lanthanide doped ACTFEL devices tested in this study are depicted in Figures 4.1-4.5. A comparison of the normalized EL spectra of ZnS:Tb and SrS:Tb ACTFEL devices is depicted in Figure 4.1. The most important aspect of Figure 4.1 is that the ZnS:Tb EL spectrum exhibits an abrupt cutoff at ~470 nm whereas three higher energy transitions ($^5D_3 \rightarrow {}^7F_6$, $^5D_3 \rightarrow {}^7F_5$, $^5D_3 \rightarrow {}^7F_4$) are clearly evident in the SrS:Tb spectrum. This is evidence that the hot electron distribution is much more heated above ~470 nm (~2.64 eV) in SrS compared to ZnS. Note that the normalized ZnS EL spectra displayed in Figure 4.1 is virtually identical to an EL spectrum obtained

for a sputtered ZnS:Tb ACTFEL device fabricated at Planar Systems; thus, we believe that our EL spectra are representative of the general behavior of ZnS and SrS phosphors and are not peculiar to our method of fabrication.

A comparison of the normalized EL spectra of ZnS:Tm and SrS:Tm ACTFEL devices is depicted in Figure 4.2. Note that the ZnS:Tm device is so dim that is was necessary to employ a frequency of 5000 Hz in order to obtain a measurable EL intensity. The ZnS:Tm EL spectra is dominated by infrared emission, which peaks at about 800 nm. The ZnS:Tm EL spectrum also exhibits a small blue emission feature, but it is much dimmer than that evident in the SrS:Tm spectrum.

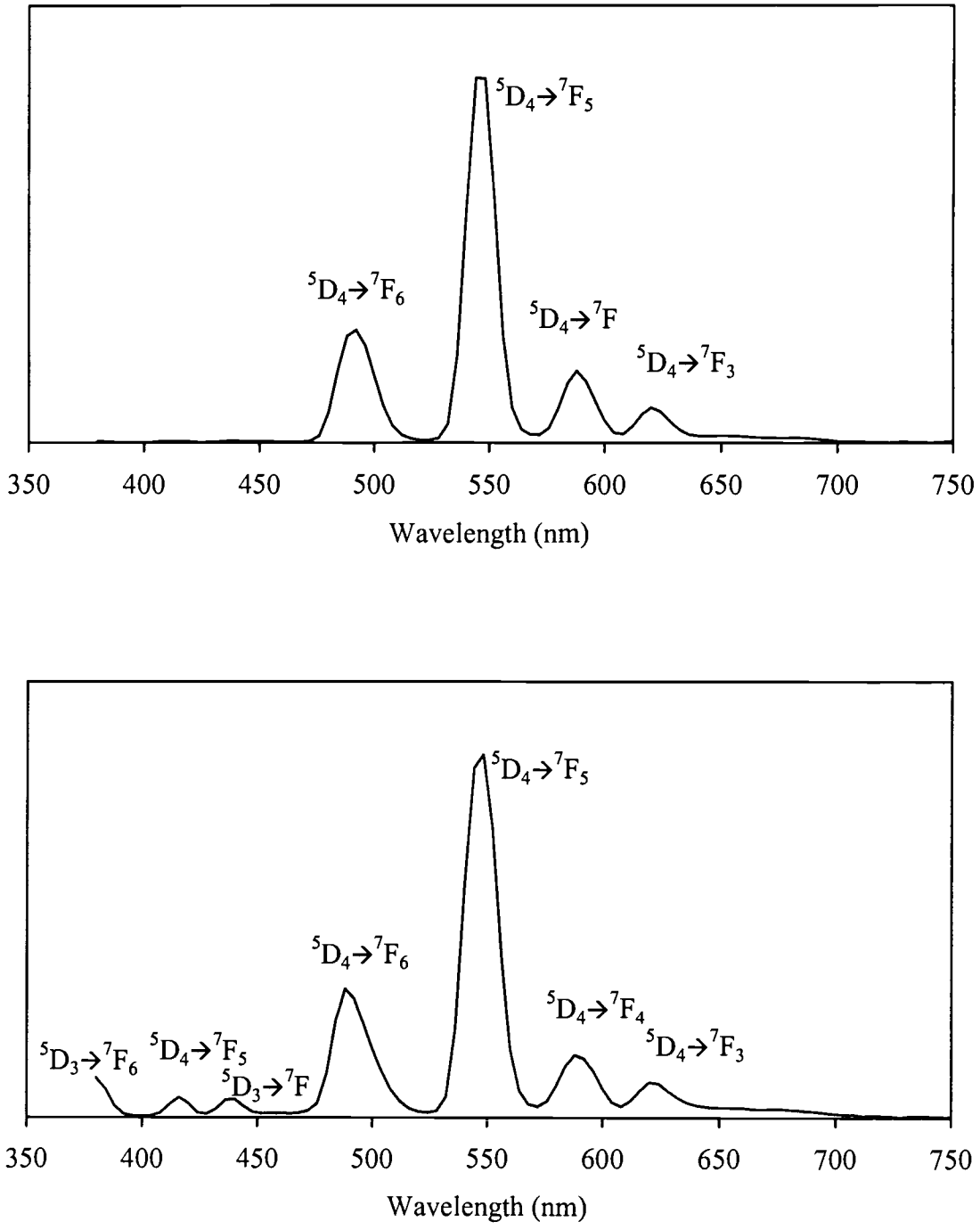

Figure 4.1. EL emission spectra for (top) ZnS and (bottom) SrS:Tb.

Additionally, the ZnS:Tm EL film exhibits a very weak EL signal out to the high energy detection limit of our spectrophotometer, i.e., 380 nm or 3.26 eV, but the signal is about 100 times weaker for ZnS than for SrS. Thus, if this EL intensity difference is ascribed to differences in the hot electron distribution, it appears that the high energy tail of the hot electron distribution in SrS is approximately 100 times larger than for ZnS even though the phosphor field for the SrS device is 1.3 MV/cm for the ZnS device (see Table 4.1).

A comparison of the normalized EL spectra of ZnS:Dy and SrS:Dy ACTFEL devices is given in Figure 4.3. Note that two SrS:Dy EL spectra are included (unaged and aged for 12 h at 40 V above threshold at 1000 Hz) since this device exhibited an unusual color shift with aging. This aging color shift arises from a suppression of part of the high energy EL intensity during aging; the aging mechanism giving rise to this trend is not understood at this time. The primary point to notice from Figure 4.3 is that the intensity of the SrS:Dy ACTFEL spectral features is enhanced for both of the high energy peaks ($^4F_{9/2} \rightarrow {}^6H_{15/2}$ and $^4F_{9/2} \rightarrow {}^6H_{13/2}$) as well as for the lower energy peaks ($^4F_{9/2} \rightarrow {}^6H_{11/2}$ and $^4F_{9/2} \rightarrow {}^6H_{9/2}$). Since all of these peaks have a common $^4F_{9/2}$ excited state, this intensity trend is consistent with SrS having a hotter electron distribution than ZnS. Note, however, that the relative peak heights of the SrS spectra differ appreciably from that observed in ZnS.

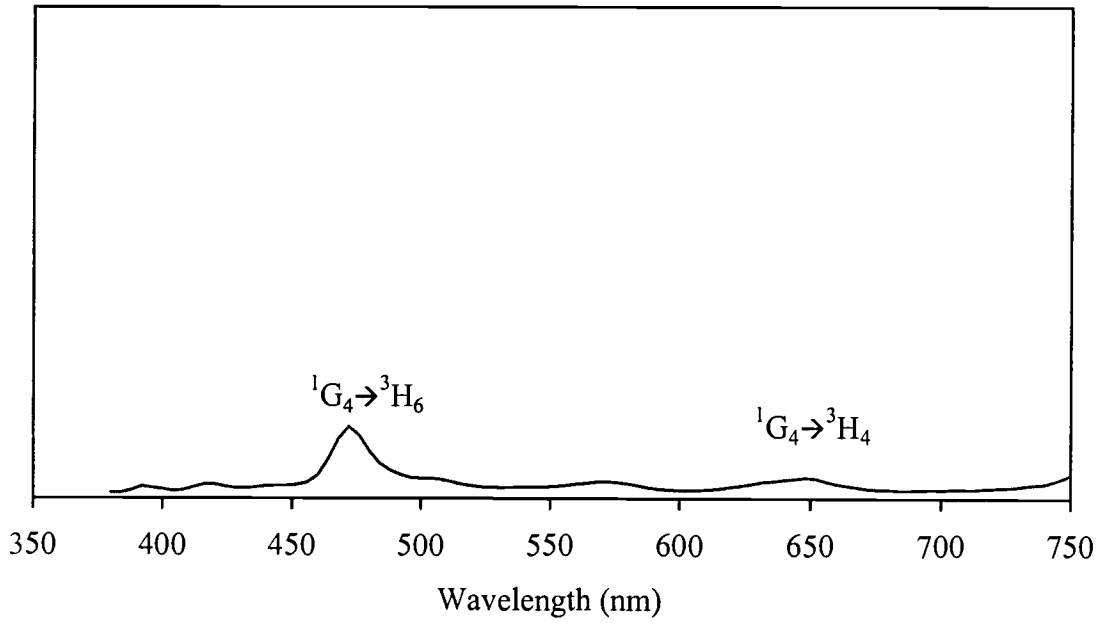

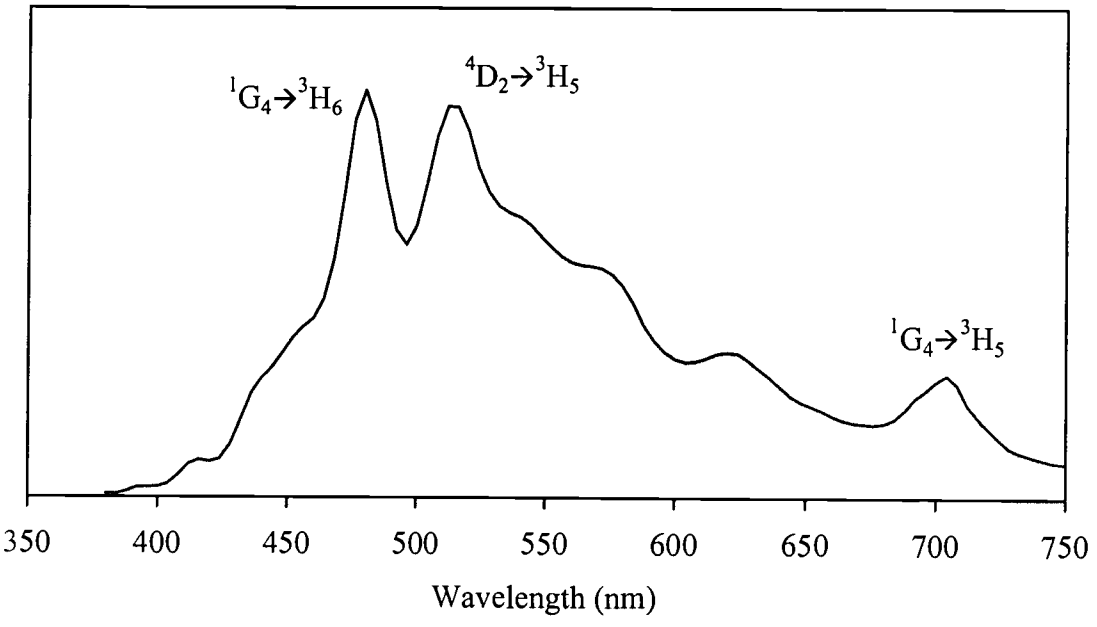

Figure 4.2. EL emission spectra for (top) ZnS and (bottom) SrS:Tm.

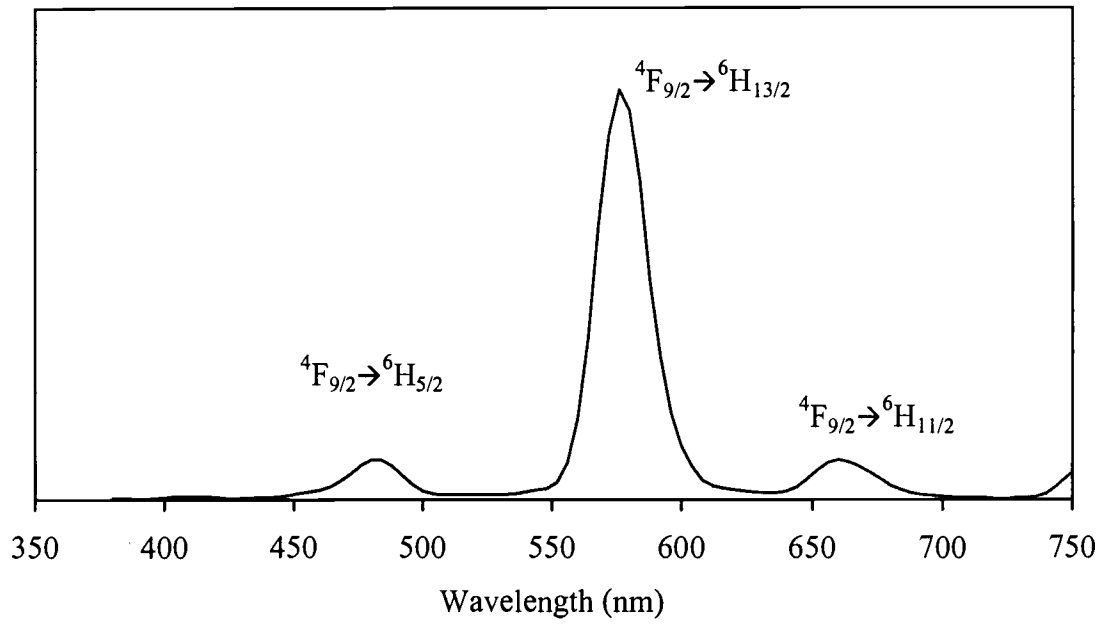

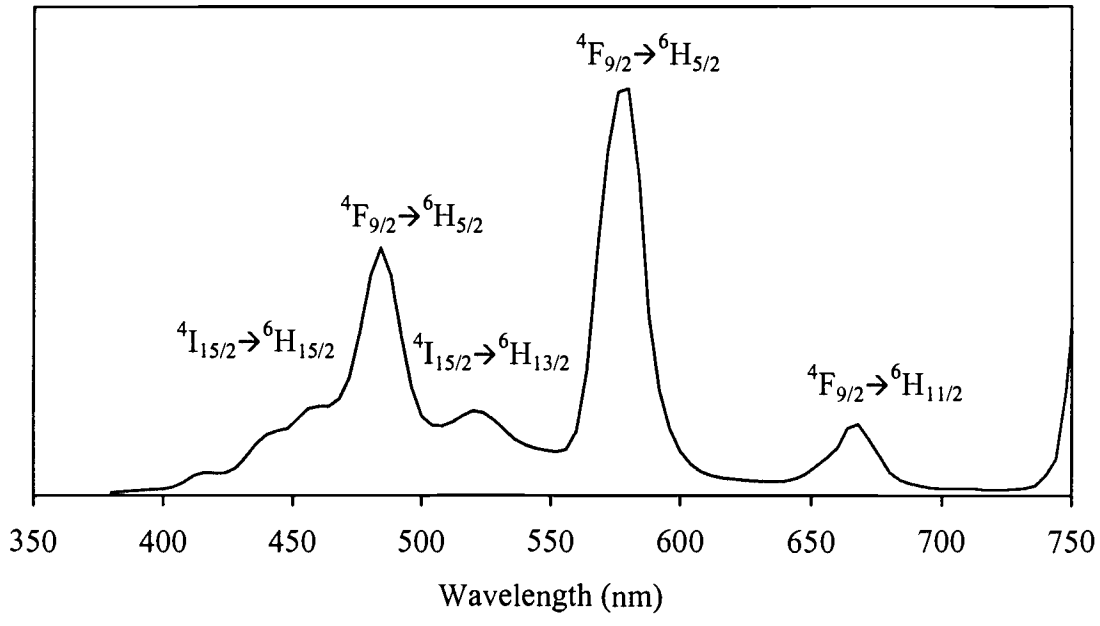

Figure 4.3. EL emission spectra for (top) ZnS and (bottom) SrS:Dy.

A comparison of the normalized EL spectra of ZnS:Ho and SrS:Ho ACTFEL devices is given in Figure 4.4. These two EL spectra are dramatically different. These differences arise primarily from the fact that the electrons in ZnS are not energetic enough to excite the higher energy $^5F_1$, $^5G_5$, and $^5G_4$ excited states. Since the electron distribution in SrS is sufficiently energetic to populate these excited states, four EL emission peaks not seen in ZnS are present in SrS (i.e., $^5G_4 \rightarrow {}^5I_8$, $^5G_5 \rightarrow {}^5I_8$, $^5F_1 \rightarrow {}^5I_8$, $^5G_4 \rightarrow {}^5I_6$). Moreover, the weak $^5F_3 \rightarrow {}^5I_8$ EL peak in ZnS becomes very strong in SrS, presumably because of the much hotter SrS electron distribution.

A comparison of the normalized EL spectra of ZnS:Er and SrS:Er ACTFEL devices is given in Figure 4.5. The most significant aspect of Figure 4.5 is the new EL peaks (i.e., $^4G_{11/2} \rightarrow {}^4I_{15/2}$, $^2H_{9/2} \rightarrow {}^4I_{15/2}$, and some other minor peaks) present in SrS that are not present in ZnS. Of particular significance is the fact that for SrS the most intense peak is the $^4G_{11/2} \rightarrow {}^4I_{15/2}$ UV peak located at about 385 nm (~3.22 eV); this suggests that the SrS electron distribution may actually peak at energies corresponding to the UV portion of the electromagnetic spectrum. If true, it is conceivable that the SrS electron distribution is sometimes too energetic for optimal ACTFEL performance. Whether this is the case cannot be unambiguously determined from the present study. Figure 4.5, however, provides very convincing evidence that the electron distribution in SrS is much hotter than in ZnS, even though the average fields are 1.2 and 1.8 MV/cm, respectively.

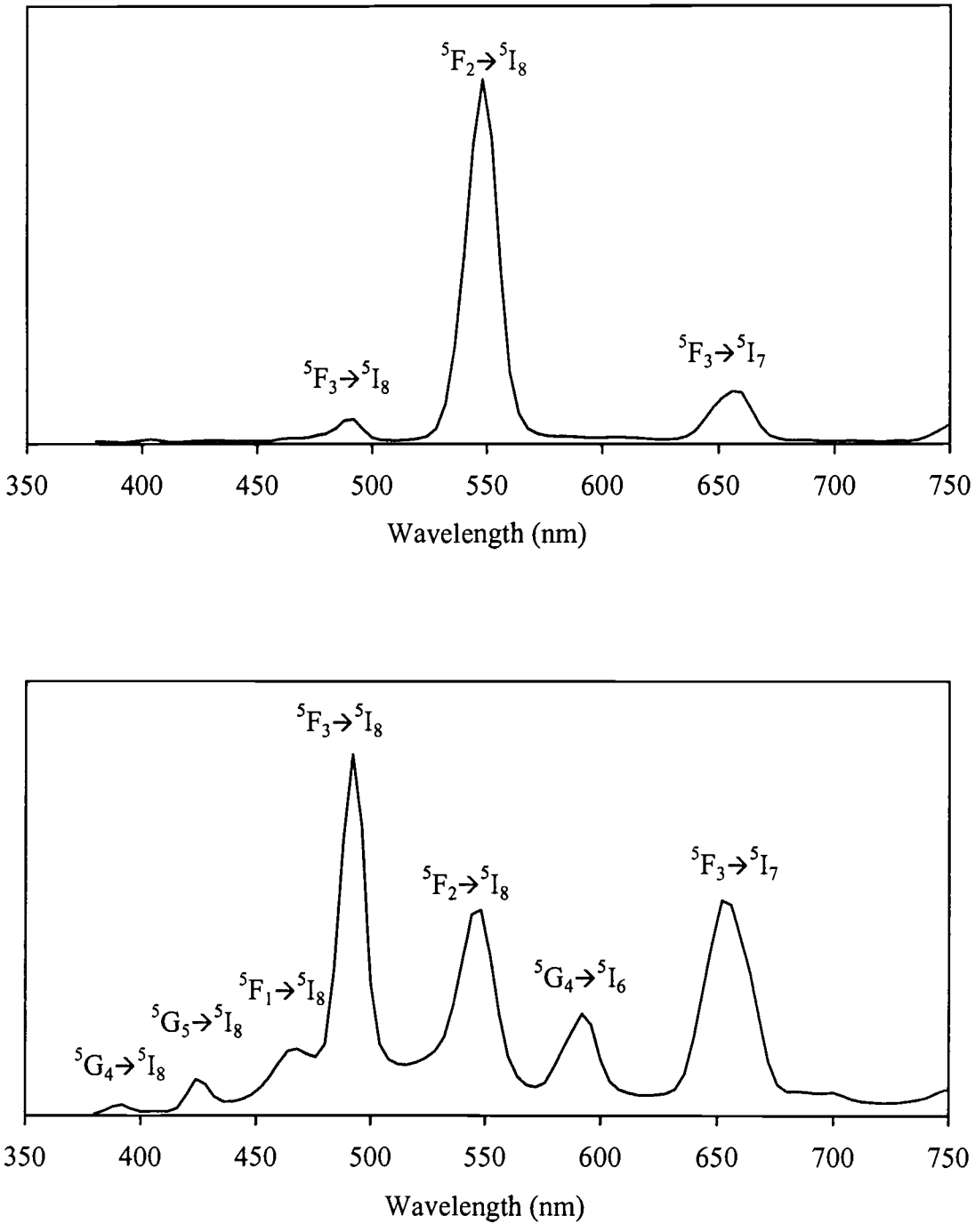

Figure 4.4. EL emission spectra for (top) ZnS and (bottom) SrS:Ho.

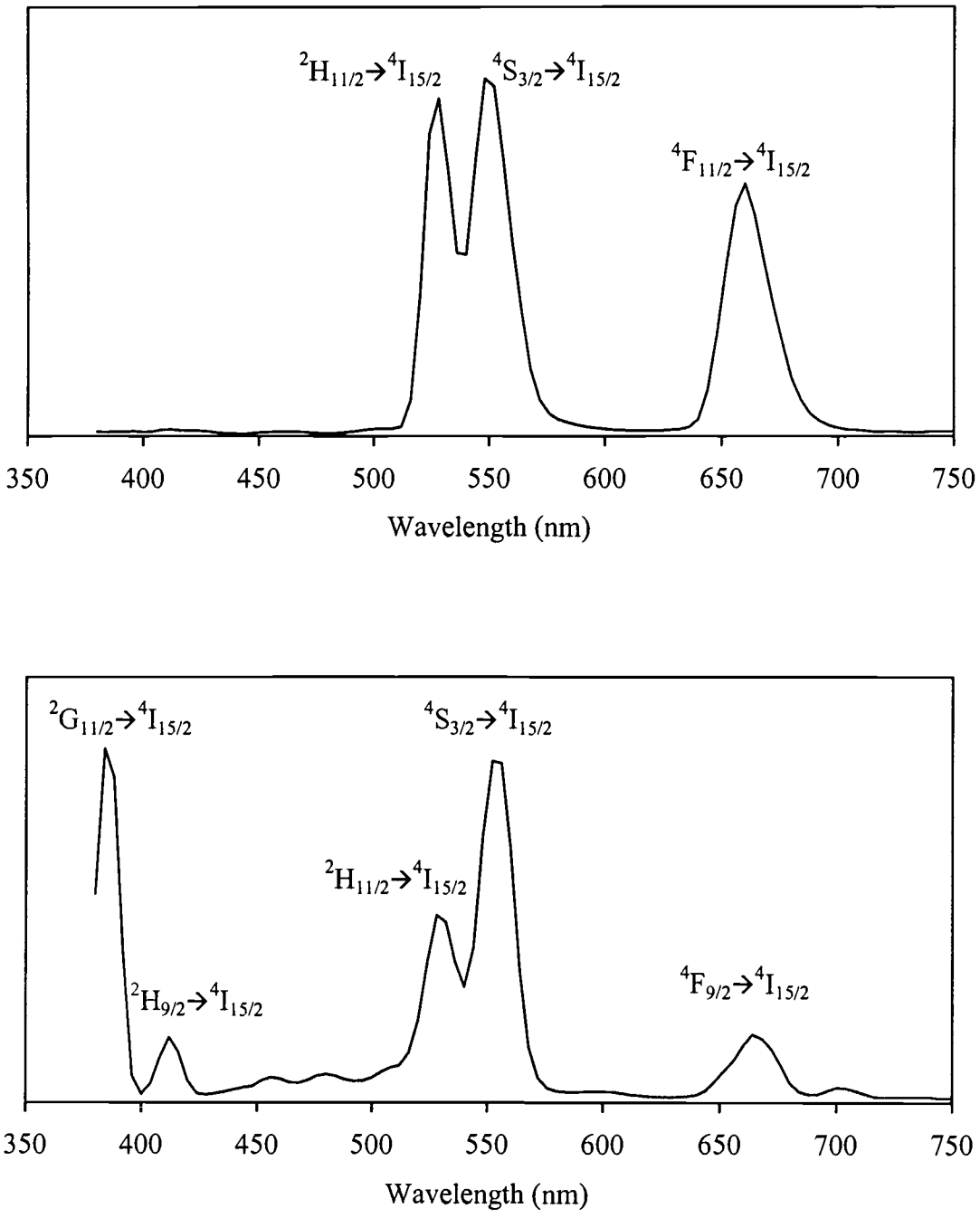

Figure 4.5. EL emission spectra for (top) ZnS and (bottom) SrS:Er.

A summary of selected properties of these devices is given in Table 4.1. The data in the first three columns represent, respectively, an assessment of the relative amount of capacitance-voltage (C-V) overshoot, transferred charge capacitance (dQ_{max}/dV_{max}) overshoot, and trailing edge (TE) luminescence found in each device. These three measurements are useful for estimating the relative amount of positive space charge present in these devices.[9-18] Considerable C-V or dQ_{max}/dV_{max} overshoot or high TE luminescence implies that significant space charge exists in the phosphor, hence, the electric field across the phosphor layer is not uniform. Additionally, the existence of the TE emission is strong evidence that the excitation of luminescent impurities occurs via a luminescent impurity ionization process instead of impact excitation.[10,11,16] The percentages included in the table reflect the peak of the overshoot compared to the insulator capacitance for C-V and dQ_{max}/dV_{max} measurements and the peak intensity of the TE edge luminescence compared to the peak intensity of the leading edge luminescence. The fourth column of Table 4.1 contains the steady-state phosphor field (F_{ss}) as estimated via Q-F_p analysis for an applied voltage of 40 V above threshold. F_{ss} is evaluated as the constant, or nearly constant, vertical part of a Q-F_p curve that occurs during the rising edge portion of the applied voltage wave form above turn-on.[9] It is important to note that F_{ss} is a relatively good estimate of the phosphor field for ACTFEL devices that do not possess space charge; in contrast, for ACTFEL devices with positive space charge, F_{ss} is a measure of the average electric field in the phosphor and the cathode (anode) field is larger (smaller) than

F_{ss}. Finally, the last three columns of Table 4.1 include luminance (L) at 40 V above threshold and 1000 Hz (except ZnS:Tm which is so dim that a frequency of 5000 Hz was used), and the color coordinates (CIEx, CIEy) for ZnS and SrS ACTFEL devices doped with various lanthanide luminescent impurities.

Table 4.1. Summary of data for SrS and ZnS:Ln ACTFEL devices.

Phosphor	C-V Overshoot	dQ_{max}/dV_{max} Overshoot	TE Luminescence	F_{ss} (MV/cm)	L (cd/m^2)	CIE x	CIE y
ZnS:Tb	None	None	None	1.9	23.1	0.31	0.59
SrS:Tb	Small (10%)	Moderate(60%)	Yes (10%)	1.45	17.2	0.32	0.55
ZnS:Tm	None	Small (10%)	None	2.1	0.7	0.27	0.27
SrS:Tm	Large(150%)	Large (100%)	None	1.3	13.5	0.29	0.40
ZnS:Dy	None	None	None	1.95	11.6	0.47	0.47
SrS:Dy	None	None	Yes (15%)	1.45	11.5	0.34	0.38
(aged)	None	None	Yes (1%)	1.4	7.7	0.43	0.44
ZnS:Ho	None	None	None	1.9	4.4	0.31	0.63
SrS:Ho	Small (30%)	Moderate(60%)	None	1.3	22.4	0.31	0.43
ZnS:Er	None	Moderate(40%)	None	1.8	7.5	0.31	0.35
SrS:Er	Small (15%)	Large (100%)	None	1.2	35.0	0.28	0.58

Some interesting trends are observed from analysis of Table 4.1. First, note that differences in the CIE coordinates of the SrS and ZnS are all consistent with SrS ACTFEL devices having a "blue shift" in which the spectra are shifted to higher energies. This is consistent with SrS having a hotter electron distribution. Second, note that all of the ZnS devices have a significantly larger average phosphor field of 1.8 – 2.1 MV/cm compared to the 1.2 – 1.45 MV/cm average phosphor field found for SrS ACTFEL devices. Third, note that the C-V and the

dQ_{max}/dV_{max}-V_{max} overshoot trends and the TE luminescence trends are consistent with ZnS ACTFEL devices having very little, if any, positive space charge, whereas all of the SrS ACTFEL devices tested appear to possess some positive space charge. Thus, these results suggest that the electric field is more uniform in ZnS phosphors that in SrS phosphors, since positive space charge seems to always be present in SrS phosphors. The presence of positive space charge means that the cathode (anode) field is significantly larger (smaller) than the average fields reported in Table 4.1. Undoubtedly, part of the improved high energy performance of SrS compared to ZnS ACTFEL devices is associated with the presence of this space charge. However the very large differences seen in Table 4.1 between the average phosphor fields of SrS and ZnS ACTFEL devices lead us to suspect that in addition to its tendency to form more positive space charge, the high field transport properties of SrS are superior to those of ZnS. Fourth, note that very little, if any, TE luminescence is detected in the ACTFEL devices tested. This implies that the luminescent impurity excitation mechanism for these devices is primarily impact excitation, not impact ionization and that differences in the high energy performance of SrS an ZnS TFEL devices cannot be attributed to differences in the luminescent impurity excitation mechanism.[5-7] Thus, we conclude, in basic agreement with Okamoto et al.,[5-7] that the superior high energy performance of SrS compared to ZnS is due to a more energetic hot electron distribution in SrS compared to ZnS. Moreover, we show that at least a portion of the superior high

energy performance of SrS arises form its tendency to more readily form positive space charge than ZnS.

Further evidence that the EL trends are a consequence of SrS having a hotter electron distribution than ZnS is provided by the temperature dependence of the EL spectra. The EL spectra for ZnS:Dy and SrS:Dy ACTFEL devices at 30, 150, 300, and 360 K is given in Figure 4.6. Note in Figure 4.6(a) that the intensity of all peaks in the ZnS:Dy ACTFEL device increase as the temperature is reduced. Presumably this temperature-dependent trend is primarily due to having a hotter electron distribution at a lower temperature (due to reduced phonon scattering), although this trend is also consistent with a decrease in the rate of nonradiative recombination at lower temperature.

Moreover, note in Figure 4.6(a) that when the high energy portion of the EL spectra is magnified for the ZnS:Dy ACTFEL device, a high energy transition [likely $^4M_{21/2} \rightarrow {}^6H_{15/2}$ but may also contain $(^4I_{13/2}, {}^4K_{17/2}) \rightarrow {}^6H_{15/2}$] at about 405 nm (~3.06 eV) becomes evident and its intensity also increases with decreasing temperature. This observation shows that a very small number of hot electrons are present in ZnS up to an energy of ~3.06 eV, but that the electron distribution in ZnS is cooler than in SrS, as evident from Figure 4.6(b) which depicts the temperature dependence of the EL spectra for a SrS:Dy ACTFEL device. It is interesting that not all of the peaks displayed in Figure 4.6(b) increase monotonically with decreasing temperature; subtle aspects of these temperature-dependent EL spectra is the subject of ongoing research.

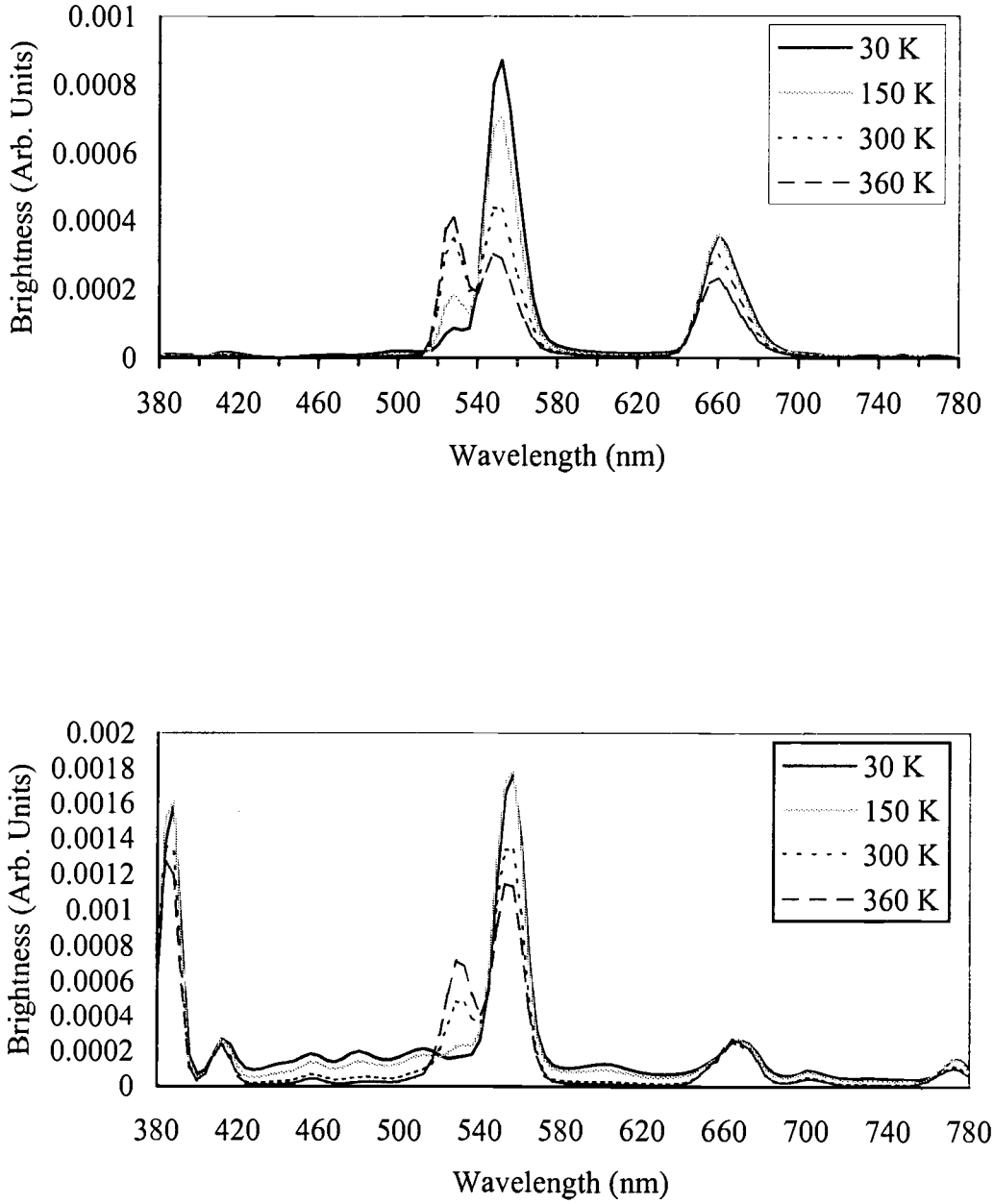

Figure 4.6. EL emission spectra for (top) ZnS:Dy and (bottom) SrS:Dy at temperatures of 30, 150, 300, and 360 K.

The main point to recognize from a comparison of Figure 4.6 is that it is further evidence that the electron distribution is significantly hotter in SrS than in ZnS.

A very important conclusion of this study is that ZnS is not an appropriate phosphor for blue ACTFEL applications since its hot electron spectrum is inadequately heated to efficiently excite short wavelength luminescent impurities. Figures 4.1-4.5 indicate that the ZnS hot electron distribution cuts off at approximately 440 – 470 nm (~2.64 – 2.82 eV), and that the intensity of the high energy tail decreases rapidly at energies nearing this cutoff. This cutoff agrees quite well with high-field transport Monte Carlo simulations reported by Dur et al., which show that the main peak of the hot electron distribution cuts off at about 2.5 eV at a phosphor field of 2.0 MV/cm.[19] In contrast to ZnS, from Figures 4.1-4.5 there is no evidence for a cutoff in the SrS hot electron distribution out to the range of our detector (380 nm or 3.26 eV). Moreover, Figure 4.1(b) and particularly Figure 4.5(b) suggest that the SrS hot electron distribution is well populated even out to ~3.26 eV.

As a final comment, note that the luminances given in Table 4.1 for our devices are very low compared to state-of-the-art, optimized ACTFEL devices. For example, the luminance of true blue (CIEx = 0.17, CIEy = 0.13) SrS:Cu, Ag ACTFEL devices has been reported[20] to be 20 cd/m^2 at 40 V above threshold and of greenish-blue (CIEx = 0.26, CIEy = 0.47) SrS:Ce, Cl ACTFEL devices has been reported to be 142 cd/m^2 at 50 V above threshold.[21] These luminances are higher than most of the luminances given in Table 4.1, even though they are obtained at 60

Hz and those given in Table 4.1 are obtained at 1 kHz. However, the primary point of performing a lanthanide doping study is not to obtain high brightness and efficiency, but rather to assess the high field transport potential of a given phosphor. Monte Carlo simulation studies of high-field transport in ACTFEL devices indicate that the hot electron distribution is primarily determined by the basic band structure and electron-phonon properties of the bulk phosphor.[19,22,23] These studies also show that the hot electron distribution does not depend critically on the type or concentration of defects present in the phosphor since defects give rise to ionized or neutral impurity scattering, which is of negligible importance in determining the hot electron distribution. In contrast, the defect properties appear to be of fundamental importance in establishing the ACTFEL device luminance and efficiency. Therefore, performing a lanthanide doping study is a viable way to assess the high-field transport potential of a phosphor, even when the phosphor luminance and efficiency are poor.

Conclusions

A comparative study of the ZnS and SrS ACTFEL device doped with the same lanthanide impurities demonstrates SrS to be superior high-field electron transport material compared to ZnS. At least a portion of this superior electron transport performance is a consequence of the tendency of SrS to more readily form positive space charge. However, the fact that the average phosphor field in SrS is noticeably less than that of ZnS and the significantly better high energy

performance of all of the SrS devices tested suggests that the electron high-field transport properties of SrS are superior to ZnS. ZnS does not appear to be a viable ACTFEL phosphor for blue color applications since its hot electron distribution appears to be inadequately heated to efficiently excite short wavelength luminescent impurities. Finally, lanthanide doping studies, such as reported here, appear to offer a viable way to assess the high-field transport potential of a new ACTFEL phosphor, even when the phosphor luminance and efficiency are poor.

Acknowledgments

This work was supported by the National Science Foundation under Contract N. DMR 9710207 and by Defense Advanced Research Projects Agency under the Phosphor Technology Center of Excellence, Grant No. MDA 972-93-1-0030. We wish to thank Sey-Shing Sun of Planar Systems for providing substrates and for useful suggestions.

References

1. Ono, Y.A. *Electroluminescent Displays*. World Scientific (1995).
2. Chase, E.W; Hepplewhite, R.T.; Krupka, D.C.; Kahng, D. *J Appl Phys.* **40**, 2512 (1969).
3. Kobayashi, H.; Tanaka, S.; Shanger, V.; Shiiki, M.; Kunou, T.; Mita, J.; Sasakura, H. *Phys. Status Solidi A.* **88**, 713 (1985).
4. Jayaraj, M.K.; Vallabhan, C.P.G. *J Electrochem. Soc.* **138**, 1512 (1991).
5. Okamoto, S; Nakazawa, E. *Jpn. J. Appl. Phys., Part 1.* **34**, 521 (1995).

6. Okamoto, S.; Nakazawa, E.; Tsuchiya, Y. *Jpn. J. Appl. Phys., Part 1.* **28**, 406 (1989).

7. Okamoto, S; Nakazawa, E. *Jpn. J. Appl. Phys., Part 1.* **28**, 521 (1995).

8. Golewski, M.; Leskela, M. *CRC Crit. Rev. Solid State Mater. Sci.* **19**, 199 (1994).

9. Wager, J.F.; Keir, P.D. *Annu Rev. Mater. Sci.* **27**, 223 (1997).

10. Tanaka, S.; Yoshiyama, H.; Mikami, Y.; Nishiura, J.; Ohshio, S.; Kobayashi, H. *Proc. Soc. Inf. Disp.* **29**, 77 (1988).

11. Singh, V.P.; Morton, D.C. *IEEE Trans. Electron Devices.* **36**, 54 (1989).

12. Neyts, K.A.; Corlatan, D.; De Visschere, P.; Van den Bossche, J. *J. Appl. Phys.* **75**, 5339 (1994).

13. Ohmi, K.; Inoue, S.; Tanaka, S.; Kobayashi, H. *Appl. Phys. Lett.* **64**, 3464 (1994).

14. Corlatan, D.; Neyts, K.A.; De Visschere, P. *J. Appl. Phys.* **78**, 7259 (1995).

15. Ohmi, K.; Ishitani, K.; Tanaka, S.; Kobayashi, H. *Appl. Phys. Lett.* **67**, 944 (1995).

16. Neyts, K.; Soininen, E. *IEEE Trans. Electron Devices.* **42**, 1086 (1995).

17. Meyers, R.; Wager, J.F. *J. Appl. Phys.* **81**, 506 (1997).

18. Hitt, J.C.; Keir, P.D.; Wager, J.F. *J. Appl. Phys.* **83**, 1141 (1998).

19. Dur, M.; Saraniti, M.; Goodnick, S.M.; Redmer, R.; Reigrotzki, M.; Fitzer, N.; Stadele, M.; Vogl, P. Presented at the *9th International Workshop on Inorganic and Organic Electroluminescence and the Fourth International Conference on the Science and Technology of Display Phosphors*, Bend, Oregon, September 14-17, 1998.

20. Sun, S.S. Presented at the *9th International Workshop on Inorganic and Organic Electroluminescence and the Fourth International Conference on the Science and Technology of Display Phosphors*, Bend, Oregon, September 14-17, 1998.

21. Velthaus, K.O.; Huttl, B.; Troppenz, U.; Herrman, R.; Mauch, R.H. *SID 97 Digest*, 4 (1997).

22. Bhattachayyra, K.; Goodnick, S.M.; Wager, J.F. *J. Appl. Phys.* **73**, 3390 (1993).

23. Dur, M.; Goodnick, S.M.; Shankar, S.; Wager, J.F.; Reigrotzki, M.; Redmer, R. *J. Appl. Phys.* **83**, 3176 (1998).

CHAPTER 5

LUMINESCENCE OF Cu DOPED CaS, SrS, AND BaS

For Publication in *Journal of Luminescence*

Abstract

The blue-emitting phosphor SrS:Cu has recently been developed for applications in thin-film electroluminescent (EL) displays. We have demonstrated that the same phosphor system can be used to generate the most efficient saturated green EL devices reported to date. While this phosphor system has been studied for more than 40 years, there remains considerable uncertainty concerning the origins of blue vs. green emission. A new model emphasizing the structural environment of the Cu atom in its ground state is used to account for new and previously reported data on the SrS:Cu system. The model will be described, extended to emission colors in other Cu-doped alkaline-earth sulfides, and used to account for the performance characteristics of EL devices.

Introduction

Alkaline-earth sulfide phosphors have been known and studied for decades.[1] Among these materials, the host SrS doped with Cu has been developed as a useful phosphor. From early work, it came to be generally regarded as an efficient green-emitting material.[2] Later, more detailed experiments revealed that Cu could be induced to emit either blue or green light.[3] Interest in the compound heightened following a report on its use as a bright and stable blue-emitting phosphor in alternating current thin-film electroluminescent (ACTFEL) devices.[4] Later, efficient green-emitting devices were produced by including an alkali-metal codopant into the phosphor layer.[5] Despite the long history and numerous studies

on the properties of the SrS:Cu system, considerable uncertainties remain concerning the nature of the Cu centers that give rise to variable color luminescence.[6] In this contribution, we will attempt to clarify the nature of these centers and suggest additional efforts that might provide further insight into this problem.

Experimental

For all samples, unless otherwise noted, the concentrations of Cu^{+}, Y^{3+}, and Na^{+} were 0.2, 1.0 and 1.0 atom %, respectively.

Preparation of CaS

Stoichiometric amounts of $CaCO_3$ (Cerac, 99.95%), $CuSO_4 \cdot 5H_2O$ (Alfa Aesar, 99.995%), and $Y(NO_3)_3 \cdot 6H_2O$ (Cerac, 99.99%) were ground and heated under a flowing stream of H_2S (g) (Matheson, 99.5%) for 1 h at 1473 K. The sample was reground and the heating process was repeated. To confirm the purity of CaS, powder X-ray diffraction (XRD) patterns were obtained by using a Siemens D5000 diffractometer equipped with Cu Kα radiation.

Preparation of $Sr_{1-x}Ba_xS$

Stoichiometric amounts of $SrCO_3$ (Alfa Aesar, 99.995%), $BaCO_3$ (Cerac, 99.9%), $CuSO_4 \cdot 5H_2O$ (Alfa Aesar, 99.995%), $Y(NO_3)_3 \cdot 6H_2O$ (Cerac, 99.99%), and $NaNO_3$ (Alfa Aesar, 99.9%) were ground and heated under a flowing stream of

$H_2S(g)$ (Matheson, 99.5%) for 1 h at 1323 K. The samples were reground and reheated under the same conditions. Powder XRD patterns were obtained, cell parameters were refined with the computer program Cellref.

A concentration quenching curve was obtained for $SrS:Cu^+,Na^+$ by holding the concentration of Na^+ constant at 2%, varying the Cu concentration from 0.005% to 0.75%, and measuring the relative intensity of each sample.

Room-temperature emission and excitation spectra were obtained by using procedures described elsewhere.[7] Low-temperature spectra and thermal-quenching curves were obtained by using a liquid nitrogen cooled cryostat Conductus LTC-10 temperature controller.

Emission lifetimes were collected at room temperature and 77 K by using a 10-ns laser pulse at 266 nm that was produced by frequency quadrupling the 1064 nm laser emission of Nd:YAG. The data were collected and the lifetimes determined by using a method described elsewhere.[8]

Results and Discussion

Cu atoms enter substitutional sites in the rock-salt structure of the alkaline-earth sulfides as formally Cu^{1+} ions. As such, the lowest-energy absorption and emission processes are associated with transitions between the ground state $3d^{10}4s^0$ and excited state $3d^94s^1$ electron configurations. If the Cu atoms simply substitute onto a cation site having O_h symmetry, the free-ion terms will split according to the energy-level diagram depicted in Figure 5.1. The primary emission will then result

from a transition between the lowest excited state ^3E_g and the ground state $^1A_{1g}$. From symmetry considerations, this relaxation is allowed through vibronic coupling, so the transition is temperature sensitive, and the resulting emission band is broad.

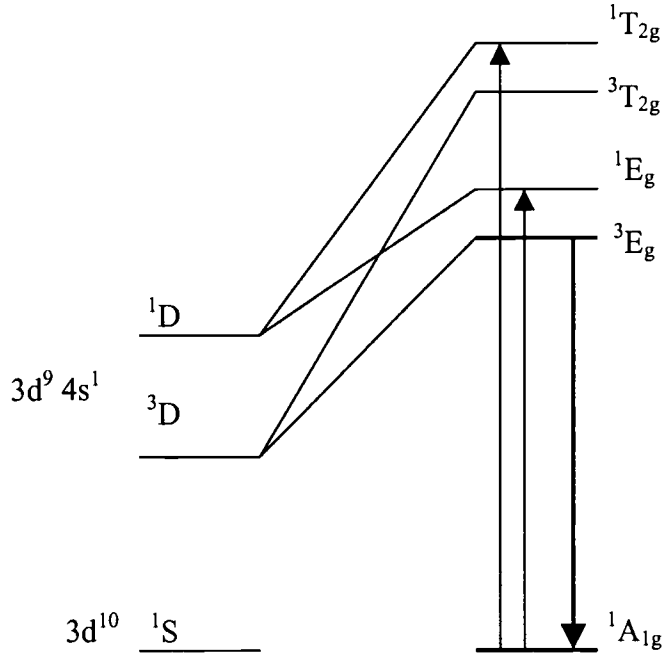

Figure 5.1. Cu^+ energy level diagram as free ion and in octahedral crystal field.

Two important considerations, however, complicate this simple picture. Since the Cu atoms enter the SrS matrix as +1 cations, some type of charge compensation must be present. In addition, motional behavior of Cu^+ in rock-salt structures, notably the halides, has been examined in considerable detail.[9] When substituted onto a large site, the Cu^+ ion can move out of the center of the site, creating an off-center potential. For Cu^+ substituted in SrS, the relevant radii are

$r(Cu^{+})$ = 0.096 nm and $r(Sr^{2+})$ = 0.112 nm. As the Cu^{+} cation is considerably smaller than the Sr^{2+} cation, an off-center displacement might be expected to occur. Other than our own recent contributions, the effects of charge compensation have not previously been considered in the context of Cu emission in this system; likewise, the effects of an off-center displacement on the emission properties of Cu have not been examined.

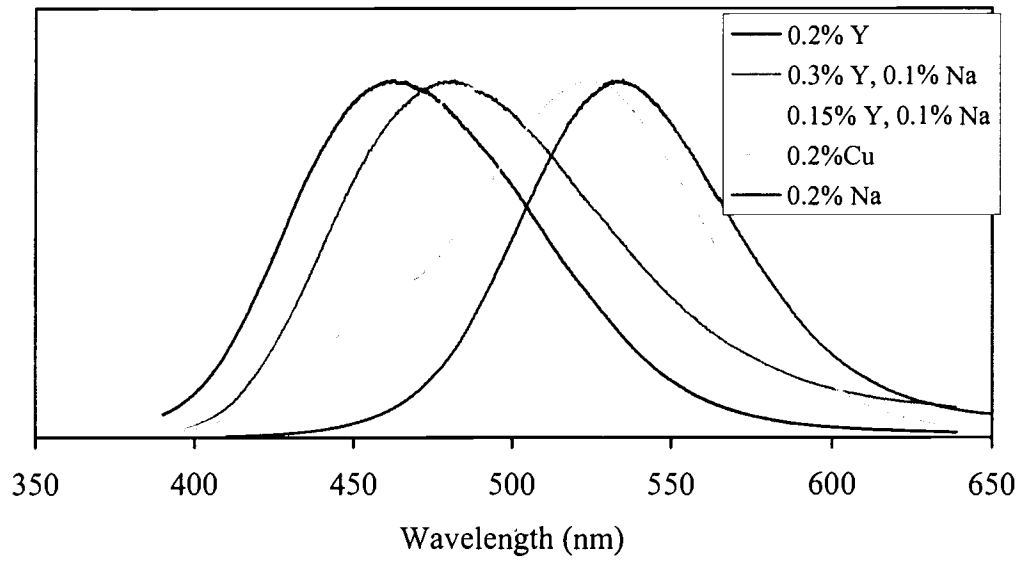

Figure 5.2. Emission spectrum for SrS codoped with Na, Y, and 0.2% Cu.

The compositions of the phosphor samples in this work have been prepared in such a way as to provide control over the emission color; examples are given in Figure 5.2. In controlling the emission color, we hope to be able to better understand the nature of the emission centers. By providing charge compensation through incorporation of a +3 codopant, e.g., Y^{3+} or La^{3+}, or a –1 anion, e.g., Cl^{-}, a predominantly blue emission is observed (*cf.* Figure 5.2.) By incorporating +1

alkali cations, e.g., Na^+ or K^+, the material can be dressed with S vacancies, and the resulting material exhibits a saturated green emission (*cf.* Figure 5.2.) It is important to realize that these emission colors are largely independent of Cu^+ dopant concentrations. For example, SrS doped with concentrations of Cu^+ and La^{3+} as high as 1 at% exhibit an emission band nearly indistinguishable from the blue-emission spectrum (0.2% Y^{3+}) of Figure 5.2. This result contrasts to previous findings on uncompensated samples wherein green emission is observed for Cu^+ concentrations approximately an order of magnitude lower, i.e., 0.1 at%.[10] We also note that the emission band of the Na^+- and K^+-doped samples is also largely independent of the Cu^+ concentration.

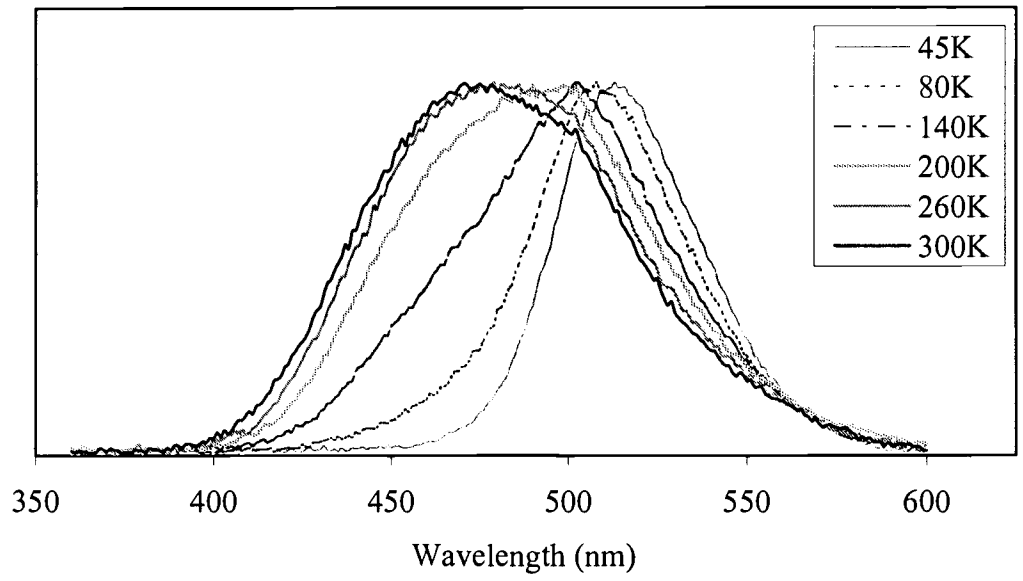

Figure 5.3. Emission of charge compensated SrS:Cu at various temperatures.

On cooling the blue-emitting materials, the peak of the emission band is observed to shift from the blue to the green portion of the spectrum (Figure 5.3.) The ratio of the green to blue bands is plotted as a function of temperature in Figure 5.4. Similar findings have been reported for uncompensated powders[8] and films.[6] On cooling the green-emitting Na^{+-} and K^{+}-doped samples, essentially no change in the emission spectrum is observed and only limited thermal quenching is evident. From these results, it would appear that predominantly three different types of Cu luminescent centers are responsible for the observed luminescence: an on-center position, a shallow off-center position, and a deep off-center position.

On the basis of lifetime data and the relative strength of the excitation transition $^1A_g \rightarrow {}^1E_g$, it is generally agreed that the green emission band resulting from cooling the room-temperature blue-emitting samples is associated with an off-center position of the Cu^+ ion.[6,8] Our results on the charge-compensated samples are similar to those reported previously. We observe a more significant $^1A_g \rightarrow {}^1E_g$ excitation signal on cooling and a single-exponential lifetime of 77 μs at 80 K. Each of these results is consistent with an off-center positioning of the Cu^+ ion and the results of previous reports.

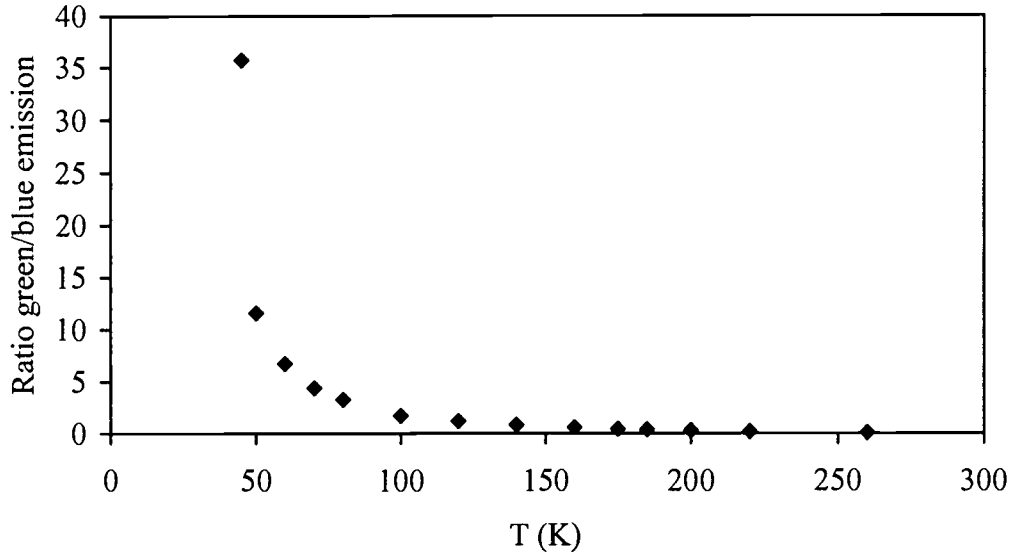

Figure 5.4. Contribution of green/blue emission centers at various temperatures.

The nature of the high-energy blue-emitting species, however, has not clearly been delineated. Some consideration has been given to its assignment as the on-center position,[6] although greater emphasis has been placed on a two-level, excited-state model[6,11] wherein the excited ^3E_g level is split into T_{2g}(higher energy) and T_{1g}(lower energy) levels. On heating samples from 80 K, it is proposed that the T_{2g} level becomes thermally populated and the Stokes shift is subsequently reduced because of the thermal expansion of the lattice, resulting in a change of emission color from green to blue.

We favor a different model that is consistent with the off-center, on-center models that have been proposed for Cu^+ in alkali halides.[7] Some of the results that have been observed for these halide matrices are summarized in Table 5.1. From detailed spectroscopic studies, it has been established that Cu^+ substitutes cleanly

for Na^+ in NaCl by occupying the center of the substitutional site.[6,12] Because of the larger cation-anion distance in NaBr, however, a so-called shallow potential well, off-center Cu^+ position dominates at low temperatures. For KCl, the long K-Cl distance provides a site that is too large for the Cu^+ ion. As a result it occupies a deep potential, off-center position that is characterized by spectroscopic properties that differ significantly from those expected for Cu^+ in a site having O_h symmetry.[13] From comparison of the Sr-S distance, 0.300 nm, with those of the alkali metals, we would expect Cu^+ in SrS to behave similar to that of Cu^+ in NaBr, where the Na-Br distance is 0.298 nm.

Table 5.1. Summary of copper doped alkali halides.

System	M-X distance (nm)	Ground-state Cu position
NaCl:Cu	0.282	on center
NaBr:Cu	0.298	shallow off center
KCl:Cu	0.314	deep off center

Considerable evidence exits for such a shallow, off-center position of Cu^+ in SrS at low temperatures and an on-center position at high temperatures. We believe all of the available data on this system are consistent with blue emission from an on-center Cu position and green emission from an off-center position. The relevant free-energy diagram for this displacement is diagrammed in Figure 5.5. On cooling blue-emitting samples, a greater occupation of the lower-energy, green-emitting site occurs. The displacement and attendant local distortion of the site

leads to an increased oscillator strength. The increase in the Cu-centered excitation band (formally $^1A_g \rightarrow {}^1E_g$) on cooling, as we and others have observed,[6] is consistent with the displacement. In addition, the measured lifetime, 110 μs, for the blue emission (460 nm) at 80 K,[6] is longer than that, 80 μs, for the green emission (530 nm) at 80 K. These lifetimes indicate independent excited states rather than the equilibrium model involving transitions (blue and green) from the excited state. More detailed studies, however, should be conducted to verify these results.

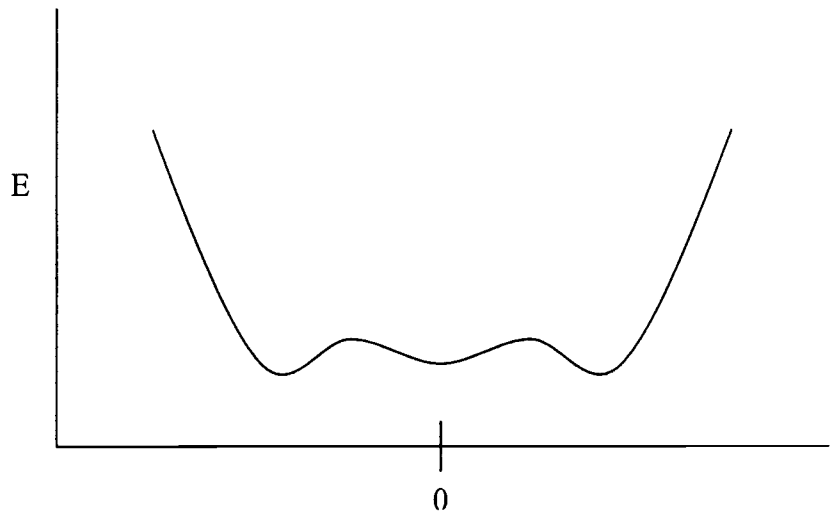

Figure 5.5. Ground state potential well for charge compensated SrS:Cu.

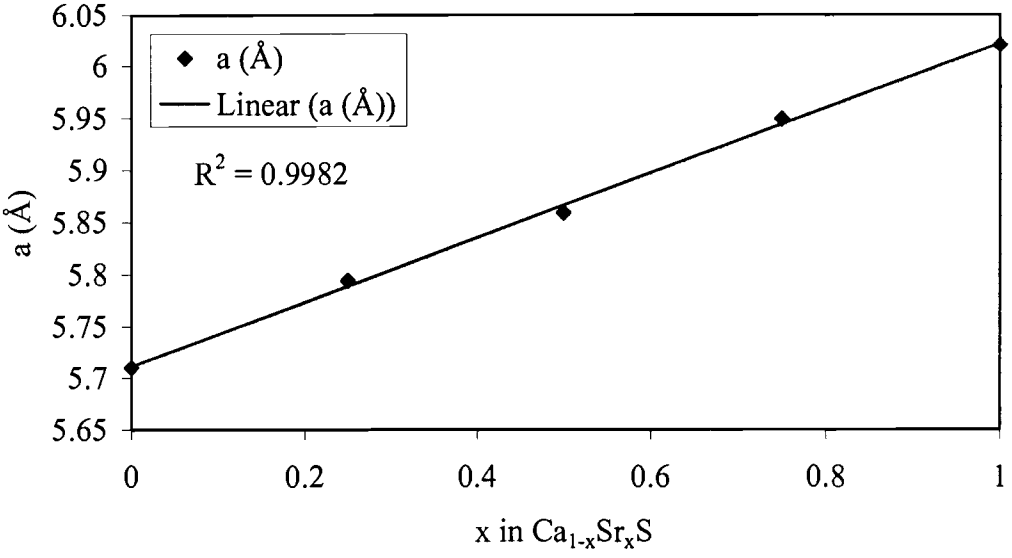

Figure 5.6. Cell parameters for the solid solution $Ca_{1-x}Sr_xS$:Cu.

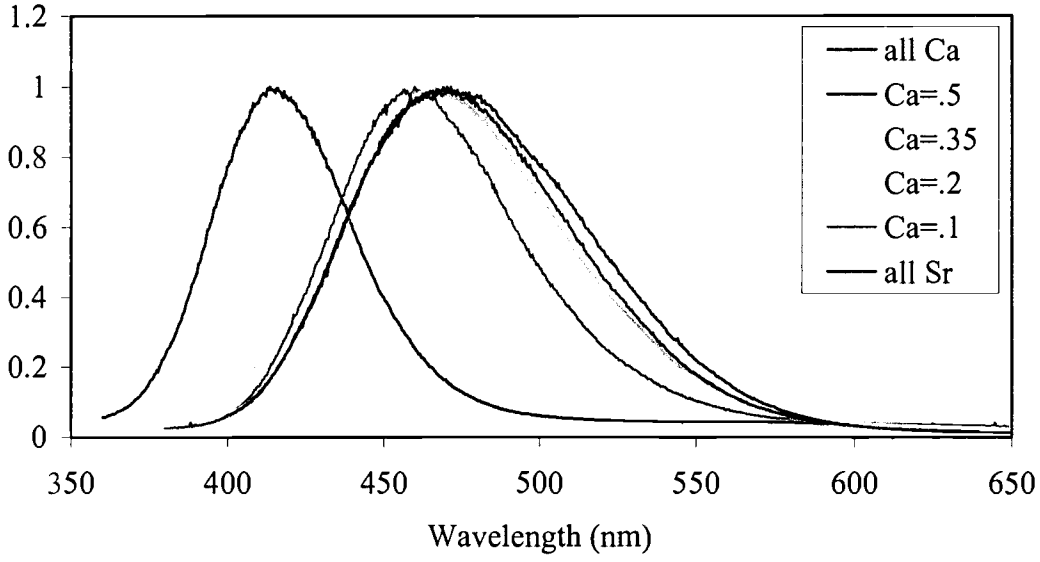

Figure 5.7. Room temperature emission of $Sr_{1-x}Ca_xS$:Cu, Y.

If there is an activation energy associated with the on-, off-center model (Figure 5.5,) a first-order phase transition would be anticipated at a critical pressure and temperature. The ratio of the green to blue emission bands (Figure 5.4) provides a result that is consistent with such a transition. The characteristics of this plot change rather dramatically near a temperature of 100 K, and this temperature corresponds to the central barrier height between the on- and off-center positions.

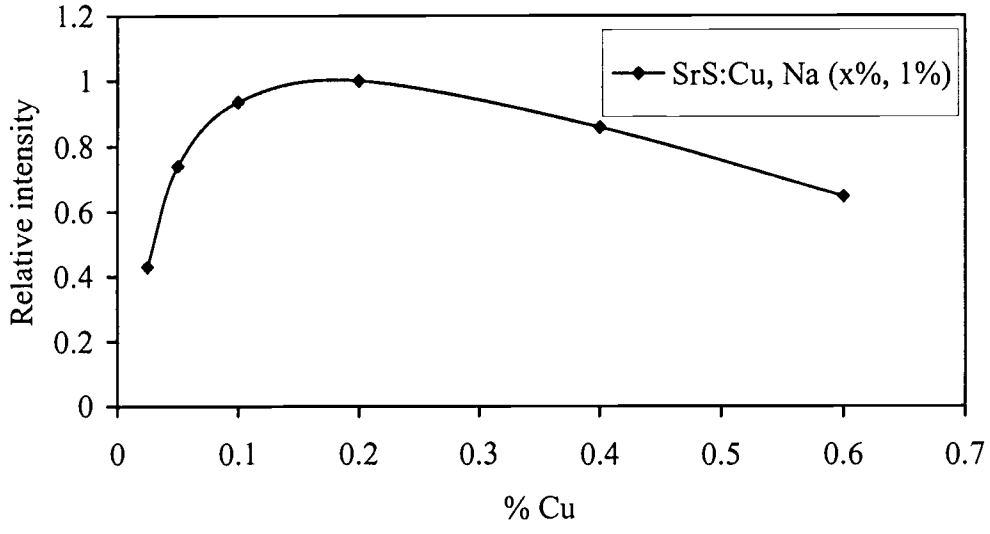

Figure 5.8. Concentration quenching curve of SrS:Cu, Na.

Unlike the changes in emission behavior that are observed in the charge-compensated materials, the green emission of the alkali-metal codoped samples persists from 80 to 298 K. The position of the emission band is also independent of Cu concentration, allowing the measurement of the concentration quenching curve (Figure 5.8.) Like the blue-emitting samples, the optimum brightness is observed

at a dopant concentration near 0.2 at%. We have further found that this emission exhibits only modest thermal quenching (Figure 5.9,) the measured luminescence lifetime at 80 K is 12 μs. This lifetime is comparable to the 15-μs value that is observed in conjunction with the 80-μs value in the uncompensated powders[3] and films.[6] From the concentration dependence of Cu emission in SrS, this emission has been associated with the presence of Cu pairs.[3] On the basis of our measurements, which indicate concentration-independent behavior, we assign this emission to a Cu center that is associated with a S vacancy. In effect, it is a very deep off-center position that is stabilized by the presence of the vacancy. It is readily observed in our powder samples because of the high concentration of alkali-metal cations and generated S vacancies. For the uncompensated powders and films, samples lightly doped with Cu^+ contain fewer S vacancies. As a result, the Cu^+ occupies sites either with or without the vacancy, and this leads to the double exponential behavior of the emission in the green at low temperatures that has been observed by others, i.e., the long lifetime is associated with the shallow off-center position and the short lifetime with the deep, off-center vacancy association.

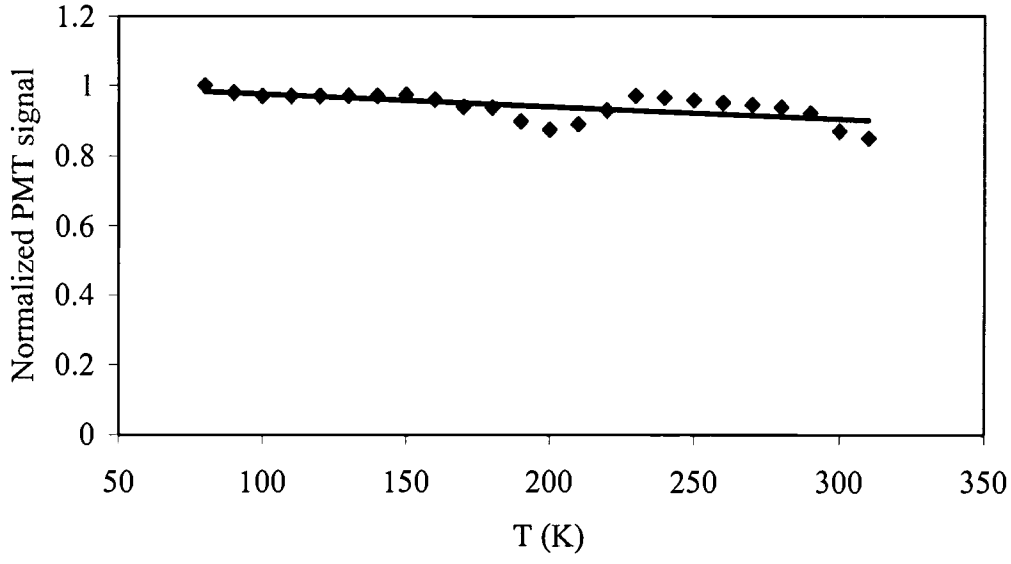

Figure 5.9. Thermal quenching of SrS:Cu,Na.

One of the unique characteristics of the off-center, on-center displacement behavior is the response to pressure. By increasing the pressure on a material exhibiting an off-center displacement, the lattice parameter can be decreased and the ion forced back onto the center position.[7] Relative to Figure 5.5, the well associated with the off-center position becomes shallower with increasing pressure, leading to its destabilization with respect to the on-center position. These effects can be observed either by applying direct pressure or by decreasing the lattice parameter through appropriate chemical substitutions. In the SrS:Cu system, the lattice parameter can be decreased by substituting Ca for Sr in the solid-solution series $Sr_{1-x}Ca_xS$. This series has previously been examined in both powders[8] and thin films,[14] and we have reproduced these results. A plot of the cell parameters according to stoichiometry is depicted in Figure 5.6, indicating a true solid solution

in the system. As shown by the emission behavior in Figure 5.7, a gradual diminution of the Cu green luminescence component is observed with increasing Ca concentration. Previously, the green luminescence component in the Ca poor samples has been associated with an inhomogeneous distribution of Ca and Sr atoms in the solid solution, i.e., some regions of the samples have been assumed to be rich in Ca and other regions rich in Sr.[8,12] This model implies a phase segregation for the (Ca,Sr)S samples, although no evidence for strain or such segregation is evident from the peak widths of the X-ray diffraction patterns; the system is better represented as a true solid solution. We believe the decrease in the contribution of the green component to the emission with increasing Ca concentration is merely a reflection of the decreasing lattice parameter and a destabilization of the off-center Cu position. The net result is a single, on-center emission center at high Ca concentrations.

We have demonstrated that increasing the pressure of the Cu^+ ion in the SrS lattice, i.e., reducing the unit-cell volume by substitution of Ca for Sr, leads to destabilization of the off-center position (Figure 5.5.) Conversely, by decreasing the pressure of the system, i.e., substitution of Ba for Sr, we can expect the system to exhibit a deep off-center position. The solid solution $Sr_{1-x}Ba_xS$ was synthesized and powder XRD patterns were obtained. The cell parameters are plotted in Figure 5.10.

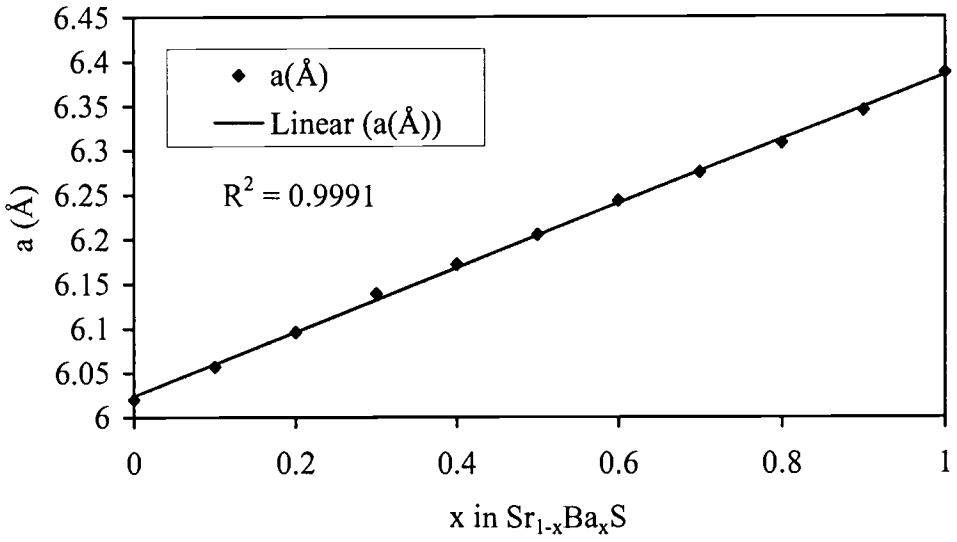

Figure 5.10. Cell parameters for solid solution $Sr_{1-x}Ba_xS$:Cu, Na.

The room temperature emission spectra are depicted in Figure 5.11. Since the Ba-S distance is large (0.312 nm,) one would expect BaS to behave similarly to KCl, where the K-Cl distance is 0.314 nm.

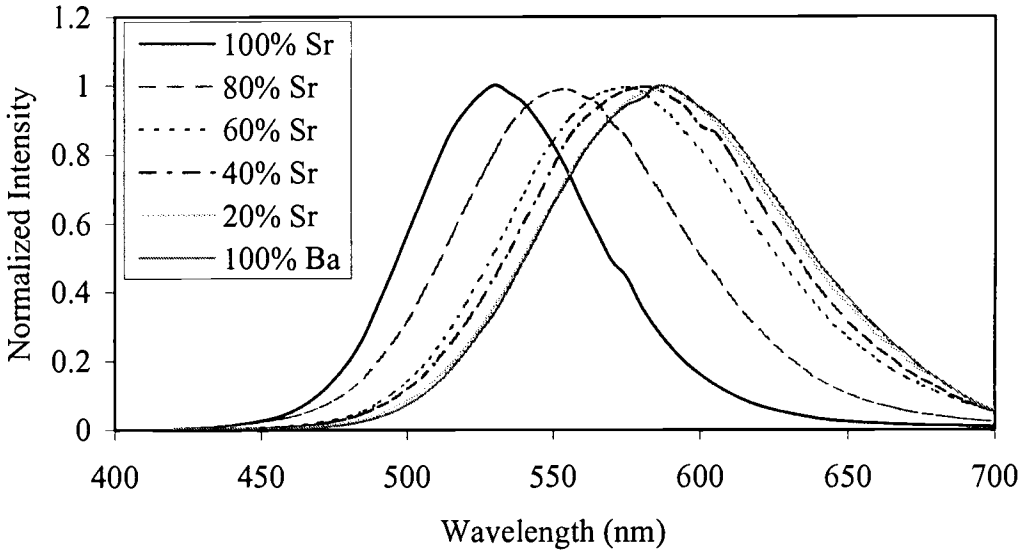

Figure 5.11. Room temperature emission spectra of $Sr_{1-x}Ba_xS$:Cu, Na.

The lifetime of BaS:Cu is ~6 μs at 300 K, and ~7 μs at 77 K. These short lifetimes are consistent with the Cu^+ ion occupying a deep off-center position. Piccirilli and Spinolo measured the lifetime of KCl:Cu^+ and observed a similar trend, that is, the lifetime is somewhat temperature independent from room temperature to 80 K.[15]

A summary of the relative Cu ground-state position in alkaline earth sulfides is given in Table 5.2.

Table 5.2. Summary of ground-state Cu position in alkaline earth sulfides.

System	M-S distance (nm)	Ground-state Cu position
CaS:Cu	0.284	on center
SrS:Cu	0.300	shallow off center
BaS:Cu	0.312	deep off center

Conclusions

We have introduced a new model to account for new and previously reported data on the SrS:Cu system. By examining the solid solutions with Ca and Ba, the emission and excitation spectra, and the lifetimes at different temperatures, we have concluded that there are three ground-state Cu positions: an on center position, a shallow off center position, and a deep off center position. These correspond well with the results reported for the Cu doped alkali halides.

References

1. Lenard, P.; Schmidt, F.; Tomascheck, R. Handb. Exp. Phys., Vol. 23, Akadem Verlagsges, Leipzig) 1928.

2. Lehmann, W., *J. Electrochem. Soc.* **117**, 1389 (1970).

3. Yamashita, N. *Jpn. J. Appl. Phys., Part 1.* **30**, 3335 (1991).

4. Sun, S.-S. *Conference Record of the 1998 International Display Research Conference*, Seoul, Korea (1998).

5. Li, D.; Clark, B.L.; Keszler, D.A.; Keir, P.D.; Wager, J.F. *Chem. Mater.* **12**, 268 (2000).

6. Li, W.M.; Ritala, M.; Leskela, M.; Niinisto, L.; Soininen, E.; Sun, S.-S.; Tong, W.; Summers, C.J. *J. Appl. Phys.* **86**, 5017 (1999).

7. Akella, A.; Keszler, D.A. *Mater. Res. Bull.*, **30**, 105 (1995).

8. Diaz, A. Ph.D. Thesis, Oregon State University, 1997.

9. Holland, U.; Lüty, F. *Phys. Rev. B: Condens. Matter.* **19**, 4298 (1979).

10. Yamashita, N.; Ebisumori, K.; Nakamura, K. *Jpn. J. Appl. Phys.* **32**, 3846 (1993).

11. Barthou, C.; Benoit, J.; Benalloul, P.; Garcia, A.; Fouassier, C. *Proc. 10th Inter. Conf. Inorg. Org. Electrolumin.* Hamamatsu, Japan (2000).

12. Payne, S.A.; Goldberg, A.B.; McClure, D.S. *J. Chem. Phys.* **81**, 1529 (1984).

13. Payne, S.A. *Phys. Rev. B.* **36**, 6125 (1987).

14. Mohammed, E.; Park, W.; Tong, W.; Stock, S.R.; Summers, C.J. *Proc. 6th Inter. Conf. Sci. Tech. Display Phosphors.* San Diego, CA (2000).

15. Piccirilli, M.; Spinolo, G. *Phys. Rev. B.* **4**, 1339 (1971).

CHAPTER 6

HYDROTHERMAL DEHYDRATION: A CONVENIENT SYNTHESIS METHOD FOR SOLIDS

For publication in *Inorganic Chemistry*

Abstract

A simple, low-temperature method has been developed to produce crystalline oxides from hydroxylated precipitates, obviating the need for firing several hundred degrees above the dehydration temperature. The compounds Zn_2SiO_4 and $SnSiO_3$ are readily prepared in crystalline form by using this technique.

Introduction

Among reactions in aqueous solutions, most chemists are generally introduced first to the precipitation reaction. In many cases, these reactions can be readily executed to produce simple anhydrous, crystalline solids with formulations ranging from $BaSO_4$ to PbI_2. As such, precipitation can be considered to be a convenient, low-temperature synthesis method. Success in the production of an anhydrous, crystalline product, however, rests on the feeble acidities and basicities of the aqua ions involved in the reaction. If the values of the hydrolysis constants pK_a and pK_b of the aqua ions are sufficiently small or negative, extensive hydrolysis occurs, and the solid precipitates as a hydroxo species. Attempts to dehydrate such products at modest temperatures invariably lead to the production of undesirable, amorphous products. Of course, these products can subsequently be crystallized by heating at temperatures of a few to several hundred degrees above their dehydration points. To achieve truly low-temperature preparation of materials, a variety of procedures, including sol-gel[1] and hydrothermal methods[2-5]

have been devised and adapted for the production of crystalline solids. Sol-gel and related techniques generally involve multiple steps, varying the levels of complexity, and moderate to high reagent costs.

The production of an amorphous material in the drying process of a hydrated, hydroxo precipitate is associated with the kinetic stabilization that occurs in the absence of nucleation centers. After all, the thermodynamically favored products in these systems are generally the crystalline inorganic material and water. To prevent the formation of an amorphous product, the dehydration process should be done under conditions that provide and opportunity for nucleation and grain growth. As we describe here for the preparation of crystalline Zn_2SiO_4 and $SnSiO_3$, this result can be achieved by conducting the dehydration under hydrothermal conditions at temperatures near 398 K and lower.

Experimental

The synthesis method for each material is described below. The Teflon-lined reaction vessel (Parr Instruments) has a capacity of 23 mL. In each case, no additional water was added to the vessel.

Zn_2SiO_4

1.79 g of $ZnSO_4 \cdot H_2O$ (Aldrich, 99.9%) and 0.92 g of Na_4SiO_4 (Alfa-Aesar, reagent grade) were each dissolved separately in 20 mL of deionized H_2O. A precipitate forms on mixing these solutions; the resulting mixture was stirred and

heated (338 K) for 30 min. The wet, white precipitate was collected by filtration and immediately placed in a Teflon-lined high-pressure reaction vessel at 423 K for 12 h. The resulting product was a dehydrated, fine crystalline powder; approximately 1 mL of clear water was present in the Teflon container, completely separated from the powder.

$SnSiO_3$

Sn^{2+} is unstable in air, so all preparations were completed under flowing N_2(g). 0.92 g of Na_4SiO_4 were dissolved in 20 mL H_2O. 1.25 g of $CuSO_4 \cdot 5H_2O$ (Alfa-Aesar, 99.999%) were dissolved in deionized H_2O. 3 g of Sn metal (Cerac, 99.8%) were added to the copper solution and allowed to stir under N_2 for 30 min. The $SnSO_4$ (aq) solution was filtered (to remove the precipitated Cu metal) such that the mother liquor was added directly to the Na_4SiO_4 (aq) solution. This precipitate was stirred under bubbling N_2 for 30 min then filtered and added to the reaction vessel. The precipitate was heated at 478 K for 12 h.

Powder XRD patterns were obtained for Zn_2SiO_4 using a Phillips diffractometer equipped with Cu Kα radiation. Powder patterns for the $SnSiO_3$ were obtained using a Siemens D5000 diffractometer equipped with Cu Kα radiation.

Results and Discussion

Zn_2SiO_4

Zn_2SiO_4 is a common phosphor host, and its preparation by both low- and high-temperature methods has been extensively studied.[6,7] On mixing solutions of $ZnSO_4$(aq) and Na_4SiO_4(aq), a precipitate forms. Since pK_b for SiO_4^{4-}(aq) is approximately –8, extensive hydrolysis occurs and the precipitate is expected to be a hydroxylated product. Dehydration of this material in air at 473 K leads to the production of an amorphous product, as indicated in Figure 6.1. The broad peak in the X-ray diffraction pattern is indicative of an amorphous product. If the precipitate, however, is collected by filtration and placed in a Teflon-lined high-pressure reaction vessel at 473 K for 12 h, a highly crystalline product is formed. As observed in Figure 6.2, the product is crystalline. The sharpness of the X-ray diffraction (XRD) lines is consistent with the high crystallinity of the sample. In fact, on opening the reaction vessel, small beads of clear water are completely separated from the fine white powder.

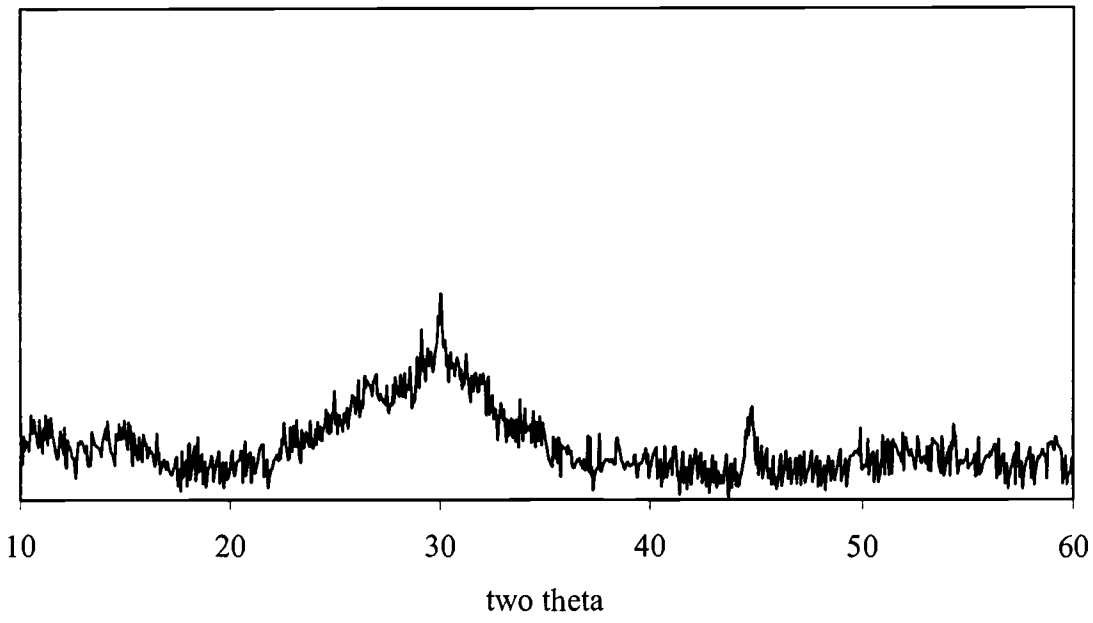

Figure 6.1. Powder XRD pattern of amorphous Zn_2SiO_4. The broad peak is indicative of an amorphous material.

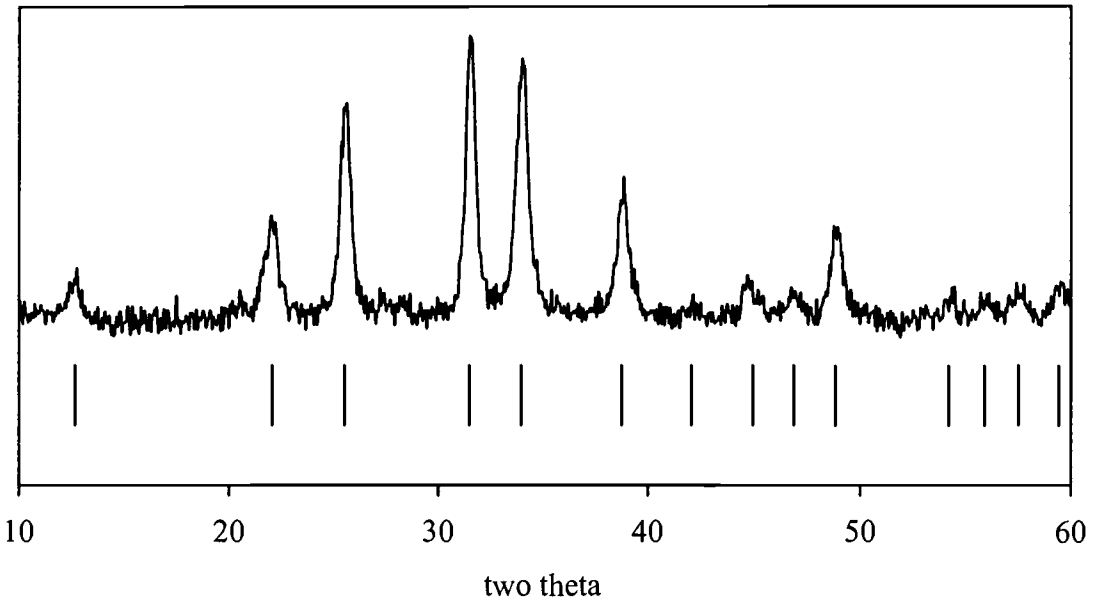

Figure 6.2. Powder XRD pattern of crystalline Zn_2SiO_4 after hydrothermal dehydration. Tick marks represent reported peaks from the JCPDF.

Since it is well known that Zn_2SiO_4 can be prepared by a variety of low-temperature methods, these materials do not provide a rigorous test of the hydrothermal dehydration method. The preparation of Sn^{2+} compounds represents a better case study.

$SnSiO_3$

The general solid-state chemistry of oxides that contain Sn^{2+} is largely undeveloped, in part, because of the disproportionation reaction that occurs on heating SnO:

$$2\ SnO \rightarrow Sn + SnO_2$$

Here, a general low-temperature synthesis method could provide an attractive means for the development of a more extensive knowledge of oxide chemistry of Sn^{2+}. In their original assessment of the phase diagram, Slonimskii and Tseidler characterized the system $SnO\text{-}SiO_2$ as a simple eutectic, i.e., no compound formation was detected.[9] Later, Carbo-Nover and Williamson annealed the glass composition $1SnO{:}1SiO_2$ and produced small crystalline spherullites embiggened in the glass matrix. These were determined by electron microprobe analysis to have the same composition as the glass, i.e., $SnSiO_3$.[10] Due to the disproportionation of SnO, heating these mixtures is obviously not a practical synthesis route.

A precipitation reaction involving $Sn^{2+}(aq)$ and $SiO_4^{4-}(aq)$ would offer a low-temperature route to the production of a crystalline product, but the small

values of pK associated with the aqua ions results in the precipitation of a hydroxylated product. Attempts to dehydrate the precipitate under normal conditions lead to amorphous products. If the hydrothermal dehydration technique is utilized, however, a well-crystallized product is obtained. The XRD powder pattern (Figure 6.3) exhibits diffraction peaks consistent with those previously reported for $SnSiO_3$.[10] Importantly, no reaction is observed by direct interaction of SnO and SiO_2 at various pH levels under the same hydrothermal conditions. This indicates that hydrothermal dehydration is a convenient method for producing oxides containing Sn^{2+} at relatively low processing temperatures.

We have recently produced single crystals of the tin silicate by a low-temperature vapor transport method. The crystal structure of this phase as well as some more general considerations and applications of the hydrothermal dehydration of precipitates to the production of powders, thin-films,[11] and luminescent materials will appear in forthcoming contributions.

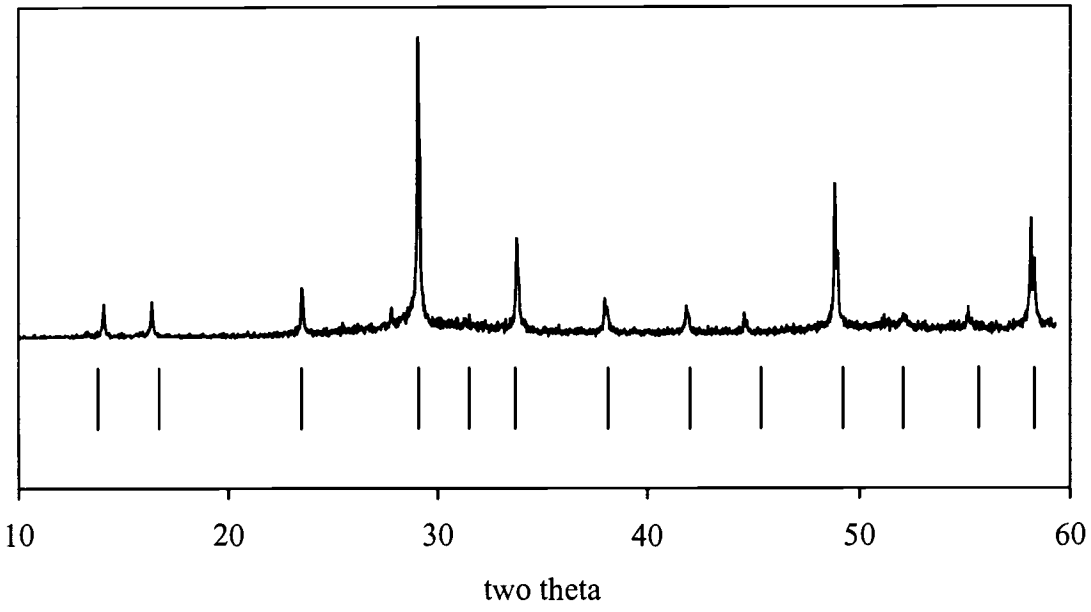

Figure 6.3. Powder XRD pattern of $SnSiO_3$. Tick marks represent peaks reported in the JCPDF.

Conclusions

Zinc silicate, Zn_2SiO_4, has been prepared at low temperatures of 398 K by hydrothermal dehydration of the precipitate. Allowing the precipitate to dehydrate under non-equilibrium conditions (i.e., oven drying without the use of a high-pressure vessel), results in the formation of an amorphous precipitate. By using this method, tin silicate, $SnSiO_3$, has been synthesized at temperatures below 400 K. Due to the disproportionation of Sn^{2+} caused by conventional synthetic methods, hydrothermal dehydration provides a low-temperature alternative for making Sn^{2+} containing compounds.

Acknowledgments

This work was supported by the National Science Foundation. We thank Prof. T. Cho for discussions during the initial stages of the work.

References

1. Pierre, A.C. *Introduction to Sol-Gel Processing.* Kluwer Academic, Boston (1998).

2. Lencka, M.M.; Oledzka, M.; Riman, R. *Chem. Mater.* **12**, 1323 (2000).

3. Harrison, W.T.A.; Dussack, L.L.; Jacobson, A.J. *J. Solid State Chem.* **125**, 234 (1996).

4. Korzenski, M.B.; Kolis, J.; Long, G.J. *J. Solid State Chem.* **147**, 390 (1999).

5. Zang, F.; Zaralij, P.Y.; Whittingham, M.S. *Mater. Res. Bull.* **32**, 701 (1997).

6. Morimo, R.; Matae, K. *Mater. Res. Bull.* **24**, 175 (1989).

7. Li, Q.H.; Komaraneni, S.; Roy, R. *J. Mater. Sci.* **30**, 2358 (1995).

8. Slonominskii, B.I.; Tseidler, A.A. *Sb. Trud. Gos. Nauchnoissled. Inst. Tsver Metal.* **15**, 173 (1959).

9. Carbo-Nover, J.; Williamson, J. *Phys. Chem. Glasses* **8**, 164 (1967).

10. Solis, J.L.; Lantto, V. *Phys. Scr.*, **69**, 281 (1996).

11. Clark, B.L.; Keszler, D.A.; Bender, J.P.; Wager, J.F. *Ext. Abstr., Internat. Conf. Sci. Technol. Display Phosphors.* 145 (2000).

CHAPTER 7

PHOTO- AND ELECTRO-LUMINESCENCE OF ZINC GERMANATE ACTFEL DEVICES

For Publication in Applied Physics Letters

Abstract

Manganese-doped zinc germanate and silicate powders exhibit bright green photoluminescence with excellent chromaticity, affording a variety of applications in displays and lighting. A large number of high- and low-temperature methods have been developed for the synthesis of $Mn:Zn_2SiO_4$. In this contribution, we describe a very simple, low-cost method for the production of Zn_2SiO_4 and Zn_2GeO_4 at low temperature. We also describe methods for generation of crystalline, luminescent Mn-doped films at temperatures as low as 398 K. Sputtered zinc germanate thin films generally require annealing temperatures near 873 K to obtain optimal ACTFEL device performance. Recently, we have developed a unique process methodology that yields crystalline zinc germanate and silicate powders at temperatures as low as 398 K. Electroluminescence from these films will be compared with those prepared by conventional sputtering techniques, which have recently yielded a brightness of over 100 cd/m^2 at 40 volts above threshold (60 Hz) and CIE coordinates of $x = 0.3$ and $y = 0.6$, indicating saturated green emission.

Introduction

Among reactions in aqueous solution, most chemists are generally first introduced to the precipitation reaction. These reactions can be a convenient, low-temperature method to produce a crystalline material. Whether or not the product is crystalline, however, depends on the relative acidities and basicities of the

aqueous ions in solution. If the values of the hydrolysis constants pK_a or pK_b are sufficiently small or negative, extensive hydrolysis will occur, and the solid will precipitate as a hydroxo species.

Take for example, the reactions used to form $SnWO_4$ and $PbWO_4$; pK_a for the $Sn^{2+}(aq)$ ion is 3.4 versus 7.7 for $Pb^{2+}(aq)$. From this, we would expect the $SnWO_4$ to precipitate as a hydroxylated and amorphous species whereas the $PbWO_4$ should precipitate as an anhydrous, crystalline product. These predictions are easily confirmed by performing the reactions at neutral pH, drying the products in air, and obtaining X-ray diffraction (XRD) powder patterns.[1]

An amorphous precipitate can be made crystalline by placing the hydroxylated precipitate in a Teflon lined reaction vessel at 473 K for four hours. This process is called hydrothermal dehydration and allows the product to dry under equilibrium conditions, allowing for nucleation and grain growth of the crystalline product. No additional water is added; in fact, on opening the reaction vessel, small beads of clear water are found completely separated from the remaining powder.

Zinc silicate is a common phosphor host, and its preparation by both low- and high-temperature methods has been studied.[2,3] On mixing solutions of $ZnSO_4(aq)$ and $Na_4SiO_4(aq)$, a precipitate is formed. Since pK_b for the $SiO_4^{4-}(aq)$ is –8, extensive hydrolysis occurs. Drying this product in air at 473 K results in an amorphous product. If the hydrothermal dehydration technique is used, however, the product is crystalline.

Since sputtered zinc silicate and germanate films are amorphous; a similar technique can be used to grow crystalline films at temperatures as low as 398 K. When this low-temperature technique is optimized, it could have a significant effect on the processing conditions of oxide ACTFEL devices.

Experimental

Approximately 8000 Å of zinc germanate were sputter-deposited onto four glass substrates previously coated with a transparent conductor (ITO) and an insulator (ATO.) Four different anneals were performed: (1) standard furnace anneal at 873 K for 4 h, (2) furnace anneal under steam at 873 K for 4 h, (3) rapid thermal anneal (RTA) at 873 K for two minutes, and (4) hydrothermal anneal at 398 K for 4 h. ACTFEL devices were completed by adding SiON and Al as the top insulator and conductor, respectively.

Results and Discussion

Results of the different annealed samples are quite surprising, especially when comparing the PL to the EL intensities. On the basis of the PL data (Table 7.1) of the different annealed samples, one would think that this hydrothermal annealing technique would be a suitable, low-temperature technique for producing oxide ACTFEL devices.

Table 7.1. Relative PL intensities of annealed Zn_2GeO_4:Mn thin-films.

Sample	Relative Intensity (%)
Furnace (873 K, 4 h)	100
Steam (873 K, 4 h)	98
RTA (873 K, 2 min)	25
Hydrothermal (398 K, 4 h)	80

In comparing the XRD data for the various annealed films (Figure 7.1), note that the crystallinity of the hydrothermal annealed thin-film is much greater than the others. The B_{40} values (Table 7.2) for the ACTFEL device annealed in a standard furnace, however, indicate that this might be the ideal annealing condition for zinc germanate films.

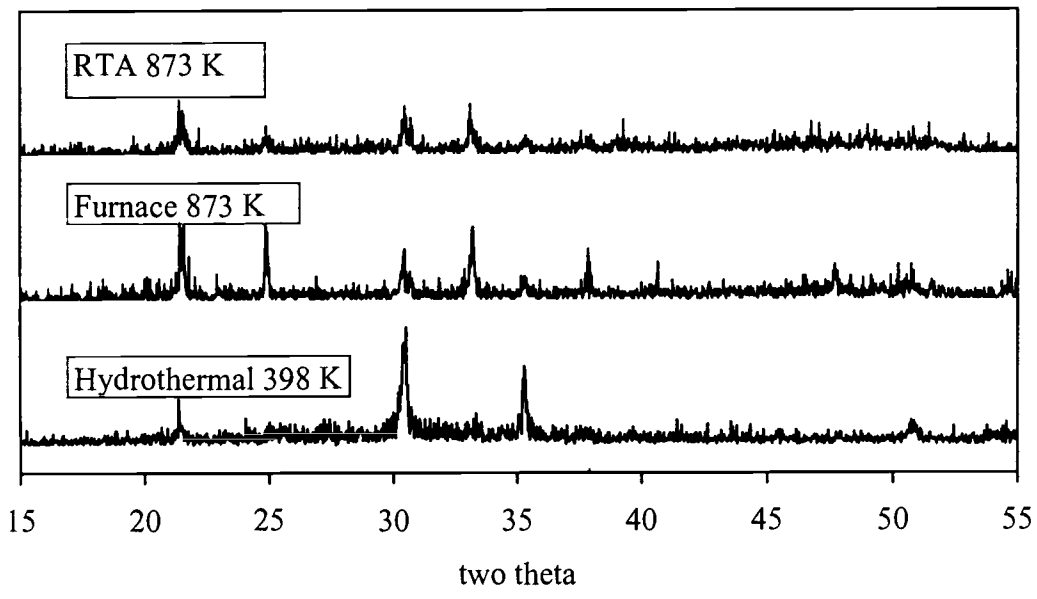

Figure 7.1. XRD patterns of zinc germanate thin-films.

The brightness vs. voltage (B-V) and efficiency vs. voltage (E-V) curves for the furnace annealed and hydrothermal annealed thin films are depicted in Figures 7.2 and 7.3. All data is summarized in Table 7.2. Although the relative PL intensities for the furnace and hydrothermal annealed films are comparable, the luminances of the respective ACTFEL devices are quite different.

Table 7.2. Summary of Zn_2GeO_4 ACTFEL devices – all devices characterized at 60 Hz driving voltage except Hydrothermal anneal, which was carried out at 1 kHz.

Sample	B_{40} (cd/m^2)	E_{40} (lm/W)
Furnace (873 K, 4 h)	105	0.33
Steam (873 K, 4 h)	85	0.42
RTA (873 K, 2 min)	60	0.21
Hydrothermal (398K, 4 h)	0.76	0.02

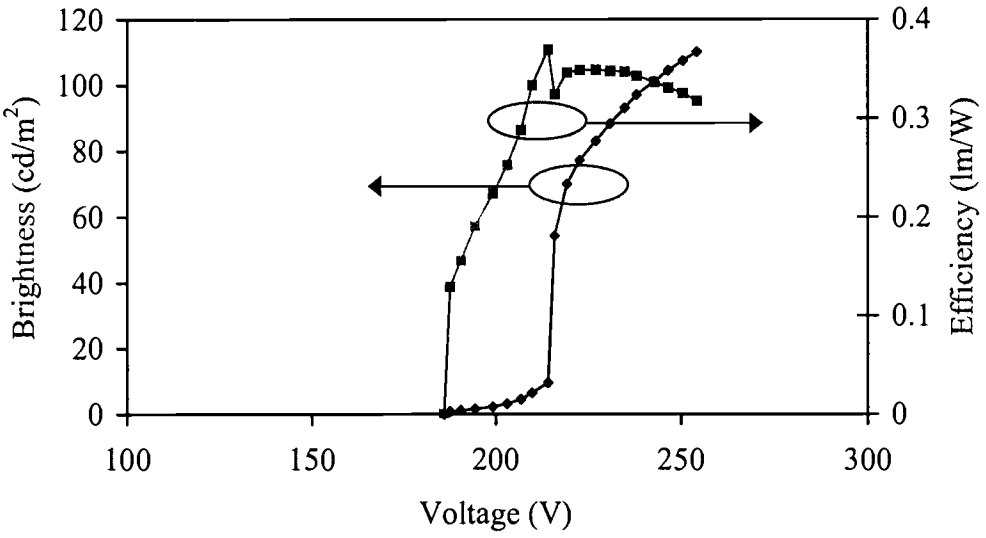

Figure 7.2. B-V and E-V of standard furnace annealed zinc germanate ACTFEL devices.

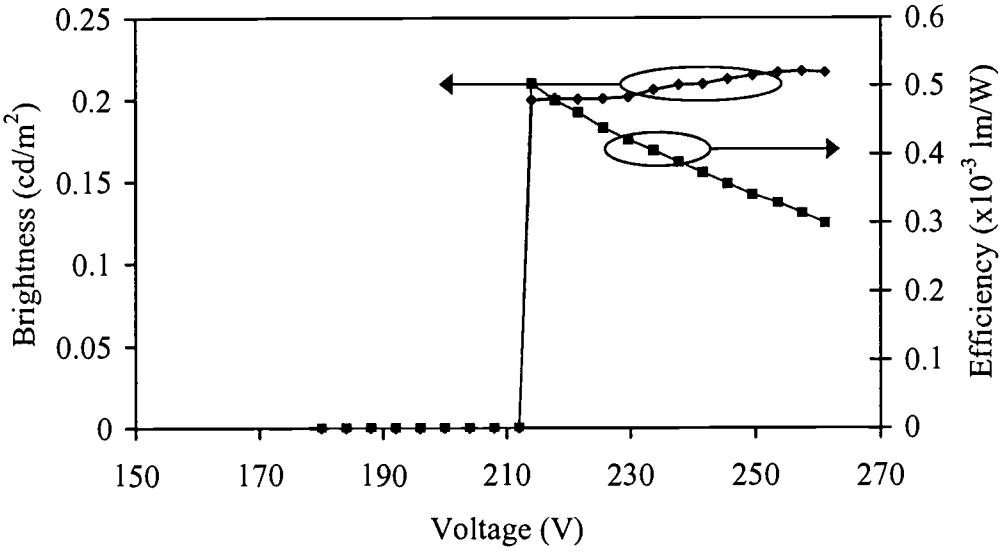

Figure 7.3. B-V and E-V of hydrothermal annealed zinc germanate ACTFEL devices.

We have noticed that if the standard furnace annealed thin-films are held in the furnace longer than 4 hours, the crystallinity increases and the ACTFEL device performance is similar to that of the hydrothermal annealed device. On the basis of the milky white appearances of each of the thin films, and the "spottiness" of light coming from the devices, we believe this is due to the high crystallinity of the film. During the anneal, tremendous grain-growth occurs causing islands of zinc germanate, rather than a homogeneous coverage. These islands may also act as a wave-guide causing light to exit at an angle.

Conclusions

We have developed a low-temperature method - hydrothermal dehydration - for production of zinc silicate and germanate powders. This method has been

modified and adapted for ACTFEL materials such that as-deposited thin-films are annealed at temperatures as low as 398 K. The PL intensity for the low-temperature method was quite high - 80% of the furnace annealed sample. To date, the technique, however, has led to milky films and poor ACTFEL performance. The same performance has been observed for standard furnace-annealed samples that remain at 873 K for longer than 4 hours. These observations lead us to believe that the poor performance of the devices results from formation of large grains in the film. With some modifications in the processing conditions, we expect to attain improved device performance by using this low-temperature technique.

References

1. Clark, B.L. and Keszler, D.A. *In press, Inorg. Chem.*
2. Morimo, R.; Matae, K. *Mater. Res. Bull.* **24**, 175 (1989).
3. Li, Q.H.; Kormaraneni, S.; Roy, R. *J Mater. Sci.* **30**, 2358 (1995).

CHAPTER 8

LOW TEMPERATURE SYNTHESIS OF FORSTERITE BY HYDROTHERMAL DEHYDRATION

For publication in Journal of Solid-State Chemistry

Abstract

Forsterite, Mg_2SiO_4, is prepared by a nontoxic, low-temperature hydrothermal dehydration technique. By carefully heating the precipitate from the reaction of $Mg(NO_3)_2(aq)$ and $Na_4SiO_4(aq)$, crystalline forsterite can be obtained at temperatures as low as 698 K.

Introduction

Research interest on Mg_2SiO_4, forsterite, involves many disciplines, including geology, biology, and chemistry. It is important in geochemical reactions involving the formation of crystalline basalt.[1] Biologists have studied the natural crystallization of forsterite, as it occurs by biomineralization from bacteria in the mountains of South Africa.[2] It has many commercial uses, including a scratch-resistant coating,[3] an anti-reflection coating,[4] and perhaps most importantly, a solid-state, tunable laser.[5] Traditional, solid-state syntheses of forsterite have proven difficult because of the large difference in melting points of MgO and SiO_2. To circumvent these problems, chemists have developed many techniques, including specific heat treatments with intermittent grindings,[6] coprecipitation with $SiCl_4$,[7] and various sol-gel methods.[8-11]

The traditional solid-state synthesis of forsterite involves heating stoichiometric mixtures of the oxides MgO and SiO_2. It is difficult to prepare single-phase material because of the high stability of MgO and SiO_2, their unreactivity, and their considerable difference in melting points, 3125 and 1973 K,

respectively. Forsterite melts at 2183 K, therefore conventional synthesis temperatures must be at or above 1900 K. Slightly lower synthesis temperatures were reached by using intermittent grinding of the oxides.[12] By adding water in the grinding step, Temujin and co-workers were able to lower the synthesis temperature to 1163 K.[13]

Researchers have examined even lower temperature techniques, such as the sol-gel method, to produce crystalline forsterite. In the sol-gel method,[14] a colloidal route is used to produce inorganic oxides or ceramics, with an intermediate stage that includes a sol and/or gel state. A *sol* is a colloidal suspension of solid particles in a liquid. For it to exist, the particles in the liquid must be small enough such that the atomic dispersion forces are greater than the gravitational force exerted on the particles. A *gel* is a porous 3-dimensionally interconnected solid network. An appropriate set of precursors is combined to form a sol and the gel is formed after evaporation of the liquid. Precursors generally involve metal alkoxides, $M(OR)_n$, such as $Mg(OCH_3)_2$ and $Si(OC_2H_5)_4$ or metallic salts, MX_n, such as $MgCl_2$ and $Mg(NO_3)_2$.

Preparation of forsterite by using the above precursors as well as silicon tetrachloride has been demonstrated.[8,9] Obviously, these experiments need to be done under inert, controlled conditions because of both the toxicity of the starting materials and the relative hydrolytic instability of alkoxide compounds. The sol-gel method employed by Park et al[9,10] required a variety of complicated steps, many of which needed to be performed under inert atmosphere. Fairly low

crystallization temperatures near 1273 K were achieved by facilitation with hydrogen peroxide.[15] Further modification of the method resulted in crystalline forsterite at temperatures near 1073 K.[16]

According to the phase diagram presented by Bowen and Tuttle,[17] forsterite forms at temperatures near 650 K and pressures near 2000 psi by reacting brucite, $Mg(OH)_2$, with serpentine, $Mg_3Si_2O_5(OH)_4$, according to the following reaction:

$$Mg(OH)_2 + Mg_3Si_2O_5(OH)_4 \rightarrow 2Mg_2SiO_4 + 3H_2O \qquad (1)$$

Not only are these starting materials non-toxic, but it is not necessary to do the experiment under inert conditions.

We previously demonstrated a unique method for producing oxide materials at low temperatures.[18] The method, called hydrothermal dehydration, involves precipitation of a hydroxylated species, followed by dehydration of the precipitate under equilibrium conditions. This process leads to nucleation and grain growth, resulting in a crystalline material. In this communication, we demonstrate this safe, low-cost, low-temperature technique for preparation of forsterite. Insofar as we know, the synthesis temperature, 698 K, is the lowest yet reported for the preparation of crystalline forsterite under low-pressure conditions.

Experimental

5.12 g of $Mg(NO_3)_2 \cdot 6H_2O$ (Mallinckrodt, reagent grade) and 1.84 g Na_4SiO_4 (Alfa-Aesar, reagent grade) were dissolved separately in 50 mL of distilled, deionized H_2O. Upon mixing the two solutions, a precipitate formed. The

precipitate was stirred and heated at 343 K for approximately 1 h. After filtration, the wet, white precipitate was placed in a platinum crucible and enclosed in an Inconel high-pressure reaction vessel (Parr Instruments.) No additional water was added. The vessel was placed in a furnace at room temperature and was heated at 5 K/h to 698 K, held for 4 hours, then cooled to room temperature at 50 K/h. On opening of the bomb, the white precipitate was separated from approximately 2 mL of H_2O.

Powder x-ray diffraction (XRD) patterns were obtained by using a Siemens D5000 X-ray diffractometer equipped with Cu Kα radiation. Data were obtained over the range $2 \leq 2\theta \leq 60$ at 0.02 ° intervals.

Results and Discussion

Upon mixing the two aqueous solutions, $Mg(NO_3)_2(aq)$ and $Na_4SiO_4(aq)$, a precipitate forms. Since pK_b for $SiO_4^{4-}(aq)$ is –8, extensive hydrolysis will occur, leading to the following reaction:

$$SiO_4^{4-}(aq) + 2H_2O \rightarrow SiO_2(OH)_2^{2-}(aq) + 2OH^-(aq) \qquad (2)$$

This results in the formation of a hydroxylated precipitate when Mg^{2+} (aq) is added. The hydroxylated precipitate is most likely not simply amorphous forsterite; rather, it is a well-mixed, stoichiometric combination of brucite and serpentine with some additional waters of hydration. We will represent this stoichiometry by using the formula $Mg(OH)_2 \cdot Mg_3Si_2O_5(OH)_4 \cdot (H_2O)_n$; the powder XRD pattern of the

precipitate without heat treatment (Figure 8.1) is indicative of an amorphous material.

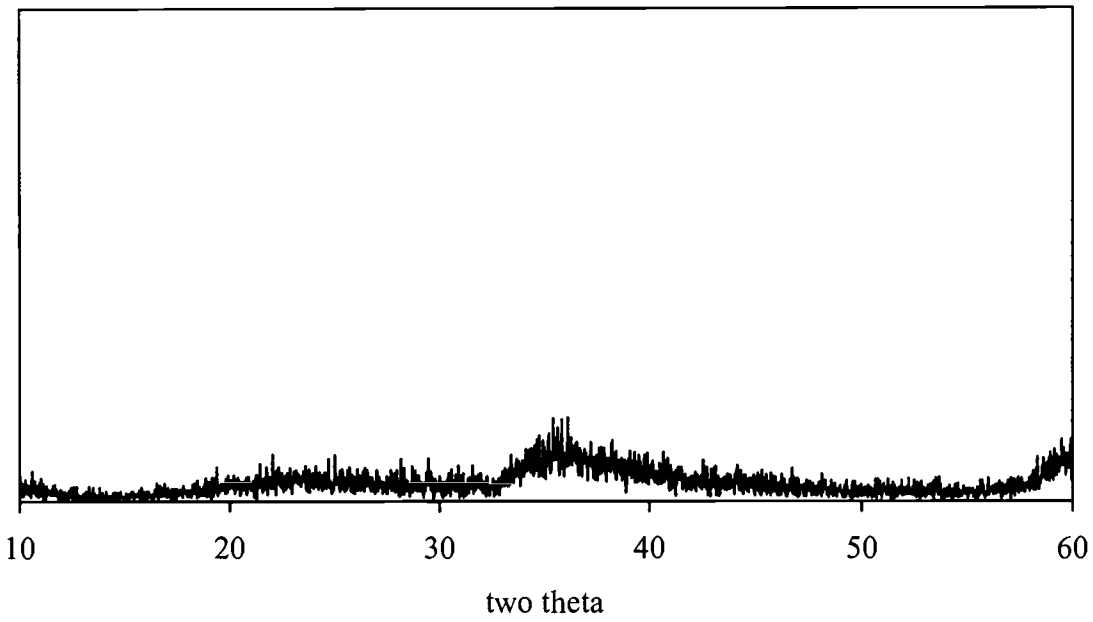

Figure 8.1. Powder XRD pattern of as-precipitated $Mg(OH)_2 \cdot Mg_3Si_2O_5(OH)_4 \cdot (H_2O)_n$.

To follow the course of the reaction, the products were removed from the reaction vessel and were analyzed by XRD following selected heat-treatment steps (Table 8.1.)

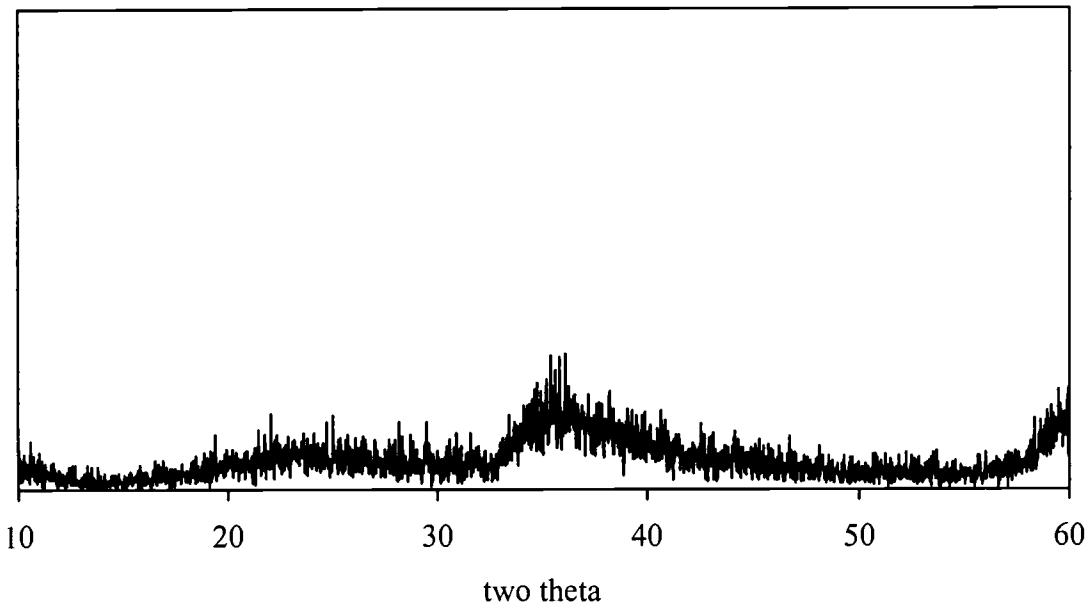

Figure 8.2. Powder XRD pattern of precipitate after heating under hydrothermal dehydration conditions at 473 K.

Table 8.1. Results from different hydrothermal dehydration temperatures. F=forsterite, B=brucite, S=serpentine, E=enstatite.

Sample #	Maximum Temperature	Phases Present
1	As precipitated (no heating)	Amorphous
2	473 K	Amorphous
3	523 K	Amorphous
4	623 K	Amorphous B, S, F
5	673 K	Crystalline B, S, F
6	698 K	Crystalline F, E

From room temperature to 523 K, no discernible crystalline phase can be detected in the XRD patterns; the pattern for the 473-K sample is depicted in Figure 8.2. After the 673 K treatment, crystalline forsterite is present in small amounts, but additional peaks can be associated with serpentine and brucite.

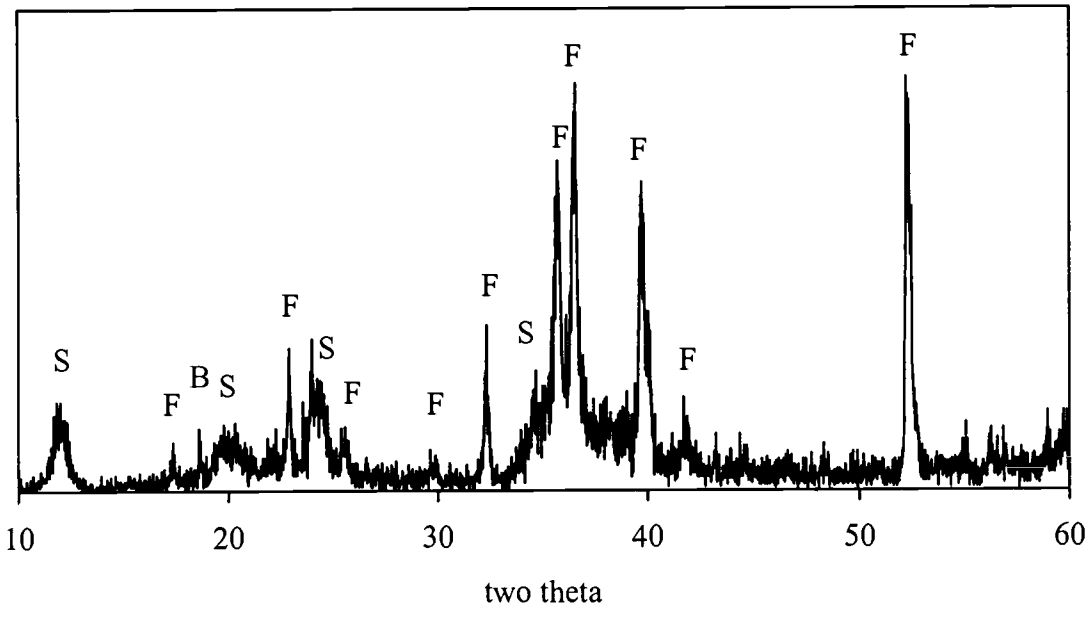

Figure 8.3. Powder XRD pattern for Mg_2SiO_4 heated at 673 K. F=forsterite, B=brucite, S=serpentine.

Increasing the temperature slightly to 698 K causes the remaining brucite and serpentine to react completely, resulting in the formation of forsterite (Figure 8.4.) Peak positions are in good agreement with those available from the JCPDF powder diffraction file.[19] No additional peaks from serpentine or brucite are present. There is, however, one additional peak resulting from enstatite, $MgSiO_3$. Phase disappears when heated to higher temperatures (Figure 8.5.) We believe 698

K is the lowest reported synthesis temperature for the preparation of crystalline forsterite.

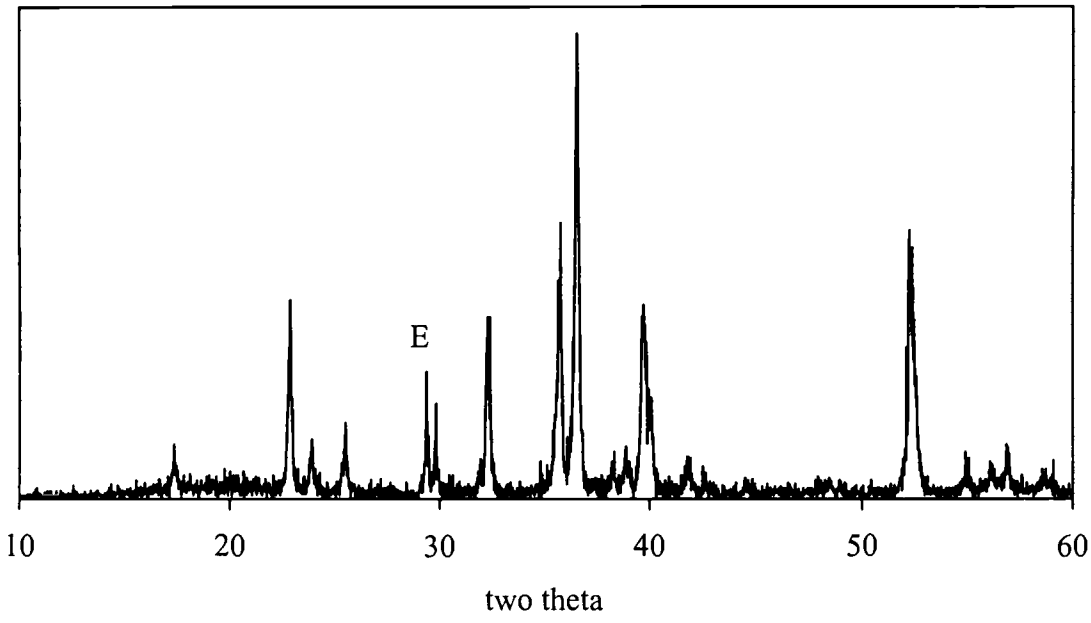

Figure 8.4. Powder XRD pattern of crystalline forsterite prepared at 698 K using hydrothermal dehydration.

Heating the sample in an open container at 1273 K for 12 h results in an improvement in the crystallinity, as evident from the sharpening of the diffraction peaks given Figure 8.5. Also note from Figure 8.5 that the enstatite peak has disappeared, leaving forsterite as the only phase present.

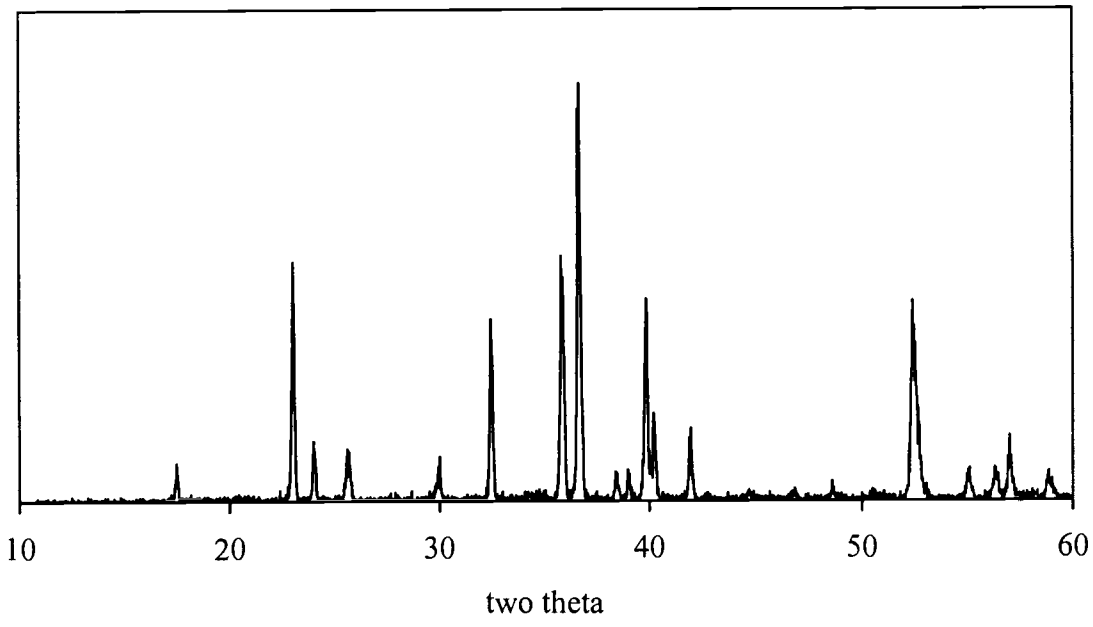

Figure 8.5. XRD pattern of forsterite, prepared by precipitation, hydrothermal dehydration, and standard furnace heating.

Conclusions

By using the hydrothermal dehydration method, we have produced crystalline forsterite at temperatures as low as 698 K. Equilibrium is established allowing for nucleation and grain growth; heating the precipitate under normal conditions (i.e., without a high pressure vessel) results in an amorphous material.

References

1. Presnall, D.C.; Dixon, S.A.; Dixon, J.R.; O'Donnell, T.H.; Brenner, N.L.; Schrock, R.L. *Contrib. Meneral. Petrol.* **66**, 203 (1978).

2. Gorbushina, A.A.; Boettcher, M.; Brumsack, H.; Krumbein, W.E.; Vendrell-Saz, M. *Geomicrobiol. J.* **18**, 117 (2001).

3. Dunton III, G.R.; Green, L.Q. U.S. Patent 3,887, 994 (1968).

4. Yoldas, B.E.; O'Keefe, T.W. *Appl. Opt.* **18**, 3133 (1979).

5. Petricevic, V.; Gayen, S.K.; Alfano, R.R.; Yamagishi, K.; Anzai, H.; Yamaguchi, Y. *Appl. Phys. Lett.* **52**, 1040 (1988).

6. Cooper, R.F.; Kohlstedt, D.L. *Tectonophysics.* **92**, 35 (1984).

7. Yamaguchi, O.; Nakajima, Y.; Simizu, K. *Chem. Lett.* **5**, 401 (1976).

8. Mitchell, M.B.D.; Jackson, D.; James, P.F. *J. Sol-Gel Sci. Tech.* **15**, 211 (1999).

9. Park, D.G.; Higuchi, M.; Dieckmann, R.; Burlitch, J.M. *Bull. Korean Chem. Soc.* **19**, 927 (1998).

10. Park, D.G.; Burlitch, J.M.; Geray, R.F.; Dieckmann, R.; Barber, D.B.; Pollock, C.R. *Chem. Mater.* **5**, 518 (1993).

11. Devi, P.S.; Gafney, H.D.; Petricevic, V.; Alfano, R.R.; He, D.; Miyano, K.E. *Chem. Mater.* **12**, 1378 (2000).

12. Swanson, H.E.; Targe, E. *Natl. Bur. Stand. Circ. 539.* **1**, 83 (1953).

13. Temuujin, J.; Okada, K.; Mackenzie, K.J.D. *J. Solid State Chem.* **138**, 169 (1998).

14. Pierre, A.C. Introduction to Sol-Gel Processing. Kluwer Academic Publishers, Boston (1998).

15. Burlitch, J.M.; Beeman, M.L.; Riley, B.; Kohlstedt, D.L. *Chem. Mater.* **3**, 692 (1991).

16. Park, D.G.; Duchamp, J.C.; Duncan, T.M.; Burlitch, J.M. *Chem. Mater.* **6**, 1990 (1994).

17. Bowen, N.L.; Tuttle, O.F. *Bull. Geol. Soc. Am.* **60**, 447 (1949).

18. Clark, B.L.; Keszler, D.A. *Inorg. Chem. In press.*

19. JCPDF card #34-0189.

CHAPTER 9

CONCLUSIONS AND RECOMMENDATIONS FOR FUTURE STUDIES

Conclusions

Several important phosphors for use in alternating-current thin-film electroluminescent (ACTFEL) devices have been synthesized and studied. Particular attention was paid to synthesis of a bright and efficient green ACTFEL SrS:Cu phosphor by using codopants, solid solution, and ceramic processing techniques.

A new model describing the emission of charge compensated SrS:Cu was introduced. By comparing our data to previously reported data for this system and NaBr:Cu, we concluded that the ground-state Cu position in SrS is similar to that of NaBr; it occupies a shallow off center position. This model was used to explain the emission characteristics of charge compensated SrS:Cu at low temperatures. Introducing S vacancies into SrS by adding alkali-metal cations leads to a reduced coordination around the Cu^{+} ion. This Cu-vacancy complex was described as a deep off-center ground-state Cu position.

A similar trend was observed by examining Cu doped calcium and barium sulfides and comparing the results to other alkali halides. The ground-state Cu position in CaS is similar to that of NaCl:Cu, i.e., it occupies an on-center position. Conversely, the ground-state Cu position in BaS is a deep off-center position,

similar to that of KCl:Cu. We believe this comparison to be valid because of the similar cell parameters and distances involved in the alkali halides and the alkaline earth sulfides.

The use of the phosphor SrS:Cu for ACTFEL applications was studied. Charge compensation of the phosphor, e.g., through addition of Y^{3+} or Cl^-, resulted in bright and efficient blue emission. Creating vacancies through addition of alkali metal cations, e.g., Na^+ and K^+, resulted in very bright and efficient green emission. The efficiencies reported here are highest observed for a saturated green-emitting ACTFEL device. All the ACTFEL results correspond well with the photoluminescent results.

A study of emission characteristics of ZnS and SrS doped with various lanthanide dopants was performed. By comparing the emission spectra for each phosphor, as well as the electrical characteristics, it was concluded that the hot electron distribution appears to be inadequately heated to efficiently excite short wavelength luminescent impurities. For this reason, we concluded that ZnS would not make an efficient ACTFEL phosphor for blue emitting applications.

In the second half of this thesis, a simple approach was examined for the synthesis of refractory silicates at low temperatures. Three silicates were prepared in this study: Zn_2SiO_4, $SnSiO_3$, and Mg_2SiO_4. Zn_2SiO_4 has previously been synthesized at low temperatures, so its preparation did not represent a particularly difficult problem. $SnSiO_3$, however, had only been prepared at temperatures of 823 K or higher. We reported a synthesis temperature of 398 K. We believe this

method will prove to be very important for the preparation of Sn^{2+} oxides because of the propensity of Sn^{2+} to lose oxygen and subsequently oxidize at high temperatures. As noted in the Appendix, $SnWO_4$ has also been prepared by using this technique. The preparation of Mg_2SiO_4 was accomplished at temperatures as low as 698 K. Although the resulting powder was not completely single phase, heating the sample at 1273 K for 12 hours resulted in a single phase material of crystalline Mg_2SiO_4. We believe this is a major accomplishment considering previous low temperature synthesis studies of Mg_2SiO_4 required many complex steps and toxic materials that needed to be handled under controlled conditions. Hydrothermal dehydration relies on nontoxic starting materials and it involves only a few, simple steps.

Recommendations for Future Studies

An observant researcher will identify many unanswered questions that arise during a lengthy research project. Because of many factors, however, these unanswered questions cannot be answered all at once. Fortunately, these questions give rise to new research projects for future graduate students. Here, a few suggestions for future studies will be offered.

Diffuse Reflectance of SrS:Cu

Previously reported results on Cu doped alkali halide phosphors involved examining the absorption properties of Cu versus temperature. From these results,

the researchers were able to determine the oscillator strength and then conclude the nature of the Cu site, i.e., on center, shallow off center, etc. These absorption studies were done by using single crystals of the alkali halides. Single crystals of alkaline-earth sulfides, however, are very difficult to grow because of their high melting points and high reactivity, although growth may be more easily achieved by using flux methods. An experiment similar to that of absorption in single crystals is diffuse reflectance. In this experiment, a powder sample is used and a monochromatic light source is displayed onto the sample. A detector is placed at an angle such that only the diffuse reflected light is collected. By varying the temperature, one should obtain results similar to the absorption data reported in the literature. This would be a nice quantitative experiment that could be used to verify the use of the off-center, on-center model.

Pressure Effects of Luminescence of SrS:Cu

We have shown that by decreasing the unit cell of SrS:Cu we were able to destabilize shallow off center ground-state potential. This, in effect, is the same as increasing the pressure. By mechanically increasing the pressure, however, we would expect to obtain the same result. Kevin Bray at Washington State University deals with luminescence of materials under high pressure. Perhaps a collaborative effort between our two labs would result in further evidence of the shallow off-center model.

ab initio Calculations on SrS:Cu

Another potentially useful experiment would be to run an *ab initio* calculation on the SrS:Cu system. By doing this experiment, one could determine the preferred directions for Cu^+ ion movement in the SrS matrix. Comparing the results for a charge compensated sample versus a vacancy associated sample may also prove very interesting.

Lifetime Data on SrS:Cu

Some current theories in the literature assume the Cu^+ ion occupies a single site, no matter the temperature. One relatively simple experiment for examining this model is to obtain lifetimes at both short and long wavelengths as a function of temperature. If the excited states are not coupled, independent lifetimes will be observed. If the excited states are characterized by a coupling between on-center and off-center potentials, the lifetimes will follow a very characteristic temperature dependence.

Low Temperature Processing for Oxide ACTFEL Devices

We have demonstrated the use of hydrothermal annealing of Zn_2GeO_4:Mn thin-films for use in ACTFEL device applications. The method is far from optimized, however, and needs considerably more research. By varying a few parameters, we could possibly obtain very bright and efficient ACTFEL devices by using this low-temperature technique. The study should include varying the

amount of water used in the reaction vessel, varying the temperature used, and varying the time in the oven. It may also be beneficial to examine the effects of adding various steps after the hydrothermal anneal, such as rapid thermal annealing and standard furnace annealing.

A technique called SILAR will be helpful in creating thin films without the use of any vacuum deposition equipment. Essentially, a glass substrate is dipped into a cation solution for several seconds, rinsed, and then dipped in an appropriate anion solution forming a monolayer of film on the substrate. The process is repeated until the desired film thickness is obtained. This could then be subjected to a hydrothermal anneal, thus dehydrating the sample and producing a crystalline film.

Hydrothermal Dehydration Synthesis of Other Silicates

We know that Mg_2SiO_4 is very difficult to prepare by standard solid-state techniques. We were able to produce the material by using the hydrothermal dehydration method, therefore, less refractory silicates should be quite easy to prepare. One such material is Y_2SiO_5. This is a common phosphor used in CRT displays. By simply combining the appropriate starting materials and following the hydrothermal dehydration procedure, crystalline Y_2SiO_5 should form rather easily.

BIBLIOGRAPHY

Aia, M.A. Kokoku (Japanese patent) 39-1121, 1964.

Akella, A.; Keszler, D.A. *Mater. Res. Bull.*, **30**, 105 (1995).

Barrow, W.A.; Coovert, R.E.; Dickey, E.; King, C.N.; Laakso, C.; Sun, S.S.; Tuenge, R.T.; Wentross, R.C.; Kane, J. *Digest of 1993 SID International Symposium*, 761, 1993.

Barrow, W.A.; Coovert, R.E.; King, C.N. *Digest of 1984 SID International Symposium*, 249, 1984.

Barthou, C.; Benoit, J.; Benalloul, P.; Garcia, A.; Fouassier, C. *Proc. 10th Inter. Conf. Inorg. Org. Electrolumin.* Hamamatsu, Japan (2000).

Becquerel, E. La Lumiere. F. Didot Freres, Paris, 1867.

Benalloul, P.; Barthou, C.; Benoit, J. *J. Alloys Compnd.* 275 (1998).

Berger-Schunn, A. Practical Color Measurement. John Wiley and Sons, 1994.

Bhargava, B.N.; Gallagher, D.; Hong, X.; Nurmikko, A. *Phys Rev. Lett.* **72**, 416 (1994).

Bhattachayyra, K.; Goodnick, S.M.; Wager, J.F. *J. Appl. Phys.* **73**, 3390 (1993).

Blasse, G.; Grabmaier, B.C. Luminescent Materials. Springer-Verlag, 1994.

Bondar, V. *Mater. Sci. Eng. B.* **69**, 510.

Bowen, N.L.; Tuttle, O.F. *Bull. Geol. Soc. Am.* **60**, 447 (1949).

Burlitch, J.M.; Beeman, M.L.; Riley, B.; Kohlstedt, D.L. *Chem. Mater.* **3**, 692 (1991).

Butler, K.H. *J. Electrochem. Soc.* **100**, 250 (1953).

Butler, K.H.; Homer, H.H. *Illum. Eng.* 55, 396 (1960).

Carbo-Nover, J.; Williamson, J. *Phys. Chem. Glasses* **8**, 164 (1967).

Chase, E.W; Hepplewhite, R.T.; Krupka, D.C.; Kahng, D. *J Appl Phys.* **40**, 2512 (1969).

Clark, B.; Keszler, D.; Bender, J.; Wager, J. *Ext. Abstr., Internat. Conf. Sci. Technol. Display Phosphors.* 145 (2000).

Clark, B.L.; Keszler, D.A. *Inorg. Chem. In press.*

Clark, B.L.; Keszler, D.A.; Bender, J.P.; Wager, J.F. *Ext. Abstr., Internat. Conf. Sci. Technol. Display Phosphors.* 145 (2000).

Colvin, V.L.; Schlamp, M.C.; Alvisatos, A.P. *Nature.* **370**, 354 (1994).

Cooper, R.F.; Kohlstedt, D.L. *Tectonophysics.* **92**, 35 (1984).

Corlatan, D.; Neyts, K.A.; De Visschere, P. *J. Appl. Phys.* **78**, 7259 (1995).

Destriau, G. *J. Chim. Physique.* **33**, 587 (1936).

Devi, P.S.; Gafney, H.D.; Petricevic, V.; Alfano, R.R.; He, D.; Miyano, K.E. *Chem. Mater.* **12**, 1378 (2000).

Diaz, A. Ph.D. Thesis, Oregon State University, 1997.

Dimitrova, V.; Draeseke, A.; Tate, J.; Yokoyama, T.; Clark, B.L.; Li, D.; Keszler, D.A. *Appl. Phys. Lett.* **75**, 2353 (1999).

Dunton III, G.R.; Green, L.Q. U.S. Patent 3,887, 994 (1968).

Dur, M.; Goodnick, S.M.; Shankar, S.; Wager, J.F.; Reigrotzki, M.; Redmer, R. *J. Appl. Phys.* **83**, 3176 (1998).

Dur, M.; Saraniti, M.; Goodnick, S.M.; Redmer, R.; Reigrotzki, M.; Fitzer, N.; Stadele, M.; Vogl, P. Presented at the *9th International Workshop on Inorganic and Organic Electroluminescence and the Fourth International Conference on the Science and Technology of Display Phosphors*, Bend, Oregon, September 14-17, 1998.

Dunton III, G.R.; Green, L.Q. U.S. Patent 3,887, 994 (1968).

Edison, T.A. U.S. Patent #865367, 1896.

Feldmann, C.; Justel, T.; Ronda, C.R.; Wiechert, D.U. *J. Lumin.* **92**, 245 (2001).

Gan, L.M.; Liu, B.; Chew, C.H.; Xu, S.J.; Chua, S.J.; Loy, G.L. *Langmuir.* **13**, 6427 (1997).

Gillooly, G.R.; Rabatin, J.G. Kokoku 40-6843, 1965.

Golewski, M.; Leskela, M. *CRC Crit. Rev. Solid State Mater. Sci.* **19**, 199 (1994).

Gorbushina, A.A.; Boettcher, M.; Brumsack, H.; Krumbein, W.E.; Vendrell-Saz, M. *Geomicrobiol. J.* **18**, 117 (2001).

Harrison, W.T.A.; Dussack, L.L.; Jacobson, A.J. *J. Solid State Chem.* **125**, 234 (1996).

Harvey, E.N. A History of Luminescence. The American Philosophical Society, 1957.

Hirabayashi, K.; Kozawaguchi, H.; Tsujiyama, B. *Jpn. J. Appl. Phys.* **26**, 1472 (1987).

Hitt, J.C.; Keir, P.D.; Wager, J.F. *J. Appl. Phys.* **83**, 1141 (1998).

Holland, U.; Lüty, F. *Phys. Rev. B: Condens. Matter.* **19**, 4298 (1979).

Inguchi, T.; Takeda, M.; Kakihora, Y.; Yoshida, M. SID Digest. **5**, 84 (1974).

Inman, G.E. *Trans. Illum. Eng. Soc.* **34**, 65 (1939).

JCPDF card #34-0189.

Janesky, J.; Warren, W.; Li, D.; Keszler, D.A. Unpublished results.

Jayaraj, M.K.; Vallabhan, C.P.G. *J Electrochem. Soc.* **138**, 1512 (1991).

Jenkins, H.G.; Bowtell, J.N. *Trans. Illum. Eng. Soc.* **13**, 61 (1938).

Jenkins, H.G.; McKeag, A.H..; Ranby, P.W. *J. Electrochem. Soc.* **96**, 1 (1949).

Kahng, D. *Appl. Phys. Lett.* **13**, 210 (1968).

Kamiya, S. *Proc. 6th Int. Symp. Sci. Tech. Light Sources*, Budapest, 37, 1995.

Keir, P.D. Fabrication and Characterization of ACTFEL Devices. PhD Thesis, Oregon State University, 2000.

Keir, P.D.; Wager, J.F.; Clark, B.L.; Li, D.; Keszler, D.A. *Appl. Phys. Lett.* **75**, 1398 (1999).

Kitai, A.H. Solid State Luminescence: Theory, Materials, and Devices. Chapman and Hall, 1993.

Kobayashi, H.; Tanaka, S.; Shanger, V.; Shiiki, M.; Kunou, T.; Mita, J.; Sasakura, H. *Phys. Status Solidi A.* **88**, 713 (1985).

Koedamn, M.; Opstelten, J.J. *Lighting Res. Technol.* **3**, 205 (1971).

Koretsky, M. Electronic Materials Processing, Class Notes, Fall, 1997.

Korzenski, M.B.; Kolis, J.; Long, G.J. *J. Solid State Chem.* **147**, 390 (1999).

Lehmann, W. *J. Electrochem. Soc.* **113**, 40 (1966).

Lehmann, W. *J. Electrochem. Soc.* **117**, 1389 (1970).

Lenard, P.; Schmidt, F.; Tomascheck, R. Handb. Exp. Phys., Vol. 23, Akadem Verlagsges, Leipzig) 1928.

Lencka, M.M.; Oledzka, M.; Riman, R. *Chem. Mater.* **12**, 1323 (2000).

Lewis, J.; Waldrip, K.E.; Davidson, M.R.; Morehead, D.; Holloway, P.H.; Sun, S-S. presented at the *Fourth International Conference on the Science and Technology of Display Phosphors*, Bend, Oregon, September 14-17, 1998.

Li, D. Ph.D. Thesis, Oregon State University, 1999.

Li, D.; Clark, B.L.; Keszler, D.A.; Keir, P.D.; Wager, J.F. *Chem. Mater.* **12**, 268 (2000).

Li, Q.H.; Komaraneni, S.; Roy, R. *J. Mater. Sci.* **30**, 2358 (1995).

Li, Q.H.; Kormaraneni, S.; Roy, R. *J Mater. Sci.* **30**, 2358 (1995).

Li, W.M.; Ritala, M.; Leskela, M.; Niinisto, L.; Soininen, E. Sun, S.S.; Tong, W. Summers, C.J. *J. Appl. Phys.* **86**, 5017 (1999).

McKeag, A.H.; Ranby, P.W. U.S. Patent #2488733, 1952.

Menkara, H.M.; Park, W.; Chaichimansour, M.; Jones, T.C.; Wagner, B.K.; Summers, C.J.; Sun, S-S. presented at the *Fourth International Conference on the*

Science and Technology of Display Phosphors, Bend, Oregon, September 14-17, 1998.

Merril, J.B.; Schulman, J.H. J. Opt. Soc. Am. 38, 471 (1948).

Meyers, R.; Wager, J.F. *J. Appl. Phys.* **81**, 506 (1997).

Minami, T. *Mater. Res. Soc. Symp. Proc.* 558, 2000.

Minami, T.; Kubota, Y.; Yamada, H.; Miyata, T. *Ext. Abstr., Internat. Conf. Sci. Technol. Display Phosphors.* 207, 1997.

Minami, T.; Miyata, T.; Nakatani, T. *Proc. Electrochem. Soc.* 99, 2000.

Minami, T.; Miyata, T.; Takata, S.; Fukuda, I. *Jpn. J. Appl. Phys.* **33**, L117 (1991).

Minami, T.; Sakagami, Y.; Miyata, T. *Ext. Abstr., Internat. Conf. Sci. Technol. Display Phosphors.* 37, 1997.

Minami, T.; Yamada, H.; Yoshihiro, K. Toshihiro, Miyata. *Proc. SPIE Int. Soc. Opt. Eng.* 3242, 1997.
Mitchell, M.B.D.; Jackson, D.; James, P.F. *J. Sol-Gel Sci. Tech.* **15**, 211 (1999).
Miyata, T.; Minami, T.; Ito, J.; Takata, S. *Proc. 6th Int. Workshop Electroluminescence.* 228, 1992.

Miyata, T.; Nakatani, T.; Minami, T. *J. Lumin.* **89**, 1183 (2000).

Mohammed, E.; Park, W.; Tong, W.; Stock, S.R.; Summers, C.J. *Proc. 6th Inter. Conf. Sci. Tech. Display Phosphors*. San Diego, CA (2000).

Morimo, R.; Matae, K. *Mater. Res. Bull.* **24**, 175 (1989).

Nakajima, S.; Honda, Y.L. *J. Illum. Eng. Japan.* **40**, 305 (1956).

Neyts, K.; Soininen, E. *IEEE Trans. Electron Devices.* **42**, 1086 (1995).

Neyts, K.A.; Corlatan, D.; De Visschere, P.; Van den Bossche, J. *J. Appl. Phys.* **75**, 5339 (1994).

Ogura, T.; Mikami, A.; Tanaka, K.; Taniguchi, K.; Yoshida, M. Nakajima, S. *Appl. Phys. Lett.* **48**, 1570 (1986).

Ohmi, K.; Inoue, S.; Tanaka, S.; Kobayashi, H. *Appl. Phys. Lett.* **64**, 3464 (1994).

Ohmi, K.; Ishitani, K.; Tanaka, S.; Kobayashi, H. *Appl. Phys. Lett.* **67**, 944 (1995).

Ohnishi, H.; Yamamoto, K.; Katayama, Y. *Conference Record of the 1985 International Display Research Conference.* 159, 1985.

Ohnishi, H.; Yamasaki, Y.; Iwase, R. *Digest of 1987 SID International Symposium.* 238, 1987.

Ohring, M. The Materials Science of Thin Films. Academic Press, 1992.

Okamoto, S.; Nakazawa, E.; Tsuchiya, Y. *Jpn. J. Appl. Phys., Part 1.* **28**, 406 (1989).

Okamoto, S; Nakazawa, E. *Jpn. J. Appl. Phys., Part 1.* **34**, 521 (1995).

Ono, Y.A. Electroluminescent Displays. World Scientific, 1995.

Ono, Y.A.; Fuyama, M.; Onisawa, K.; Tamura, K.; Ando, M. *J. Appl. Phys.* **66**, 5564 (1989).

Park, D.G.; Burlitch, J.M.; Geray, R.F.; Dieckmann, R.; Barber, D.B.; Pollock, C.R. *Chem. Mater.* **5**, 518 (1993).

Park, D.G.; Duchamp, J.C.; Duncan, T.M.; Burlitch, J.M. *Chem. Mater.* **6**, 1990 (1994).

Park, D.G.; Higuchi, M.; Dieckmann, R.; Burlitch, J.M. *Bull. Korean Chem. Soc.* **19**, 927 (1998).

Payne, S.A.; Goldberg, A.B.; McClure, D.S. *J. Chem. Phys.* **81**, 1529 (1984).

Payne, S.A. *Phys. Rev. B.* **36**, 6125 (1987).

Petricevic, V.; Gayen, S.K.; Alfano, R.R.; Yamagishi, K.; Anzai, H.; Yamaguchi, Y. *Appl. Phys. Lett.* **52**, 1040 (1988).

Piccirilli, M.; Spinolo, G. *Phys. Rev. B.* **4**, 1339 (1971).

Pierre, A.C. *Introduction to Sol-Gel Processing.* Kluwer Academic, Boston (1998).

Presnall, D.C.; Dixon, S.A.; Dixon, J.R.; O'Donnell, T.H.; Brenner, N.L.; Schrock, R.L. *Contrib. Meneral. Petrol.* **66**, 203 (1978).

Ronda, C.R.; Smets, B.M.J. *J. Electrochem. Soc.* **136**, 570 (1989).

Schuegraf, K.K. Handbook of Thin-Film Deposition Processes and Techniques. Noyes Publications, 1988.

Shionoya, S.; Yen, W.H. Phosphor Handbook. CRC Press, 1999.

Singh, V.P.; Morton, D.C. *IEEE Trans. Electron Devices*. **36**, 54 (1989).

Slonominskii, B.I.; Tseidler, A.A. *Sb. Trud. Gos. Nauchnoissled. Inst. Tsver Metal.* **15**, 173 (1959).

Smets, B.; Rutten, J.; Hoeks, G.; Verlijsdonk, J. *J. Electrochem. Soc.* **136**, 2119 (1989).

Solis, J.L.; Lantto, V. *Phys. Scr.*, **69**, 281 (1996).

Stevels, A.L.N. *J. Lumin.* **17**, 121 (1978).

Sun, S.-S. *Extended Abstracts, 4th Int. Conference on Science and Technology of Display Phosphors.* Bend, OR. Society for Information Display: Santa Ana, CA, 1998.

Sun, S.S. Presented at the *9th International Workshop on Inorganic and Organic Electroluminescence and the Fourth International Conference on the Science and Technology of Display Phosphors*, Bend, Oregon, September 14-17, 1998.

Sun, S-S. presented at the *Fourth International Conference on the Science and Technology of Display Phosphors*, Bend, Oregon, September 14-17, 1998.

Sun, S-S. Private communication, May 20, 1998.

Sun, S-S.; Dickey, E.; Kane, J.; Yocum, P.N. *Proceedings of the 17th International Display Research Conference*, p. 301, 1997.

Suntola, T.; Hyvarinen, J. *Ann. Rev. Mat. Sci.* 15, 177 (1985).

Swanson, H.E.; Targe, E. *Natl. Bur. Stand. Circ. 539.* **1**, 83 (1953).

Tanaka, K.; Mikami, A.; Ogura, T.; Taniguchi, M.; Yoshida, M.; Nakajima, S. *Appl. Phys. Lett.* **48**, 1730 (1986).

Tanaka, S. *J. Crystal Growth.* **101**, 958 (1990).

Tanaka, S.; Deguchi, H.; Mikami, Y.; Shiiki, M.; Kobayashi, H. *Proc. SID.* **26**, 255 (1985).

Tanaka, S.; Mikami, Y.; Deguchi, H.; Kobayashi, H. *Jpn. J. Appl Phys.* **25**, L225 (1986).

Tanaka, S.; Ohmi, K. Fujimoto, K.; Kobayashi, H.; Nire, T.; Matsuno, A.; Miyakoshi, A. *Eurodisplay '93*, 237, 1993.

Tanaka, S.; Yoshiyama, H.; Mikami, Y.; Nishiura, J.; Ohshio, S.; Kobayashi, H. *Proc. Soc. Inf. Disp.* **29**, 77 (1988).

Tanaka, S.; Yoshiyama, H.; Nishiura, J.; Ohshio, S.; Kawakami, H.; Kobayashi, H. *Appl. Phys. Lett.* **51**, 1661 (1987).

Tayer, R.N.; Barnes, B.T. *J. Opt. Soc. Am.* **29**, 131 (1939).

Temuujin, J.; Okada, K.; Mackenzie, K.J.D. *J. Solid State Chem.* **138**, 169 (1998).
Thornton, W.A. *J. Opt. Soc. Am.* **61**, 1155 (1971).

Troppenz, U.; Huttl, B.; Storz, U.; Kratzert, P.; Velthaus, K.O. presented at the *Fourth International Conference on the Science and Technology of Display Phosphors*, Bend, Oregon, September 14-17, 1998.

Tuenge, R.T.; Kane, J. *Digest of 1991 SID International Symposium*, 279, 1991.

Vecht, A.; Gibbons, C; Davies, D.; Jing, X.; Marsh, P.; Ireland, T.; Silver, J.; Newport, A.; Barber, D. *J Vac Sci Tech.* **17**, 750 (1999).

Velthaus, K.O.; Huttl, B.; Troppenz, U.; Herrman, R.; Mauch, R.H. *SID 97 Digest*, 4 (1997).

Verstegen, J.M.P.J. *J. Electrochem. Soc.* **121**, 1623 (1974).

Vij, D.R. Luminescence in Solids. Plenum, 1998.

Vlasenko, N.A.; Poplov, I.A. *Optics & Spectroscopy.* **8**, 39 (1960).

Wager, J.F. and Keir, P.D. *Annu. Rev. Mater. Sci.* **27**, 223 (1997).

Wager, J.F.; Hitt, J.C.; Baukol, B.A.; Bender, J.P.; Keszler, D.A. *Unpublished results.*

Wager, J.F.; Keir, P.D. *Annu Rev. Mater. Sci.* **27**, 223 (1997).

Williamson, S.J.; Cummins, H.Z. Light and Color in Nature and Art. John Wiley and Sons, 1983.

Wolf, S.; Tauber, R.N. Silicon Processing for the VLSI Era, vol. 1. Lattice Press, 1986.

Xu, S.J.; Chua, S.J.; Liu, B.; Gan, L.M.; Chew, C.H.; Xu, G.Q. *Appl. Phys. Lett.* **4**, 478 (1998).

Yamaguchi, O.; Nakajima, Y.; Simizu, K. *Chem. Lett.* **5**, 401 (1976).

Yamashita, N. *Jpn. J. Appl. Phys.* **30**, 3355 (1991).

Yamashita, N.; Ebisumori, K.; Nakamura, K. *Jpn. J. Appl. Phys.* **32**, 3840 (1993).

Yoldas, B.E.; O'Keefe, T.W. *Appl. Opt.* **18**, 3133 (1979).

Yu, J.; Liu, H.; Wang, Y.; Jia, W. *J. Lumin.* **79**, 191 (1998).

Zang, F.; Zaralij, P.Y.; Whittingham, M.S. *Mater. Res. Bull.* **32**, 701 (1997).

APPENDIX A: CRYSTAL STRUCTURE OF Nd:$LaSc_3(BO_3)_4$ AND LUMINESCENCE STUDIES OF Tb:$CeAl_3(BO_3)_4$

The compound $LaSc_3(BO_3)_4$ (LSB) and $CeAl_3(BO_3)_4$ (CAB) belong to a large class of materials that crystallize in the structure of the mineral huntite, $CaMg_3(CO_3)_4$. In this appendix, the crystal structure of Nd:LSB is given. Also, excitation and emission spectra of the bright phosphor Tb:CAB are described.

Crystal Structure of Nd:$LaSc_3(BO_3)_4$

A large Czochralski grown crystal was obtained from Dr. Tom Reynolds. A smaller crystal with approximate dimensions 0.1 x 0.1 x 0.2 mm was chipped off and mounted on the end of a glass fiber with epoxy for X-ray structure analysis. Data were collected with Mo Kα radiation on a Rigaku AFC6R diffractometer. The ω–2Θ scan technique was used to collect data covering the range of indices $0 < h < 15$, $0 < k < 19$, and $-23 < l < 23$. The space group C2/c was determined based on the systematic absences $h + k = 2n + 1$ and $l = 2n + 1$ for h0l. Three reflections, chosen as standards and measured after each block of 500 data, exhibited an overall average intensity decay of 1.8%. The structure was solved and refined using the TEXSAN crystallographic software package (Molecular Structure Corporation, 1997.) The refinement converged to R = 0.034 and wR = 0.041. A summary of the crystallographic data is given in Table A.1.

Table A.1. Crystallographic data for Nd:LSB.

Diffractometer	Rigaku AFC6R
Radiation	0.71703 Å (Mo Kα)
Formula wt., amu	509.001
Unit cell	Monoclinic
a, Å	7.728(2)
b, Å	9.848(1)
c, Å	12.047(2)
V, Å^3	883.8(2)
Space group	C2/c (#15)
R	0.034
WR	0.041

Table A.2. Atom positions for Nd:LSB.

atom	x	y	z	B(eq)
La(1)	0	0.3946(2)	0.5	0.58(1)
La(2)	-0.5	-0.0345(2)	0	0.56(1)
Sc(1)	0	0.0060(3)	0	0.25(2)
Sc(2)	-0.0492(2)	0.1803(2)	0.2243(1)	0.38(2)
Sc(3)	-0.5	0.3562(3)	0.5	0.54(2)
Sc(4)	-0.4525(2)	0.1819(2)	0.2752(1)	0.43(2)
O(1)	-0.2418(6)	0.3184(4)	0.2626(4)	0.42(5)
O(2)	-0.2065(6)	-0.1256(4)	0.0029(4)	0.38(5)
O(3)	-0.2500(6)	0.0485(5)	0.2503(4)	0.60(6)
O(4)	-0.3042(6)	0.4894(5)	0.4838(4)	0.69(6)
O(5)	0.0944(7)	0.3440(5)	0.1855(4)	0.57(6)
O(6)	-0.6038(6)	0.3426(5)	0.3181(4)	0.50(6)
O(7)	0.1151(6)	0.0306(5)	0.1807(4)	0.44(6)
O(8)	-0.6047(6)	0.0285(5)	0.3180(4)	0.53(6)
O(9)	-0.0611(6)	-0.3242(4)	0.1015(4)	0.53(6)
O(10)	-0.3285(5)	0.2091(4)	0.4537(3)	0.44(4)
O(11)	0.0757(6)	0.1986(5)	0.3967(4)	0.53(6)
O(12)	-0.3472(5)	-0.3332(4)	-0.0413(3)	0.50(5)
B(1)	-0.745(1)	-0.041(1)	0.2475(9)	0.7(1)
B(2)	-0.253(1)	-0.0919(8)	0.2483(7)	0.34(9)
B(3)	-0.299(1)	0.625(1)	0.4753(9)	0.5(1)
B(4)	-0.201(1)	-0.266(1)	0.0237(8)	0.5(1)

Photoluminescence of Tb:$CeAl_3(BO_3)_4$

CAB:Tb samples were prepared by standard solid-state chemistry techniques. First, the optimum concentration of Tb was found to be 30 atom% Tb in CAB, as indicated by Figure A.1.

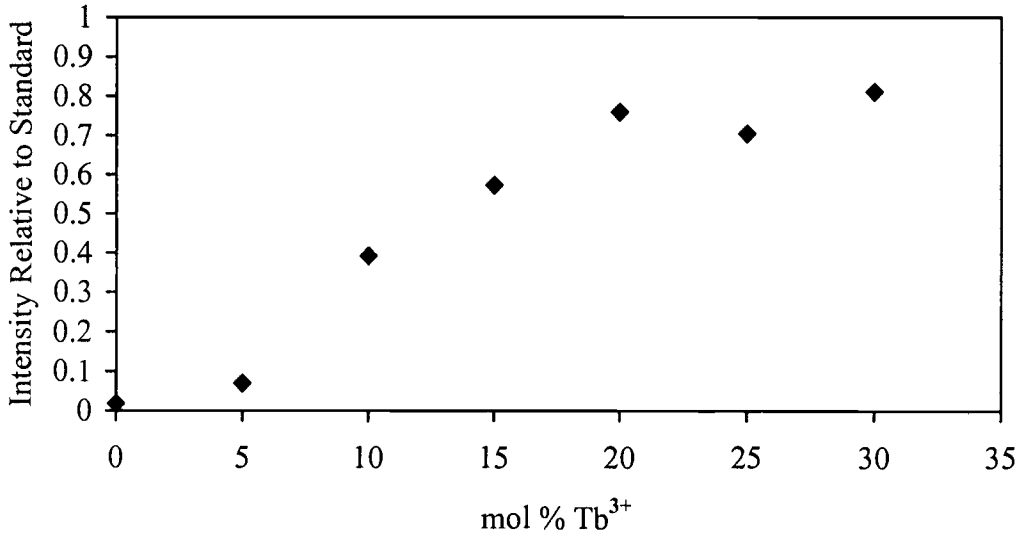

Figure A.1. Concentration Quenching of $CeAl_3(BO_3)_4:Tb^{3+}$.

The emission spectrum for CAB:Tb is given in Figure A.2. The sample was excited by 270 nm radiation. All spectra were corrected for monochromator and PMT response.

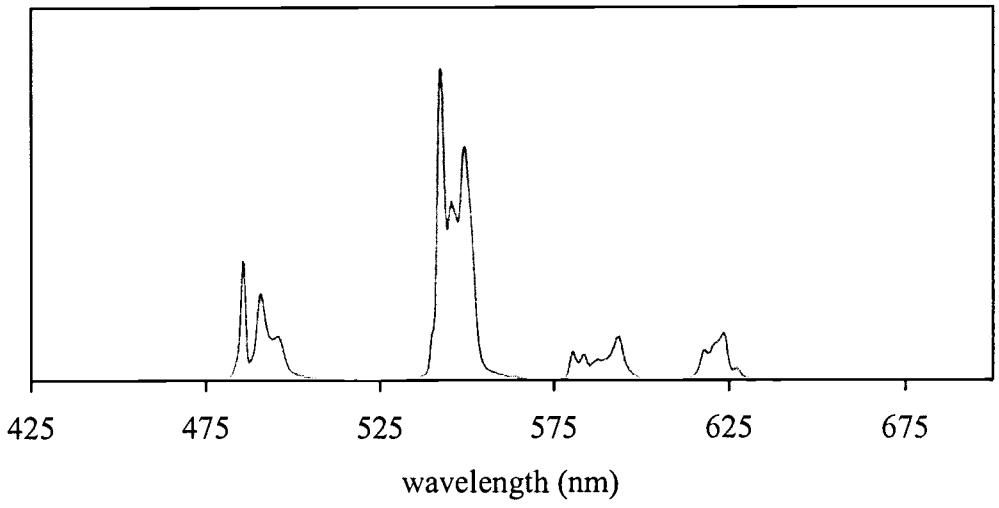

Figure A.2. Emission spectrum of $CeAl_3(BO_3)_4:Tb^{3+}$.

The VUV excitation spectra for CAB:Tb and Zn_2SiO_4:Mn is given in Figure A.3. This data was obtained at Samsung Corporation in South Korea with the help of Youhyak Kim. Note the excitation is stronger in CAB:Tb at longer wavelengths, but weaker at shorter wavelengths. For this reason, this phosphor would probably not compete well with Zn_2SiO_4:Mn for VUV applications such as plasma television displays.

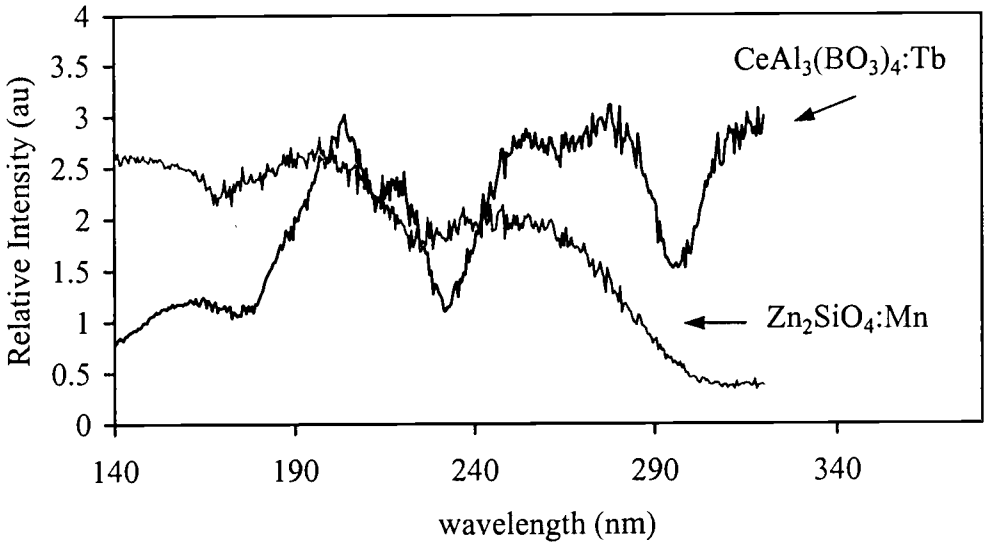

Figure A.3. VUV excitation spectrum of $CeAl_3(BO_3)_4:Tb^{3+}$.

APPENDIX B: UNFINISHED PROJECTS

In this appendix I will describe many of the projects that I could not finish during the four years that I was here at OSU. I feel that these projects would probably make for some interesting studies, especially those dealing with Sn compounds.

Synthesis of $Sn_2(WO_4)_3$ Single Crystals

The purpose of this experiment was to synthesis new Sn containing materials, specifically compounds with a mixed valance Sn, i.e., Sn^{2+} and Sn^{4+}, similar those compounds containing Bi^{3+} and Bi^{5+}. Single crystals of $Sn_2(WO_4)_3$ were grown by vapor phase transport in an evacuated silica tube, using I_2 and NH_4I as the transporting agent. More details of vapor phase transport crystal growth can be found in the literature. These crystals were black and conductive. Finding a non-twinned crystal proved difficult, however, and the structure was not solved with any degree of certainty.

Hydrothermal Dehydration of $SnWO_4$

By using the hydrothermal dehydration method, as outlined in chapters 6-8, single phase α-$SnWO_4$ was prepared. Two phases exist for $SnWO_4$: the low temperature α-phase and a high temperature β-phase. Attempts were made to make

the high temperature phase using the hydrothermal dehydration method, by varying the pH of the solutions, but these attempts were never successful.

Luminescence of SrS:Cu, Ag

Some studies were performed on the photoluminescence of SrS:Cu, Ag. This system emits in the deep blue region of the spectrum. Based on our work dealing with coordination of Cu in SrS, one would expect that the luminescence would be green, since Ag enters the matrix as a +1 cation. We believe, however, that the Ag^{+} acts as a vacancy scavenger, preserving the six-fold coordination about Cu in SrS. From the results I obtained on low temperature measurements for SrS:Cu, Ag, this seems logical, since the same green shift is observed with decreasing temperature. It's still not clear why SrS:Ag is not an efficient phosphor without the Cu present. The latest studies in the literature indicate that the Ag cannot enter the matrix without first forming an alloy with Cu, which is then incorporated into SrS. It would be interesting to study SrS:Ag to tell whether or not the Cu is really necessary. For instance, is there another way to incorporate only Ag into SrS?

$SrGa_2S_4$ and $Sr_2Ga_2S_5$ Phosphors

Two samples of $SrGa_2S_4$ and $Sr_2Ga_2S_5$ doped with Eu^{2+} were prepared. The emission of each was measured and the latter was red-shifted compared to the first. No further studies were done on this system.